

2006

The effect of base connection geometry on the fatigue performance of welded socket connections in multi-sided highmast lighting towers

Margaret K. Warpinski
Lehigh University

Follow this and additional works at: <http://preserve.lehigh.edu/etd>

Recommended Citation

Warpinski, Margaret K., "The effect of base connection geometry on the fatigue performance of welded socket connections in multi-sided highmast lighting towers" (2006). *Theses and Dissertations*. Paper 940.

This Thesis is brought to you for free and open access by Lehigh Preserve. It has been accepted for inclusion in Theses and Dissertations by an authorized administrator of Lehigh Preserve. For more information, please contact preserve@lehigh.edu.

Warpinski,
Margaret K.

The Effect of Base
Connection
Geometry on the
Fatigue
Performance of
Welded Socket...

May 2006

The Effect of Base Connection Geometry on the Fatigue Performance of
Welded Socket Connections in Multi-sided High-mast Lighting Towers

By

Margaret K. Warpinski

A Thesis

Presented to the Graduate and Research Committee

of Lehigh University

in Candidacy for the Degree of

Master of Science

in

Civil Engineering

Lehigh University

May 2006

This thesis is accepted and approved in partial fulfillment of the requirements
for the Master of Science.

April 26, 2006

Date

Dr. Robert J. Conroy
Assistant Professor, Purdue University
Thesis Advisor

Dr. John W. Fisher
Professor Emeritus
Co-Advisor

Dr. Stephen P. Pessiki
Chairperson of Department

Acknowledgements

I would like to acknowledge the Iowa Department of Transportation, the Pennsylvania Department of Transportation, and the Pennsylvania Infrastructure Technology Alliance for funding this study of high-mast lighting towers and making my education at Lehigh University possible.

To Dr. Robert Connor, thank you for sharing your knowledge throughout my graduate education. And thank you for your constant encouragement, guidance, and support in my academic and professional endeavors.

To Dr. John Fisher, thank you for your support and academic sponsorship of my research project.

To Ian Hodgson, Carl Bowman, and the members of the Infrastructure Monitoring Group, thank you for your help with my research project. This study would not have gone so smoothly or been so enjoyable without you.

I would also like to thank my wonderful friends, both near and far away, for relentlessly telling me to “chill out Meg” and for always being there for me with open ears.

To my family, thank you, because none of this would be possible without your constant support and love. To my parents, Norm and Katie, thank you for teaching me that I can accomplish anything in this world as long as I have determination. And to my younger brothers, Matt and Joe, thank you for always believing in me.

Table of Contents

List of Tables	vii
List of Figures.....	viii
Abstract.....	1
Chapter 1 Introduction.....	2
1.1 Background.....	2
1.2 High-mast Lighting Tower Features	3
1.3 Wind Loading.....	6
1.3.1 Vortex Shedding.....	6
1.3.2 Natural Wind Gusts.....	7
1.3.3 Mitigation.....	8
1.4 High-mast Lighting Tower Failures	10
1.5 High-mast Lighting Tower Design.....	11
1.5.1 Design Code in the United States.....	11
1.5.2 Design Code in Canada.....	13
1.6 Related Research	14
1.7 Scope	17
Chapter 2 Experimental Field Testing.....	26
2.1 Introduction	26
2.2 Phase 1	27
2.3 Phase 2.....	28
2.4 Test Setup	29

2.5 Field Test Results	30
2.5.1 Natural Frequencies.....	30
2.5.2 Damping Ratios.....	30
2.3.2 Measured Stresses	33
2.3.3 Effect of Anchor Nut and Leveling Nut Loosening.....	34
Chapter 3 Finite Element Modeling	44
3.1 Introduction to Modeling.....	44
3.2 BASE Finite Element Model.....	44
3.2.1 Part 1 – Beam Elements	45
3.2.2 Part 2 – Shell Elements	46
3.2.3 Part 3 – Solid Elements.....	48
3.2.4 Part 4 – Multi-point Constraints.....	50
3.3 Model Loading and Constraints	51
3.4 Submodel Study.....	53
3.5 Model Verification	54
3.5.1 Mesh Refinement	55
3.5.2 Anchor Rod Studies	56
3.5.3 Previous Calibration Studies.....	57
Chapter 4 Finite Element Parametric Study	74
4.1 Introduction to the Parametric Study.....	74
4.2 Base Plate Thickness Study.....	80
4.3 Tube Wall Thickness Study.....	84
4.4 Anchor Rod Studies.....	86

Chapter 5 Conclusions and Recommendations	110
5.1 Field Investigation Conclusions	110
5.2 Finite Element Study Conclusions	111
5.3 Future Work.....	113
Appendix A: Vertical Stress Profiles.....	115
References.....	133
Vita	135

List of Tables

Table 2.1: High-Mast Lighting Towers Tested During Phase 1.....	36
Table 2.2: High-Mast Lighting Towers Tested During Phase 2.....	37
Table 2.4: Damping Ratios of Each Tower Tested for the First Four Modal Frequencies	39
Table 2.5: Maximum Measured Stresses at Critical Locations	40
Table 2.6: Maximum Measured Stresses at Critical Locations During Anchor Bolt Loosening Study	42
Table 4.1: Constant Variables for the Finite Element Parametric Study.....	89
Table 4.2: Finite Element Parametric Study Matrix	89
Table 4.3: Study A - Base Plate Thickness Parametric Study with a Tube Wall Thickness of 0.1875"	95
Table 4.4: Study B - Base Plate Thickness Parametric Study with a Tube Wall Thickness of 0.5"	95
Table 4.5: Study C - Tube Wall Thickness Parametric Study with a Base Plate Thickness of 1.25"	103
Table 4.6: Study D - Anchor Rods Parametric Study with a Base Plate Thickness of 1.25"	107
Table 4.7: Study E - Anchor Rods Parametric Study with a Base Plate Thickness of 3.0"	108

List of Figures

Figure 1.1: Typical High-Mast Lighting Tower	20
Figure 1.2: Socket Fillet Welds: Structural and Lower	20
Figure 1.3: Hand Access Hole Detail	20
Figure 1.4: Concrete Foundation and Anchor Rod and Leveling Nut System	21
Figure 1.5: Winch Plate	21
Figure 1.6: Luminary System: (a) Luminary Installed on Top of Tower, (b) Luminary System Lying on Ground Before Tower Erection	22
Figure 1.7: von Karman Vortex Street in the Wake of a Circular Cylinder	22
Figure 1.8 – “Lock-in” phenomenon	23
Figure 1.9: Mode shapes and frequencies for the lowest four modes of the As-built tower along I-35 in Clear Lake, as determined using ABAQUS [Connor, et al., 2006]	24
Figure 1.10 Sioux City, Iowa Retrofit to Stiffen the High-mast Lighting Tower	25
Figure 1.11 – Splice Retrofit Designed by Wiss, Janney, Elstner Associates, Inc. and Installed in Clear Lake, Iowa	25
Figure 2.1: High-Mast Lighting Towers in Sioux City, Iowa	38
Figure 2.2: Pluck Test of a Pole in Sioux City, Iowa	38
Table 2.3: Natural Frequencies for the First Four Modes	39
Figure 2.5: Damping Ratio vs. Frequency	40
Figure 2.6 – Strain gage details for the As-built tower along I-29 in Sioux City, Iowa	41
Figure 2.7 – Strain gage details for the Retrofit tower along I-29 in Sioux City, Iowa	42
Figure 2.8: Localized Stress Changes Due to Poor Installation Techniques	43
Figure 3.1: Front View of the High-mast Lighting Tower Model	60
Figure 3.2: Part 1 of the BASE Model, Constructed of Beam Elements	61
Figure 3.3: Part 1 - Beam Section Sub-Division into Properties and Elements	61

Figure 3.4: Part 2 - Lower Transition - 1" shell elements to 2" shell elements.....	62
Figure 3.5: Part 2 - Base Plate and Tube Wall Mesh.....	62
Figure 3.6: Part 2 - Upper Transition – 2" Shell Elements to 4" Shell Elements	63
Figure 3.7: Part 2 - 1/16 th Section Used to Create the Entire Shell Model.....	63
Figure 3.8: Area of Overlap When Using Shell Elements.....	64
Figure 3.9: Part 3 – Solid Finite Element Model, Lower Tube, Weld, Base Plate, Leveling Nuts, and Anchor Rods.....	65
Figure 3.10: Part 3 – Solid Finite Element Model.....	66
Figure 3.11: Part 3 - Remeshed Region of the Base Plate to Allow for the Anchor Rod and Leveling Nuts	66
Figure 3.12: Shell to Solid Transition Region Around Part 3	67
Figure 3.13: Part 4 - Multi-Point Constraints at the Beam-to-Shell Interface.....	67
Figure 3.14: Part 4 - Multi-Point Constraints at the Shell-to-Solid Interface.....	68
Figure 3.15: Plan View of Point Load Applied to the High-mast Lighting Tower.....	68
Figure 3.16: Stand-off Length	69
Figure 3.17: Anchor Rods Built of Bar Elements that are Constrained at the Center Line and Anchor Rod Built of Solid Elements that is Constrained along the Outer Surface.....	69
Figure 3.18: Global Model and Submodel	70
Figure 3.19: Driven Nodes	70
Figure 3.20: Comparison of Results for the Global Model, the Submodel, and the Combined Model	71
Figure 3.21: Mesh Refinement Studies	71
Figure 3.22: Mesh Refinement Study.....	72
Figure 3.23: Study of the Length that the Anchor Rod is Restrained in the Concrete Foundation.....	72
Figure 3.24: Anchor Rod Constraint Study.....	73
Figure 4.1: Plan View of High-Mast Tower Base Including the Direction of the Applied Load	90

Figure 4.3: Case 1 Vertical Stress Profile Along The Center of the Front Face of Tube Wall	91
Figure 4.4: Case 1 Vertical Stress Contour Plot	91
Figure 4.5: Case 13 Vertical Stress Contour Plot	92
Figure 4.6: General Radial Plot of Vertical Tube Wall Stress in a Multi-Sided Tower and the Predicted Simply Beam Theory Nominal Stress	93
Figure 4.7: General Radial Plot of Vertical Tube Wall Stress in a Multi-Sided Tower at a Height of 6" Above the Base Plate and the Predicted Simply Beam Theory Nominal Stress	94
Figure 4.8: Radial Plot of Outer Vertical Tube Wall Stress at the Weld Toe for Case 6	95
Figure 4.9: Study A Results - Vertical Stress at the Tube Wall Fold vs. Base Plate Thickness for a Tube Wall Thickness of 3/16"	96
Figure 4.10: Study A Results - Normalized Vertical Stress at the Tube Wall Fold vs. Base Plate Thickness for a Tube Wall Thickness of 3/16"	97
Figure 4.11: Study B Results - Vertical Stress at the Tube Wall Fold vs. Base Plate Thickness for Tube Wall Thickness of 1/2"	97
Figure 4.12: Study B Results - Normalized Vertical Stress at the Tube Wall Fold vs. Base Plate Thickness for Tube Wall Thickness of 1/2"	98
Figure 4.13: Results of Studies A and B - Maximum Vertical Tube Wall Stress at the Tube Wall Fold vs. Base Plate Thickness for Tube Wall Thicknesses of 3/16" and 1/2"	98
Figure 4.14: Results of Studies A and B - Normalized Maximum Vertical Tube Wall Stress at the Tube Wall Fold vs. Base Plate Thickness for Tube Wall Thicknesses of 3/16" and 1/2"	99
Figure 4.15: Study A Results - Vertical Stress at the Center of the Front Side of Tube Wall vs. Base Plate Thickness for a Tube Wall Thickness of 3/16"	99

Figure 4.16: Study A Results - Normalized Vertical Stress at the Center of the Front Side of Tube Wall vs. Base Plate Thickness for a Tube Wall Thickness of 3/16”	100
Figure 4.17: Study B Results - Vertical Stress at the Center of the Front Side of the Tube Wall vs. Base Plate Thickness for a Tube Wall Thickness of 1/2”	100
Figure 4.18: Study B Results - Normalized Vertical Stress at the Center of the Front Side of the Tube Wall vs. Base Plate Thickness for a Tube Wall Thickness of 1/2”	101
Figure 4.19: Results for Studies A and B - Maximum Vertical Tube Wall Stress at the Center of the Front Side vs. Base Plate Thickness for Tube Wall Thicknesses of 3/16” and 1/2”	101
Figure 4.20: Results of Studies A and B - Normalized Maximum Vertical Tube Wall Stress at the Center of the Front Side vs. Base Plate Thickness for Tube Wall Thicknesses of 3/16” and 1/2”	102
Figure 4.21: Study A Results - Comparison Between Stress Locations.....	102
Figure 4.22: Radial Plot of Outer Vertical Stress for Cases 1 and 6	103
Figure 4.23: Results of Study C - Vertical Tube Wall Stress Along the Fold With A Base Plate Thickness of 1.25” vs. Tube Wall Thickness	104
Figure 4.24: Results of Study C - Normalized Vertical Tube Wall Stress Along the Fold With a Base Plate Thickness of 1.25” vs. Tube Wall Thickness	104
Figure 4.25: Results of Study C - Vertical Tube Wall Stress Along the Center of the Front Side With a Base Plate Thickness of 1.25” vs. Tube Wall Thickness	105
Figure 4.26: Results of Study C - Normalized Vertical Tube Wall Stress Along the Center of the Front Side With a Base Plate Thickness of 1.25” vs. Tube Wall Thickness	105
Figure 4.27: Radial Plot of Outer Vertical Stresses for Cases 1 and 13	106

Figure 4.28: Normalized Radial Plot of Outer Vertical Stresses for Cases 1 and 13.....	107
Figure 4.29: Results of Studies D and E – Normalized Vertical Tube Wall Stresses at the Fold vs. Number of Anchor Rods for Base Plate Thicknesses of 1.25” and 3.0”	108
Figure 4.30: Results of Studies D and E – Normalized Vertical Tube Wall Stresses at the Center of the Front Side vs. Number of Anchor Rods for Base Plate Thicknesses of 1.25” and 3.0”	109
Figure A.1: Case 2 – Stress Profile Along Fold	115
Figure A.2: Case 2 – Stress Profile Along Center of Front Side.....	116
Figure A.3: Case 3 – Stress Profile Along Fold	116
Figure A.4: Case 3 – Stress Profile Along Center of Front Side.....	117
Figure A.5: Case 4 – Stress Profile Along Fold	117
Figure A.6: Case 4 – Stress Profile Along Center of Front Side.....	118
Figure A.7: Case 5 – Stress Profile Along Fold	118
Figure A.8: Case 5 – Stress Profile Along Center of Front Side.....	119
Figure A.9: Case 6 – Stress Profile Along Fold	119
Figure A.10: Case 6 – Stress Profile Along Center of Front Side.....	120
Figure A.11: Case 7 – Stress Profile Along Fold	120
Figure A.12: Case 7 – Stress Profile Along Center of Front Side.....	121
Figure A.13: Case 8 – Stress Profile Along Fold	121
Figure A.14: Case 8 – Stress Profile Along Center of Front Side.....	122
Figure A.15: Case 9 – Stress Profile Along Fold	122
Figure A.16: Case 9 – Stress Profile Along Center of Front Side.....	123
Figure A.17: Case 10 – Stress Profile Along Fold	123
Figure A.18: Case 10 – Stress Profile Along Center of Front Side.....	124
Figure A.19: Case 11 – Stress Profile Along Fold	124
Figure A.20: Case 11 – Stress Profile Along Center of Front Side.....	125
Figure A.21: Case 12 – Stress Profile Along Fold	125
Figure A.22: Case 12 – Stress Profile Along Center of Front Side.....	126
Figure A.23: Case 13 – Stress Profile Along Fold	126

Figure A.24: Case 13 – Stress Profile Along Center of Front Side.....	127
Figure A.25: Case 14 – Stress Profile Along Fold	127
Figure A.26: Case 14 – Stress Profile Along Center of Front Side.....	128
Figure A.27: Case 15 – Stress Profile Along Fold	128
Figure A.28: Case 15 – Stress Profile Along Center of Front Side.....	129
Figure A.29: Case 16 – Stress Profile Along Fold	129
Figure A.30: Case 16 – Stress Profile Along Center of Front Side.....	130
Figure A.31: Case 17 – Stress Profile Along Fold	130
Figure A.32: Case 17 – Stress Profile Along Center of Front Side.....	131
Figure A.33: Case 18 – Stress Profile Along Fold	131
Figure A.34: Case 18 – Stress Profile Along Center of Front Side.....	132

Abstract

Recent failures of high-mast lighting towers and other cantilevered sign, signal, and support structures have increased awareness of the fatigue problems associated with these structures. Field investigations and extensive finite element studies performed at Lehigh University determined that the flexibility of the baseplate of a cantilevered sign structure has a drastic effect on the stress behavior in the tube wall near the welded connection [Hall, 2005].

This study investigates the effect of base connection geometry on the baseplate flexibility and fatigue performance of multi-sided high-mast lighting towers. The results of a field investigation of the dynamic properties associated with high-mast towers are discussed, followed by the results of a finite element analysis, construction techniques, assumptions, and parametric studies. The field investigation study found that the geometric properties of high-mast lighting towers have little effect on the dynamic characteristics. The parametric study found that the baseplate thickness has the most significant effect on the localized stress distribution in the tube wall. Increasing the baseplate thickness of the tower provides significant improvement to the fatigue life of the towers by reducing the maximum stresses at the baseplate-to-tube wall connection, with minimal economic impacts.

Chapter 1 Introduction

1.1 Background

This study investigates the effect of base plate connection geometry on the fatigue performance of welded socket connections in multi-sided high-mast lighting towers. High-mast lighting towers, as shown in Figure 1.1, are tall, single tube structures that support luminary fixtures used to illuminate large outdoor areas. The towers are adaptable to two types of luminary systems: systems with lowering devices and fixed mounted configurations. Although typically 80 to 150 feet tall, these segmental structures, often constructed with three or four sections, can reach heights up to 200 feet.

There are many different uses for high-mast lighting towers. They typically provide light for major highway interchanges, but can also be used to illuminate airports, parking lots, sports complexes, and industrial yards. The concept of using lighting to illuminate a street was first recorded in London in the 1400's, but has probably been around much longer. High-mast lighting towers were first developed in the 1960's after the authorization of the Federal Aid-Highway Act of 1956. The creation of the interstate system led to multi-level road intersections and a need for taller lighting structures. One benefit of using high-mast towers is that the number of individual street lights (i.e., poles) required to illuminate a given area can be drastically decreased. Additionally, as the height of a high-mast tower increases, the area that it is capable of illuminating increases. For this reason, and for monetary

reasons, the number of towers at an intersection is often decreased and the height of the structures is increased.

High-mast lighting towers are interesting structures. They are not necessary to the flow of traffic at an intersection, however they do increase visibility during the night as well as decrease the number of visibility related accidents [FHWA, 2003]. Furthermore, since fewer of them are required at an interchange, there is less likelihood of vehicular impact. Unfortunately, since there is no redundancy built into these structures, a failure could be very hazardous if a tower were to fall across multiple lanes of traffic on a highway or on property adjacent to the structure.

1.2 High-mast Lighting Tower Features

High-mast lighting towers have several important features; the weld, the hand access hole, the anchor rod and nut system, the winch plate, and the lighting system. Several types of welds are used for high-mast lighting towers, including a socket welded connection and a complete joint penetration welded (CJP) connection. The scope of this project does not include an investigation into the differences between the two types of connections and focuses only on the socket connection. The purpose of the socket weld connection is to connect the tube to the base plate. A hole or polygon (depending on the shape of the tube) is cut from the base plate large enough for the tube to fit snug inside. The tube is then welded to the base plate at two locations. This connection is typically an unequal leg fillet weld connecting the tube to the top of the base plate and a fillet weld connecting the bottom of the tube to the inside of the base plate cut out. Both types of welds are shown in Figure 1.2.

The top weld serves as a structural connection and the bottom weld serves to prevent moisture and debris from entering the tiny gap between the tube and the base plate. Moisture between the tube and base plate can create a corrosive environment that would lead to a fast deterioration of the welded connection. Previous experimental studies have shown that the socket welded connection of cantilevered sign, signal and light structures is highly susceptible to fatigue. Complete joint penetration welds (CJP) have also been used, however the fatigue strength is not necessarily improved by that much due to other factors that influence the fatigue resistance of this detail.

The hand access hole, as shown in Figure 1.3, is a reinforced hole at the base of the tower. A hole is cut from the tube wall and plates are welded perpendicular to the tube wall for reinforcement. The hand access hole provides easy access to the luminary lowering system and the electric wiring. This is another detail that is susceptible to fatigue cracking. A hand hole cover plate is included to protect the interior of the tower from debris, weather, and vandalism.

A typical high-mast tower is bolted to a concrete foundation for support as shown in Figure 1.4. The size, grade of steel, number, and configuration of the bolts depends upon the size and shape of the tower. A typical foundation may extend several feet (20 to 30 feet) below the ground surface, and depending upon the geological conditions of the area, could be supported by piles, drilled shafts, or spread footings. The anchor rods extend most of the length of the concrete foundation to ensure that there is sufficient anchorage into the concrete. Two nuts, an upper nut, also called a locking nut, and a lower nut, also called a leveling nut, are used to attach each anchor rod to the base plate. The bottom nut, as its name implies,

serves as a leveling nut and the upper nut acts to tighten the system. A typical anchor rod and nut system is shown in Figures 1.3 and 1.4. The anchor rod system is the only connection between the tower and the concrete foundation. The locking and leveling nuts are of particular importance because the nuts are the only way to transfer load from the base plate to the anchor rods. It is essential to have properly tightened nuts in order to avoid unequally distributed loads, which ultimately lead to uneven distribution of the tube wall stresses and overstressing of the tight anchor rods. Interestingly, loose leveling and anchor nuts are very common and are believed to have contributed to cracking in some structures.

The winch plate, Figure 1.5, is welded to the inside of the tower tube wall 180 degrees from the hand access hole. The winch plate has no structural significance and is only used to attach the luminary lowering divide to the inside of the tower. Of importance are the two longitudinal welds that attach the winch plate to the inside of the high-mast tower. This detail represents a longitudinal attachment which has the potential to develop fatigue cracks which could propagate through the tube wall. The lowering system is a network of cables and pulleys that raise and lower the luminaries for maintenance and cleaning. Several types of lighting systems in use today are the pulley system, the "in tension" hoisting system, and the single or double drum winch system. The towers are capable of supporting single and multiple light fixtures (typically 8 lights). See Figure 1.6 for pictures of luminaries attached to a high-mast tower.

1.3 Wind Loading

Across-wind and along-wind movements of high-mast lighting structures are typically caused by two types of wind phenomena: vortex shedding and natural wind gusts, respectively. These two wind phenomena have the potential to produce vibrations that may cause fatigue damage. To design for this type of fatigue damage, both types of wind loading are factored into the AASHTO design requirements for high-mast towers. Preventative measures may also be taken in the design stage or after installation.

1.3.1 Vortex Shedding

Vortex shedding is an aerodynamic phenomenon caused by the separation of an along-wind flow around an object, typically a smooth cylinder, and is Reynolds number dependent. At Reynolds numbers in the range of $30 < Re < 5000$ alternating vortices are shed from the backside of the cylinder and form a trail known as the von Karman Vortex Street, shown in Figure 1.7. The vortices create across-wind deflections due to an increase in static pressure on one side of the structure and a decrease on the other, such that an across-wind force acts on the structure. Alternating vortices produces alternating forces. The vortices have a primary frequency (or vortex shedding frequency) of N_s , according to the Strouhal relation:

$$S = \frac{N_s D}{U}$$

Where D is the diameter of the structure or cross-wise dimension, and U is the wind velocity. The Strouhal number, S , is dimensionless and depends on the shape of the cross-section and the Reynolds number of the flow. In the AASHTO

Specifications [AASHTO, 2001] a value of 0.18 is used for circular towers and a value of 0.15 is used for multi-sided towers.

As the frequency of the vortices approaches the natural frequency of the structure, a condition referred to as “lock-in” occurs. The frequency of the vortices no longer follows the Strouhal relation, but is constant over a range of wind speeds, as shown in Figure 1.8. The vibrations are more stable and are not as susceptible to changes in wind speeds within the “lock-in” range. When the wind speeds become large enough, turbulence caused by the across-wind deflections will disrupt the regularity of the vortices and diminish the “lock-in effect. The typical range of wind speed in which vortex shedding occurs in high-mast lighting towers is 3 to 10 mph. It is noted that during the field instrumentation portion of this project, vortex shedding was observed to occur in the range of these wind speeds for the towers monitored.

1.3.2 Natural Wind Gusts

Natural wind gusts are the most basic type of wind phenomena that can cause vibration of a high-mast lighting tower. The speed and the direction of the wind gusts are highly variable and random, as are the displacements that occur due to the fluctuating applied pressure. The accumulation of vibrations during the life of a high-mast tower may cause fatigue cracking. Often times the vibration caused by minor wind gusts will not contribute to the fatigue damage of the structure. Larger wind gusts, however, may contribute a significant number of damaging wind cycles in a single storm event. Structures that are in large open areas, such as those in the

state of Iowa, are exposed to larger natural wind gusts, and may accumulate many more cycles in a storm event than a structure located in a more densely populated area.

Unlike vortex shedding, natural wind gusts can simultaneously excite several modal frequencies. The deflection shapes of a high-mast tower in the first four fundamental modes are shown in Figure 1.9. It should be noted that the deflection shapes do not vary much among towers. Of importance is that the higher modes of vibration may not necessarily have the same damping ratio as the first mode of vibration, in fact they are usually lower. The damping ratios of higher modes of vibration will be discussed in Chapter 2. The flexibility of the towers coupled with low damping ratios contributes significantly to the accumulation of high stress-range cycles.

1.3.3 Mitigation

The various problems related to wind induced fatigue damage observed in high-mast sign structures can be mitigated in several different ways. The first method is to alter the geometric properties of the towers before and after installation. The second method is to reduce the movement of the towers by adding aerodynamic devices that disrupt the vortex streets and the third method is to use mechanical devices to reduce the vibration of the towers. This research focuses on the first method of mitigation, however a brief discussion of all three methods of mitigation are in the following paragraphs.

The easiest way to mitigate deflections of high-mast towers is to increase the stiffness of the structure. By increasing the base plate and/or tube wall thickness in the design stage the tower can be stiffened effectively reducing the possibility of cracking at the base plate-to-column connection by simply lowering the stress range. The area around the hand access hole is another critical region and can be reinforced or detailed differently to reduce cracking. Figure 1.10 is an example of distributing the stress around the hand access hole by increasing the thickness of the tube wall in that region. This retrofit example has been implemented in the state of Iowa. Although modifying the geometric properties of the towers may be the easiest solution, it can be expensive when used as a retrofit option.

High-mast towers can also be stiffened in-situ, as shown in Figure 1.11. This example of altering the geometric properties, called a splice retrofit, was designed by Wiss, Janney, Elstner Associates, Inc, for several towers in Clear Lake, Iowa. The splice retrofit fits like a glove around the tower and is bolted to the tower to ensure the distribution of load to the retrofit. This retrofit was an inexpensive solution to an immediate problem.

The second method of mitigation involves aerodynamic damping devices installed near the top of towers to disrupt the generation and regularity of the vortex streets. The most common aerodynamic damping method is the helical strake system. It has been determined that the most effective strake system has three evenly spaced rectangular strakes wrapped spirally down the tower at a pitch of one revolution in five diameters. The strakes need to have a radial height of 0.10 diameter (0.13 diameter for lightly damped structures). The most effective strakes

cover approximately 33 to 40% of the top portion of the tower [Simiu, 1996]. However, this approach may be in conflict with the traveler that slides down the pole to access the light bulbs.

Shrouds, spoilers, and slats are other types of aerodynamic devices used to mitigate the vibrations of cantilevered structures. Aerodynamic damping devices, although effective, must be designed with care to prevent the vortex streets behind the structure from regenerating.

The third method of mitigation uses mechanical dampers in structures to absorb some of the energy applied to a structure, due to wind or earthquake loadings. Ball-and-chain dampers and Dogbone dampers are several types of dampers that have been installed in high-mast towers. Ball-and-chain dampers consist of a metal ball attached to a chain that hangs inside the tower. As the tower vibrates, the ball moves around and hits the wall of the tube. This type of mechanical damper is an effective method for mitigating the movement of a high-mast tower [Dexter, et al., 2002]. Dogbone dampers can be installed internally or externally. In order to be effective, mechanical dampers must have a frequency close to the natural vibration frequency of the high-mast tower, usually a frequency associated with a higher mode (that causes double curvature).

1.4 High-mast Lighting Tower Failures

There have been several recent failures of high-mast towers. The failures have raised many questions regarding the design of these structures, especially when they are in service only a couple of years.

One tower of interest is the 140-foot high-mast tower along Interstate 29 in Sioux City, Iowa that cracked at the base connection and collapsed in November of 2003. The collapse prompted an investigation into the cause of failure of the tower. A statewide investigation of all high-mast lighting towers in Iowa was conducted and found that many of the towers in Iowa had cracks and/or loose locking and leveling nuts. Further investigations into the behavior and dynamic characteristics of high-mast lighting towers, to be discussed in Section 1.6 and Chapter 2, began in 2004.

In November 2005, a two year old high-mast lighting tower collapsed in South Dakota. This tower was 150 feet tall and had a 3/8" tube wall thickness and a 1 3/4" base plate thickness. The tower in South Dakota cracked along the tube wall-to-base plate connection and fortunately fell adjacent to the highway. A more recent collapse occurred in Kansas in March of 2006. This tower was also two years old. Unlike the other failures mentioned, fatigue cracking initiated at the top of the hand access hole detail and propagated around the tube wall.

1.5 High-mast Lighting Tower Design

1.5.1 Design Code in the United States

High-mast lighting towers in the United States are designed using the 4th edition of the AASHTO Standard Specifications for Structural Supports for Highway Signs, Luminaries and Traffic Signals [AASHTO, 2001]. Section 11 in the 4th edition of the AASHTO Specifications, titled Fatigue Design, is a result of research conducted for NCHRP report 412, *Fatigue Resistant Design of Cantilevered Signal, Sign and Light Supports* [Kaczinski, et al., 1998]. The fatigue design of these

structures is based on a nominal stress infinite life approach which requires fatigue critical details to be designed so that the nominal stress ranges fall below the constant-amplitude fatigue limit (CAFL). The infinite-life approach is used when the number of cycles at the CAFL of a particular detail is exceeded by the number of cycles that are actually experienced by the structure during its lifetime.

In the AASHTO Specifications, cantilevered structures (including signal, sign, and light supports) are assigned importance factors based upon their location. The more hazardous a structures collapse would be to its surrounding area (which includes highways and property damage), the greater the importance factor. The structures are then designed to resist each type of static equivalent load (relevant to the structure) due to wind and adjusted according to its importance factor. Finally, the modified design stresses must to fall below the required CAFL for the type of fatigue detail used in the design of the structure. The AASHTO Specifications includes a table which lists the most common fatigue details that are used in the design of signal, sign, and light supports.

High-mast lighting towers, in particular, are designed to resist equivalent static pressure ranges due to vortex shedding and natural wind gusts, acting separately. AASHTO only requires non-tapered towers to be designed to resist vortex shedding-induced loads. Towers with tapers less than 0.0117m/m (0.14in/ft) may also be required to resist the same vortex shedding-induced loads. Vortex shedding is not described in detail in the AASHTO Specifications and it only accounts for structures vibrating in the first fundamental mode. However, it has been found that high-mast towers often vibrate in the second and third modes while vortex

shedding [Connor, et al., 2006]. The AASHTO Specifications allow the use of a damping ratio of 0.50% in the calculation of vortex shedding-induced loads when experimentally determined values are unavailable. This given damping ratio may not be valid for structures vibrating in higher modes, as will be discussed in Chapter 2.

Typically, the cantilevered structures are designed based on a yearly mean wind speed of 5 m/s (11.2 mph) for most locations. However, locations exceeding this yearly mean wind speed or with more detailed wind records are designed using a separate equation. The static pressures ranges due to each wind phenomena are applied separately to a static analysis of the structure to determine the stress ranges at critical fatigue details.

1.5.2 Design Code in Canada

The Canadian Highway Bridge Design Code [CAN/CSA-S6-00, 2000] includes a procedure for designing a cantilevered structure susceptible to vortex shedding loads in any mode of vibration. The procedure was originally developed for chimneys and its applicability to high-mast lighting towers has not been verified with experimental tests. A more detailed summary and an example of this procedure can be found in the report presented to the Iowa Department of Transportation [Dexter, 2004]. It should be noted that the value used as a damping ratio when experimentally determined values are unknown is 0.75%, compared to a value of 0.50% in the AASHTO Specifications.

1.6 Related Research

There are three major deficiencies with respect to knowledge about high-mast lighting towers. They are the dynamic behavior of the structure, the fatigue resistance of the base connection, and the response to load. This study investigates the second and the third deficiencies, through the use of finite element modeling. In the last 10 years there has been a greater research focus on the fatigue performance of cantilevered sign, signal, and light structures. There has been a huge focus on the traffic signals supports in particular, but more recently there has been a greater focus on high-mast lighting towers, particularly in light of the recent failures of high-mast towers.

In the late 1970's the first major study of sign structures was performed at Lehigh University for the California Department of Transportation by Dr. John Fisher. The major result of this investigation was that the fatigue strength of the column-to-base plate connection was considerable lower than anticipated [Miki, Fisher, Slutter, 1981]. The study recommended that a Category E' be used for these types of fatigue details. Another result of importance is that fatigue cracking of the sign structures consistently occurred where the toe of the fillet weld meets the tube wall. Although the number and types of specimens tested were limited, the results of the study made it apparent that more research was needed.

The National Cooperative Highway Research Program [NCHRP] Report 412 [Kaczinski, et. al., 1998], was a result of additional failures and problems of cantilever sign structures due to fatigue. The purpose of NCHRP 412 was to develop guidelines for the fatigue design of cantilevered signal, sign and light supports. This

report updated the AASHTO Specifications by developing and evaluating the existing static wind loads due to vortex shedding and galloping [Van Dien, 1995]. The results of this report and the AASHTO Specifications were discussed in further detail in Section 1.5.1. NCHRP Report 469 [Dexter, et. al., 2002] continued the study of cantilevered sign, signal, and light supports. This report provided further recommendations to the AASHTO Specifications as well as many detailed design examples. One example was the design of a high-mast lighting tower.

The University of Texas at Austin conducted an extensive study of the fatigue characteristics of traffic signal mast arms as presented in Mark Koenigs Masters' Thesis in 2003 [Koenigs, 2003]. The results of this study showed that fatigue cracks always form at the toe of long leg of the fillet weld on the tube wall, as was previously suggested by J. Fisher. More recently, an investigation of the effects of base plate flexibility on the stress behavior of traffic signals was conducted at Lehigh University and presented in John Hall's Masters' Thesis [Hall, 2005]. Several experimental tests and an extensive finite element analysis were performed. The primary results of the study are that the base plate flexibility has a drastic influence on the stress behavior in the tube wall adjacent to the socket connection. It was determined that the geometric parameter that has the largest effect on the stresses is the base plate thickness. This investigation paved the way for this high-mast tower study. Modeling issues, such as stand-off lengths, weld profiles, and leveling nut contact provided answers to many of the uncertainties involved with modeling cantilevered structures.

Recent collapses and fatigue cracking of high-mast towers has expanded the focus of cantilevered structures that are studied to include high-mast towers. In 2003, a high-mast tower collapse in Sioux City, Iowa prompted an investigation of the cause of cracking performed by Robert Dexter for the Iowa Department of Transportation [Dexter, 2004]. This study also included the development of a retrofit procedure and an assessment of the remaining towers in Iowa. One result of this study was a set of recommendations for future design. The recommendations suggested that tube wall and base plate thicknesses should be 3/8" and 3.0", respectively. The researchers also suggested that the designer consider using round towers instead of polygonal towers. This investigation of the Iowa failure prompted additional investigations of high-mast lighting towers. The most recent study has focused on the dynamic characteristics of high-mast towers. This study was carried out for the Iowa Department of Transportation by Lehigh University in 2004 to 2005. An additional investigation focused on collecting long-term stress and wind data at two towers in use in Iowa. Chapter 2 provides a brief summary of this recent field study conducted by Lehigh University. Further information can be found in a report to be presented to the Iowa Department of Transportation this year.

Several new projects investigating the fatigue resistance of cantilevered sign, signal, and light structures are underway. Both studies are focused on the second deficiency of cantilevered structures; the fatigue resistance of the connection details. The first study is a pooled fund study lead by The University of Texas at Austin. Some of the objectives of the study include determining changes to current details that would improve the fatigue life of the structures, formulating a relationship

between the detail changes and the fatigue life, and providing a design guide and recommendations to the AASHTO Specifications for improved future designs. The second study is NCHRP Project 10-70 and is being conducted by Lehigh University. This research study is only in the beginning stages, but its objectives include establishing a fatigue stress category for existing, retrofitted, and new connection details and developing revisions to the 4th edition of the AASHTO Specifications.

1.7 Scope

The recent high-mast lighting failures described in Section 1.4, coupled with the limited knowledge of these structures provided the motivation for this research project. The objectives of this study were to evaluate the effect of base connection geometry on the base plate flexibility of multi-sided high-mast lighting towers.

Finite element parametric studies were conducted to investigate the influence of base plate thickness, tube wall thickness, and the number of anchor rods on the tube wall stresses. Two different models were used as the basis of the base plate thickness study, each with a different tube wall thickness. By varying the base plate of two different models, the effect of tube wall thickness can also be seen. Another parametric study varied the tube wall thickness of a model to determine its effect on the tube wall stress. The last parametric study performed looked at the effect of the number of anchor rods used to attach the tower to the foundation. Several modeling assumptions were also investigated.

A brief summary of the experimental field testing conducted in Iowa is in Chapter 2. A detailed explanation of the modeling assumptions and the modeling

procedure used to construct the first finite element model, called the BASE model, are in Chapter 3. A description of the parametric study that investigated base plate thickness, tube wall thickness, and the number of anchor rods is in Chapter 4. Chapter 4 also presents the results of the parametric study. The final chapter, Chapter 5, presents the conclusions for this study and recommendations for further research and design practice.

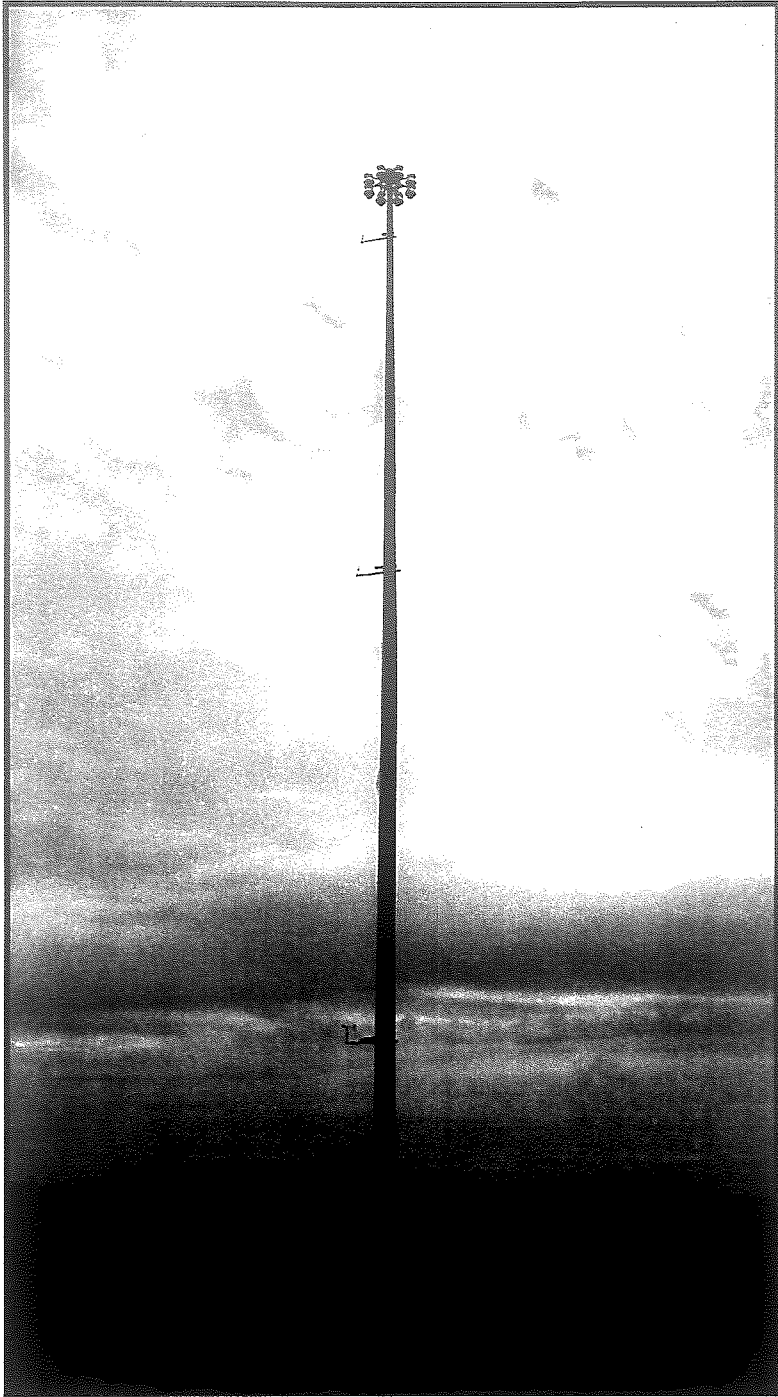


Figure 1.1: Typical High-Mast Lighting Tower

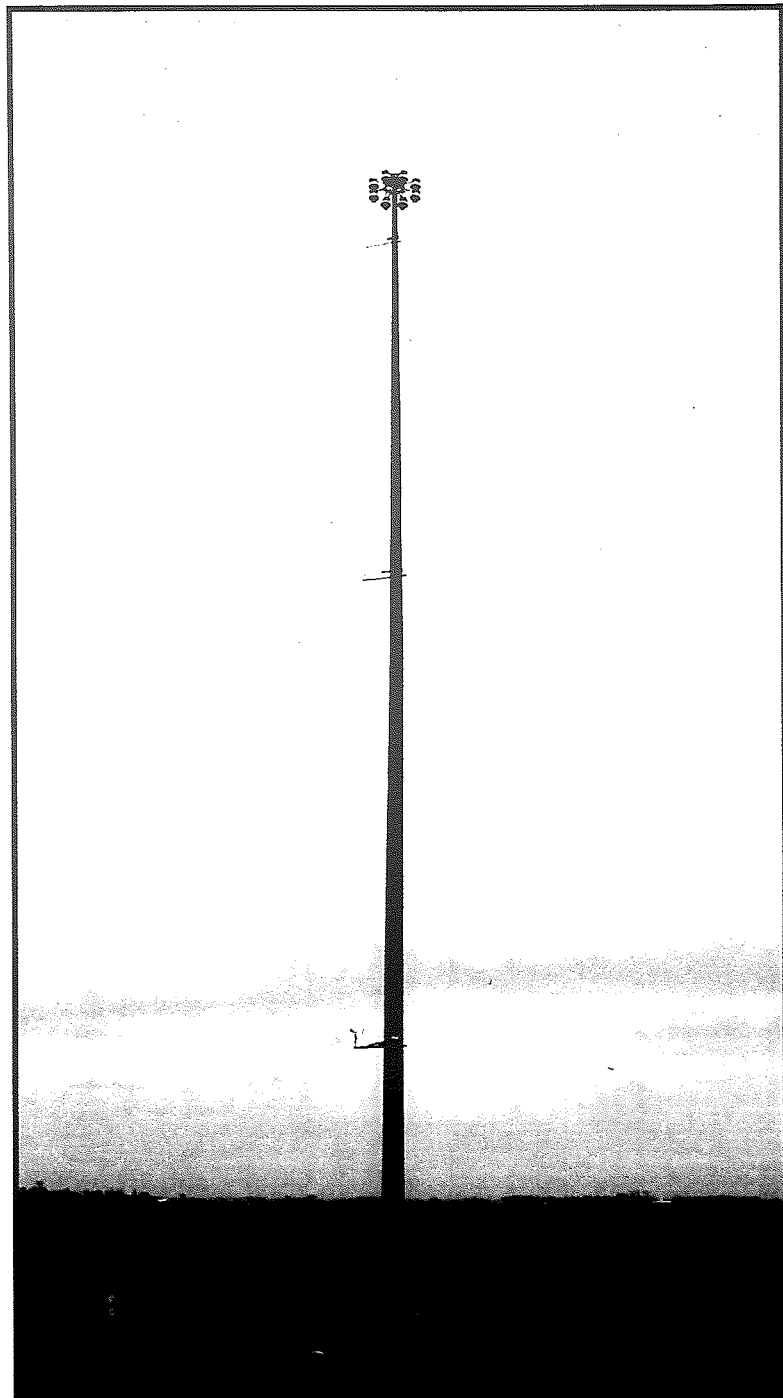


Figure 1.1: Typical High-Mast Lighting Tower

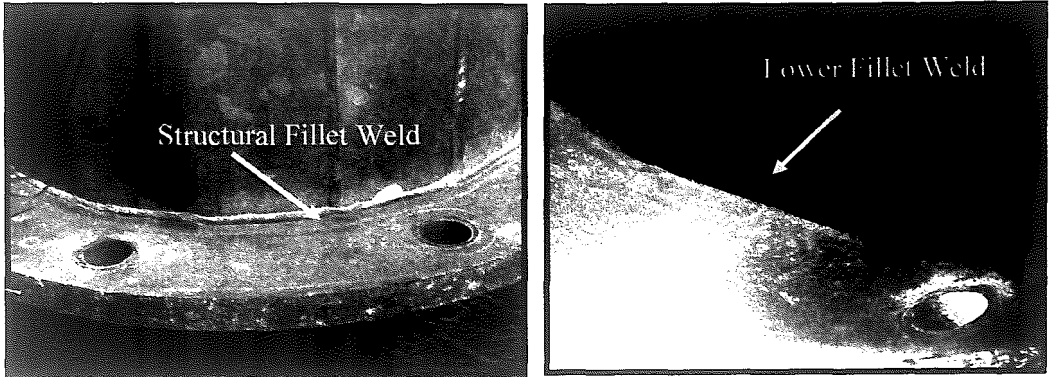


Figure 1.2: Socket Fillet Welds: Structural and Lower

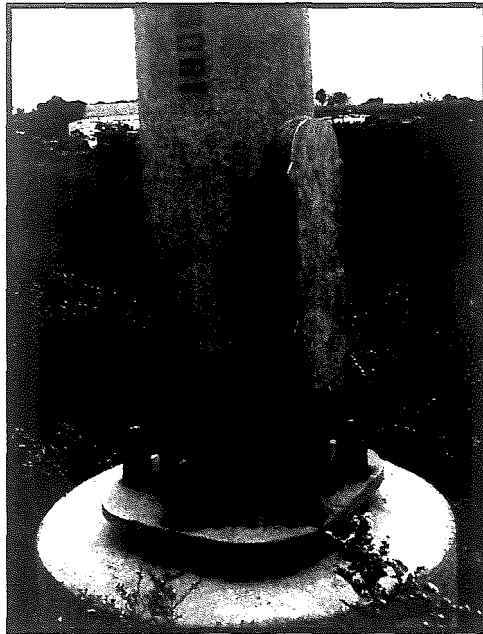


Figure 1.3: Hand Access Hole Detail

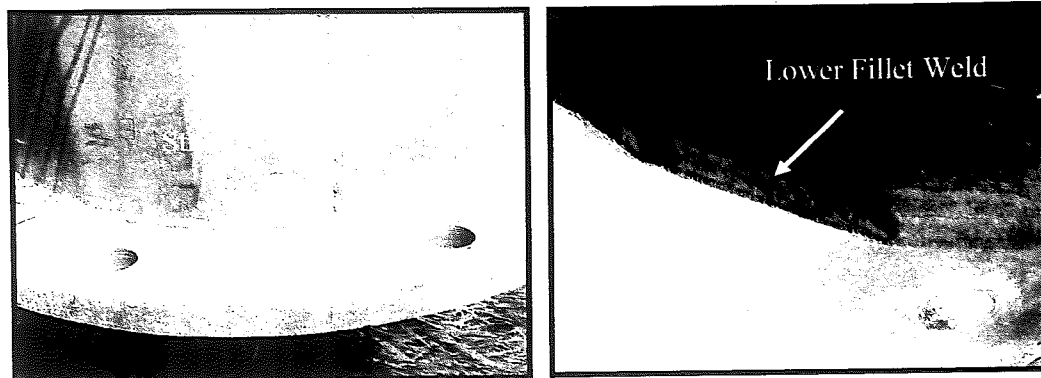


Figure 1.2: Socket Fillet Welds: Structural and Lower

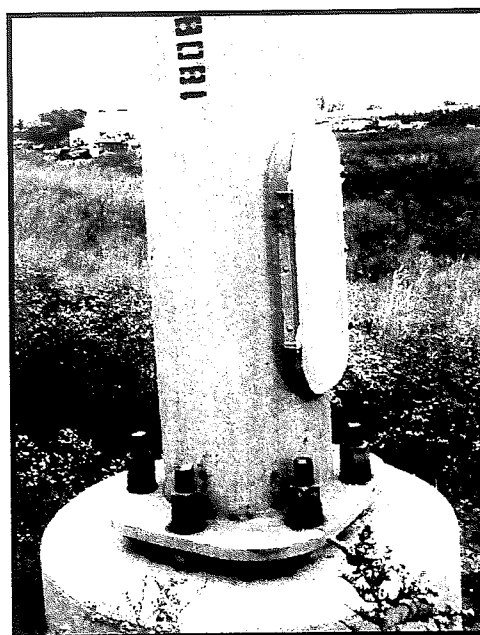


Figure 1.3: Hand Access Hole Detail



Figure 1.4: Concrete Foundation and Anchor Rod and Leveling Nut System



Figure 1.5: Winch Plate

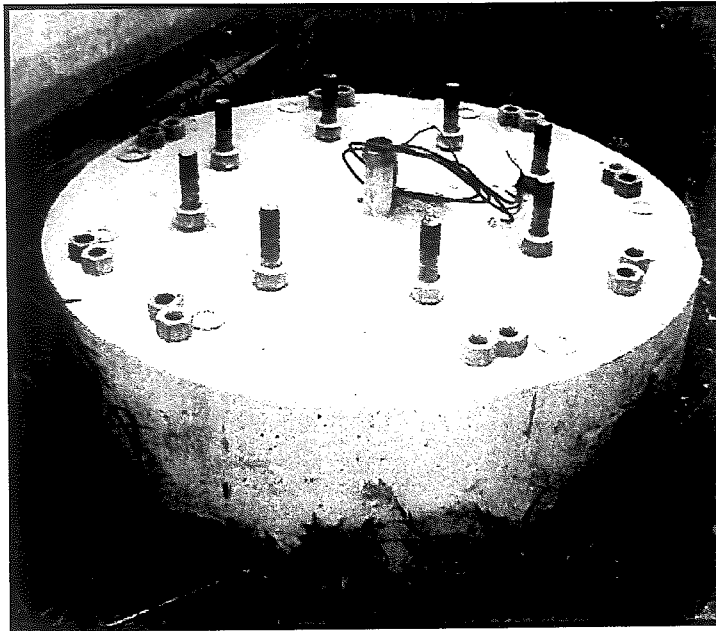


Figure 1.4: Concrete Foundation and Anchor Rod and Leveling Nut System

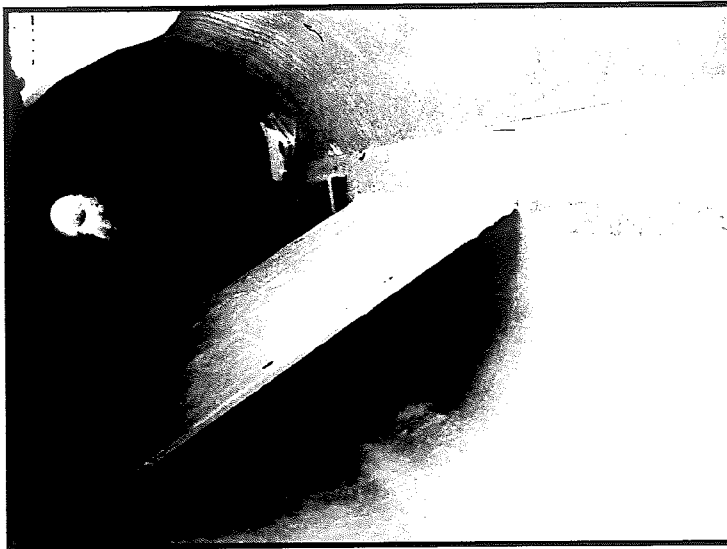
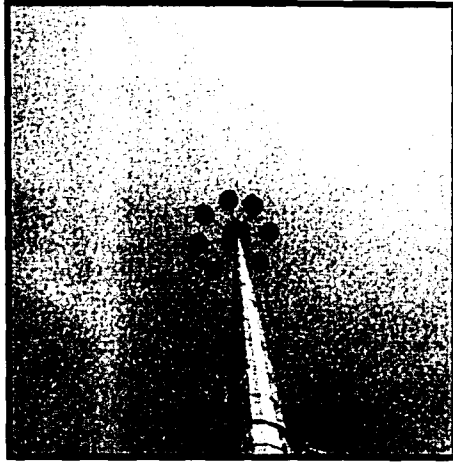


Figure 1.5: Winch Plate



(a)



(b)

Figure 1.6: Luminary System: (a) Luminary Installed on Top of Tower, (b) Luminary System Lying on Ground Before Tower Erection

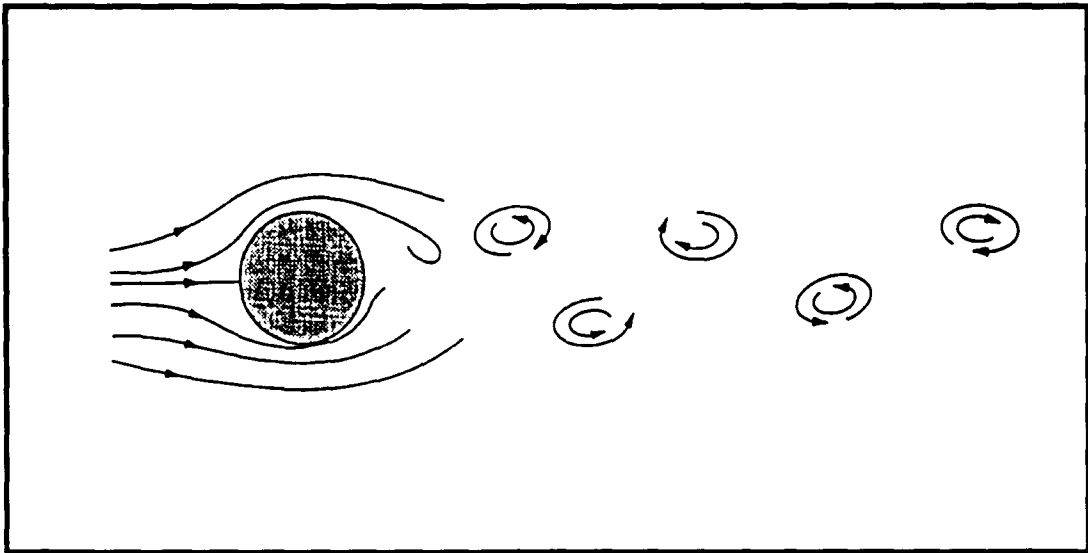
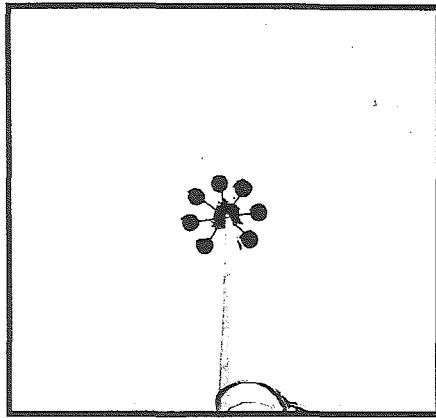
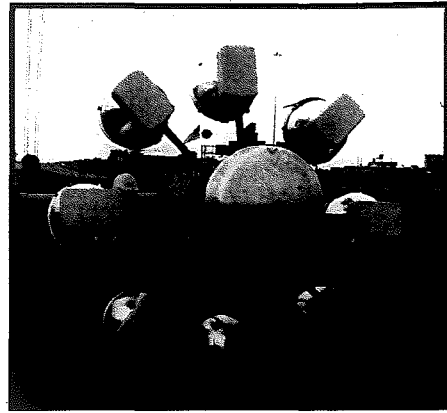


Figure 1.7: von Karman Vortex Street in the Wake of a Circular Cylinder
Source: Van Dien, 1995



(a)



(b)

Figure 1.6: Luminary System: (a) Luminary Installed on Top of Tower, (b) Luminary System Lying on Ground Before Tower Erection

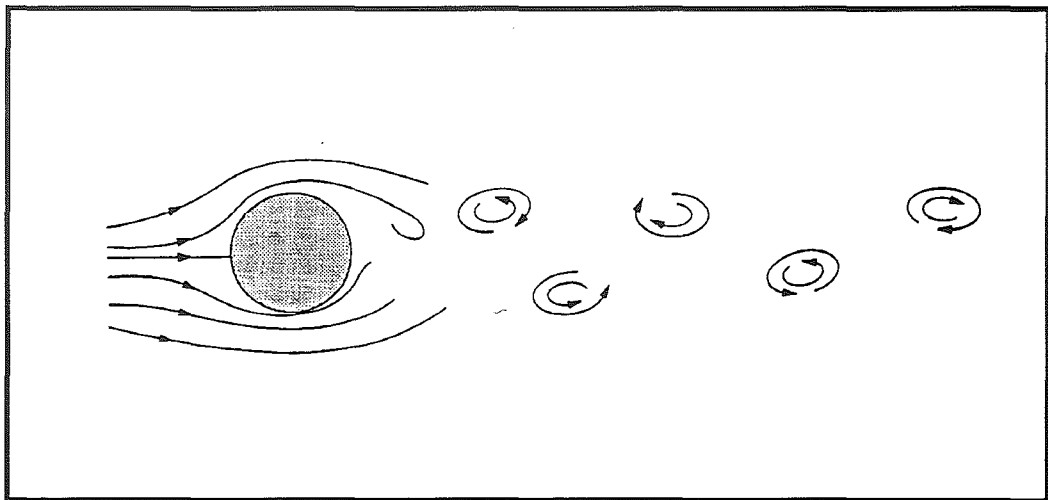


Figure 1.7: von Karman Vortex Street in the Wake of a Circular Cylinder
Source: Van Dien, 1995

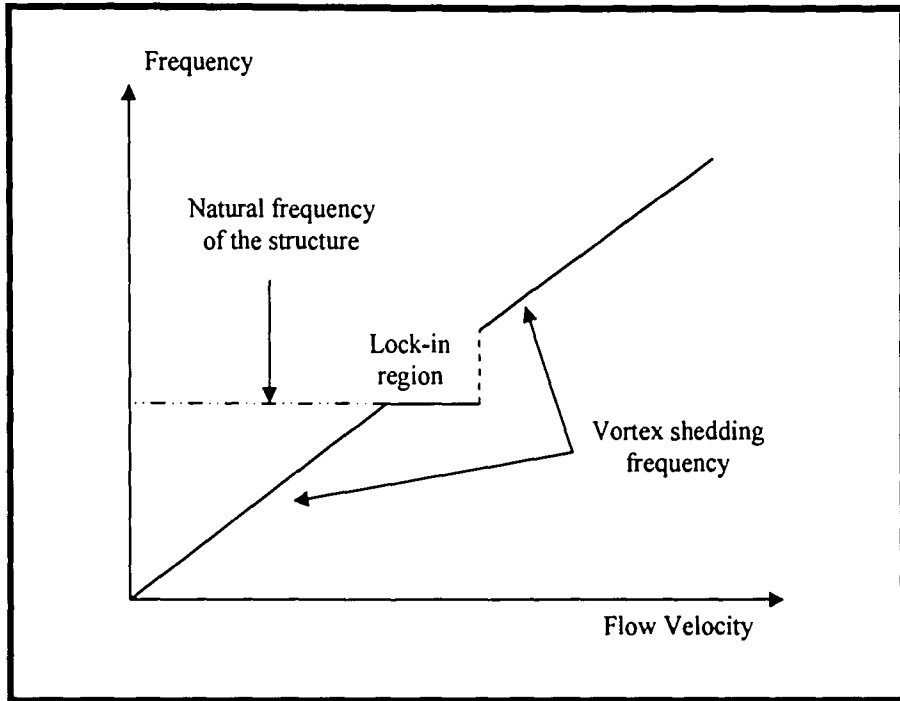


Figure 1.8 – “Lock-in” phenomenon

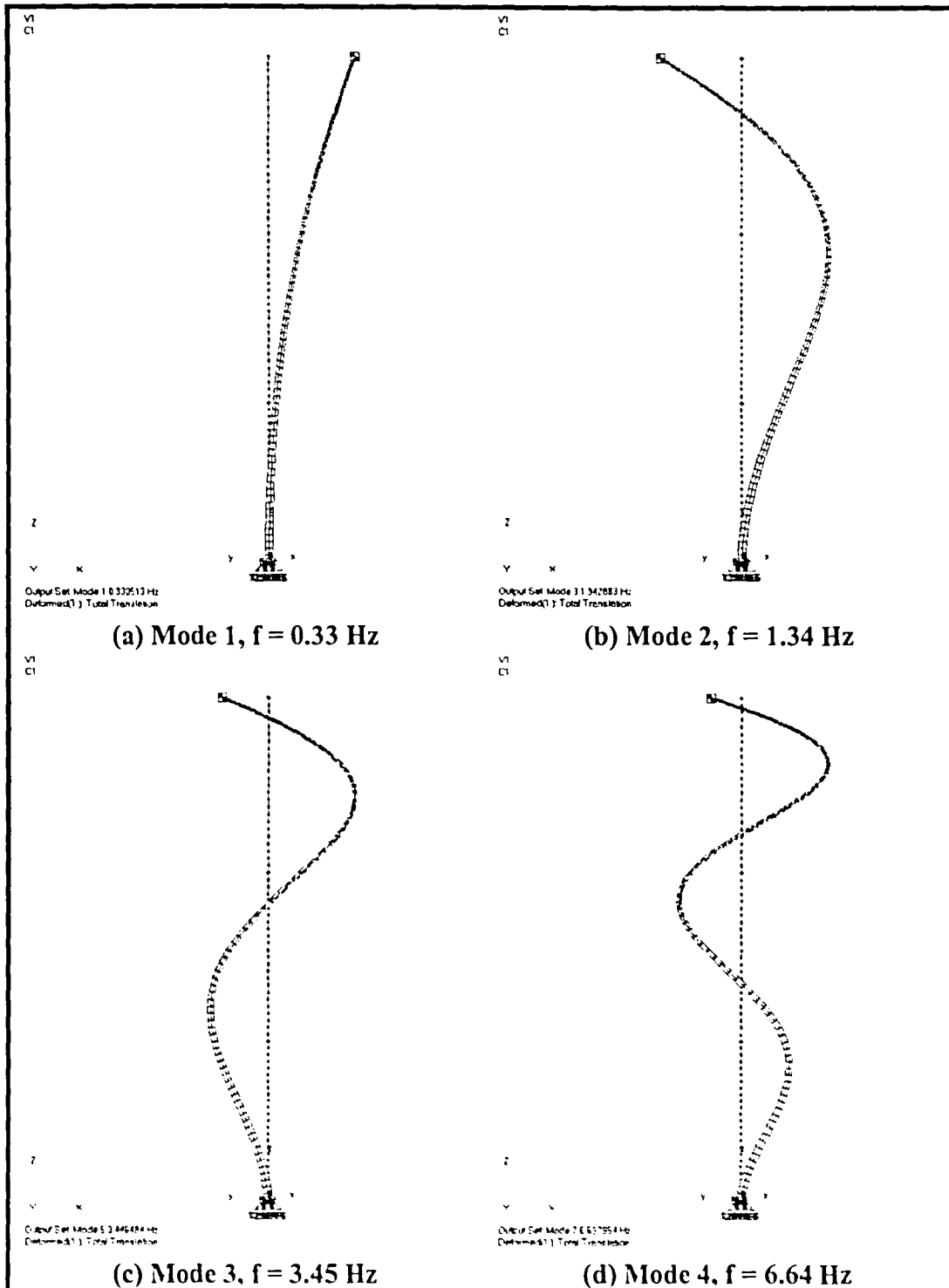


Figure 1.9: Mode shapes and frequencies for the lowest four modes of the As-built tower along I-35 in Clear Lake, as determined using ABAQUS [Connor, et al., 2006]



Figure 1.10 Sioux City, Iowa Retrofit to Stiffen the High-mast Lighting Tower



Figure 1.11 – Splice Retrofit Designed by Wiss, Janney, Elstner Associates, Inc. and Installed in Clear Lake, Iowa

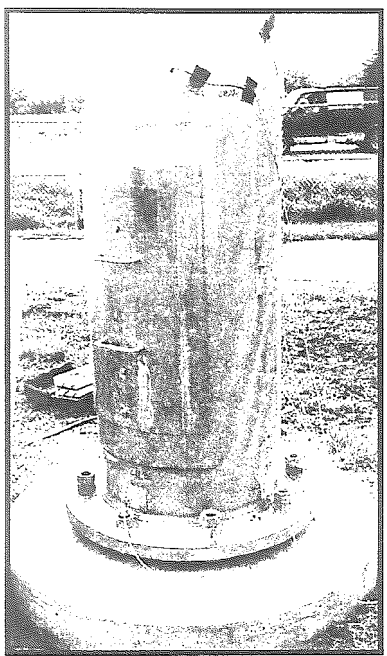


Figure 1.10 Sioux City, Iowa Retrofit to Stiffen the High-mast Lighting Tower

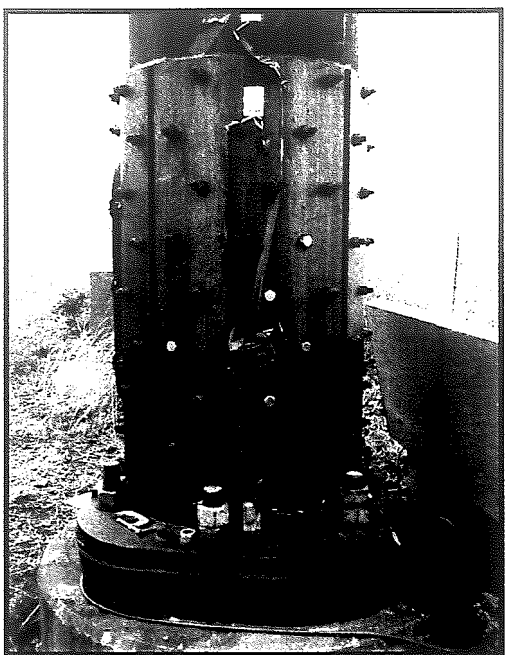


Figure 1.11 – Splice Retrofit Designed by Wiss, Janney, Elstner Associates, Inc. and Installed in Clear Lake, Iowa

Chapter 2 Experimental Field Testing

2.1 Introduction

On November 12, 2003 a 140-foot high-mast tower along Interstate 29 in Sioux City, Iowa collapsed. The wind speed at the time of the collapse was reported as 37 mph, and the maximum wind speed earlier in the day was 56 mph. Extensive work regarding the cause of the failure was carried out by the late Robert Dexter of the University of Minnesota and sub-consultants, and the results are presented in detail in a report prepared for the Iowa DOT in September 2004 [Dexter, 2004].

The collapse of the tower in Sioux City prompted a statewide investigation of all the high-mast lighting towers in Iowa. Of the 233 towers inspected, 17 galvanized high-mast towers similar to the collapsed tower, and 3 weathering steel high-mast towers near Clear Lake, Iowa had cracks. All of the cracked towers have been removed or repaired. (Cracks were recently found at the base plate connection in two other towers in November 2005 and April 2006.) The base sections of the towers in Sioux City were replaced with a retrofitted base as previously shown in Figure 1.10 and a splice retrofit, as shown in Figure 1.11, was installed on the towers near Clear Lake. Additionally, loose locking and leveling nuts were discovered at 32 towers during the investigation and a statewide retightening program was implemented.

The cracking of high-mast towers in Clear Lake, Iowa and the collapse of the tower in Sioux City, Iowa prompted further investigation into the behavior and

dynamic characteristics of the high-mast lighting towers. This chapter presents a brief overview of the experimental study of 13 high-mast lighting towers performed by Lehigh University in the state of Iowa. Further detail regarding the experimental testing can be found in the report prepared by R.J. Connor and I.C. Hodgson for the Iowa DOT [Connor, et al., 2006].

The experimental field testing conducted by Lehigh University was completed in two different phases. The first phase of this study focused on the dynamic characteristics of ten high-mast towers in the Clear Lake area. The second phase of the investigation focused on the differences in the dynamic and static behavior between the original tower, similar to the one that collapsed, and the retrofitted tower in Sioux City, Iowa.

2.2 Phase 1

During Phase 1 of the experimental study, ten high-mast towers were instrumented to various degrees and tested, as listed in Table 2.1. The towers were located at five interchanges in Clear Lake, Ames, and Des Moines, Iowa. Two towers at each interchange were tested to assess the repeatability of tests performed on identical towers. High-mast towers of varying characteristics (galvanized and weathering), geometry (height, material thickness, anchor rod pattern, etc.), and age were tested.

All ten high-mast towers were dynamically load tested by “plucking” the tower in order to obtain the vibration characteristics of the pole. Of the ten towers

tested, two were instrumented to obtain stress distributions at various details, and were included in a 12-month long-term monitoring study to obtain information regarding the response of the towers under natural wind loading. Wind speed and direction was also continuously monitored during the long-term study.

2.3 Phase 2

During Phase 2, three towers were instrumented and tested, as listed in Table 2.2. Two of the towers were located at Exit 147B of I-29 in Sioux City, Iowa. These towers were instrumented and tested to obtain their dynamic characteristics and the magnitude of stresses at critical details. The first tower, termed “As-built”, is identical to the tower that collapsed in 2003, with a 1 ¼” base plate thickness and a 3/16” tube wall thickness. The tower had previously been removed, but was re-erected specifically for this field testing. The second tower, termed “Retrofit”, is the retrofitted tower that has a new base section (36 ft. high) with a revised access hole detail, a 3” base plate thickness, and a 5/8 inch tube wall thickness. Photographs of the As-built and Retrofit towers are shown in Figure 2.1. The purpose of these tests is to compare the dynamic characteristics and the magnitude of stresses in the tube walls of the as-built and retrofit towers.

A third tower, called “Hamilton”, is located at the Hamilton Road exit of I-29. This tower was a 140-foot weathering steel tower with 12 sides (see Table 2.2). It was also dynamically load tested. The purpose of this test was to compare the dynamic characteristics of the Hamilton tower to the characteristics of the towers

from Phase 1. Only accelerometers were installed and stresses were not measured at this tower.

2.4 Test Setup

The setup for the pluck tests during both testing phases was exactly the same. One end of a steel cable was attached to a strap that was wrapped around the tower 35 feet above the base plate. The other end of the cable was attached to a fixed object in the area, such as a concrete column or the ATLSS field vehicle. Figure 2.2 shows the field testing setup. The high-mast tower was statically loaded by tightening the steel cable with a pulling device, also called a “come-along”. The load applied to the tower was monitored by a load cell which was connected in-line with the steel cable. Once the desired load was reached, the tower was quickly released or “plucked”. The quick release was achieved using a quick-release hook, which when opened, the tower vibrated freely. Plucking the tower produced a free decay vibration that was used to extract the dynamic characteristics of the tower. Ambient vibration data, from which the dynamic characteristics can also be extracted, were also recorded for 15 to 30 minutes at each of the towers.

Uniaxial accelerometers were placed on each tower for the pluck tests. The accelerometers were temporarily mounted to the tower at a height of approximately 35 feet from the top of the base plate. Strain gages were also placed at predetermined locations as for the As-built and Retrofit towers to collect stress data during the static and dynamic loading of the towers.

2.5 Field Test Results

2.5.1 Natural Frequencies

The natural frequencies of the first four modes for each high-mast tower were extracted from the raw data obtained during the Phases 1 and 2 pluck tests. The raw data collected are time-domain signals composed of many sinusoidal components. Using the fast Fourier transform (FFT), a mathematical algorithm, the raw data were transformed into a frequency domain signal, from which the natural frequencies of the first four modes for each tower was determined. In general, the natural frequencies of the first four modes for each tower fell within the same range. They are also in agreement with values determined by previous finite element analyses. The first four modal frequencies for each high-mast tower are found in Table 2.3. The first through fourth modal frequencies varied between 0.25 and 7.3 Hz.

2.5.2 Damping Ratios

Three different methods were used to determine the damping ratios of the high-mast lighting structures; one using pluck test data, and the other two using ambient vibration data. The first method, which utilizes the pluck test data, is the log decrement (LD) method. The second method, the half-power bandwidth method (HPBW), estimates the damping ratio using the response in the frequency domain (created by the FFT). The third method, the random decrement method (RD), works in the time domain to create a free decay profile similar to that of the LD method.

As previously mentioned, this field investigation is described in more detail in a report presented to the Iowa Department of Transportation.

Several damping ratios were extrapolated from each tower, using the data collected from the accelerometers and the strain gages. As discussed in the previous paragraph, both the pluck test data and the ambient test data were used to extrapolate the damping ratios. The averaged damping ratios for the first four modal frequencies for each tower were obtained and are presented in Table 2-4. Plots of frequency versus the damping ratio for each high-mast tower are shown in Figure 2.5.

Figure 2.5 includes the suggested damping ratios from the AASHTO and the CAN/CSA specifications. As discussed in Chapter 1, AASHTO recommends using a ratio of 0.5% when the actual damping ratio of the structure is unknown [AASHTO, 2001], and the Canadian Bridge Code [CAN/CSA] specifies a damping ratio of 0.75% when experimentally determined values are unavailable [CSA International, 2000]. This plot shows that the damping ratios in all four modes are in many instances considerably lower than the assumed values from the two codes. There are several difficulties with the two specifications. First, the AASHTO Specifications does not address the possibility of the damping ratios in the higher modes of vibration falling below that of the first mode. Second, the suggested damping ratios may be based on previous tests or research of cantilevered structures that have different damping characteristics from the high-mast towers.

The damping ratios in the first mode, on average, are considerably higher than the other modes. This increase could be attributed to the presence of

aerodynamic damping. Aerodynamic damping is a function of wind speed and is additive with the inherent structural damping of the tower and increases with increasing wind speed. Unfortunately, the effects of any potential aerodynamic damping could not be evaluated as part of this study.

Structures with high damping ratios require fewer cycles for the vibration to attenuate. The high-mast towers have very low damping ratios and as a result experience a high number of damaging cycles that can cause damage after the load event, which produced the initial excitation, has ended. These cycles can be accumulated during vortex shedding or following natural wind gusts. When the towers with low damping ratios are stressed beyond the constant amplitude fatigue limit (CAFL), a significant number of damaging cycles can accumulate before the stress range falls below the CAFL. This importance of high damping ratios can be seen by comparing the number of cycles required for two towers, of different damping ratios, stressed to 5 ksi to attenuate in free vibration to a stress of 2.6 ksi (CAFL of Category E'). Tower A has a damping ratio of 1% and tower B has a damping ratio of 0.1%. Using the decay of motion equation from structural dynamics, tower A reaches the CAFL after 10 cycles, while tower B requires 104 cycles to reach the same stress level. These base plate-to-tube wall connections are assumed to be an E' fatigue detail according to the AASHTO Specifications, with a CAFL of 2.6 ksi. This is the lowest fatigue category and low level stress ranges easily exceed the CAFL. Therefore, the low CAFL in combination with a low damping ratio can produce many damaging cycles on the high-mast lighting towers

and consequently significantly reduce the fatigue life. It should be noted that the designation of E' for the base plate connection is based on very few experimental tests and is currently being investigated as discussed in Section 1.6. It is very possible that this socket connection detail is even worse than its current E' designation and many structures may not be designed to account for this deficiency.

2.3.2 Measured Stresses

The maximum stresses at the critical gages for the As-built and Retrofit Sioux City towers, prior to the release of the load, are summarized in Table 2.5. All the channels reported in this Table are in-line with the applied load. Channels 1, 5, and 10 are on the tension side of the tower, and channels 2, 6, and 11 are on the compression side. Channels 1 and 2 were placed 3" above the base plate, channels 5 and 6 were 5'-9" above the base plate, and channels 10 and 11 were 8" above the base plate. Note that gages 10 and 11 were not placed in the same location on the As-built tower and have been omitted from the table. Refer to Figures 2.6 and 2.7 for the gage plans for the As-built and Retrofit towers. Also of importance is that the loads presented in the Table are the loads measured by the load cell in the inclined cable. The inclination of the cable for each tower was similar.

It should be noted that the stresses 3" above the base plate are not the maximum stresses along the height because they are located in the valley of the stress profile. This characteristic of the stress profile will be discussed in greater detail in Section 4.1. However, it should be noted that the stresses at the base plate

connection are considerably higher than the stresses in the tube wall due to localized stress concentrations.

As expected, the Retrofit tower experienced significantly lower stresses than the As-built tower due to the increased base plate thickness, increased tube wall thickness, and the reinforced access hole detail.

2.3.3 Effect of Anchor Nut and Leveling Nut Loosening

Additional tests were performed to study the effects that loose nuts due to poor installation practices or nuts that loosen over time have on the tube wall stresses. Three tests were conducted: two on the As-built tower and the third on the Retrofit tower. During the first test, one nut was loosened, the load was applied and released, then a second nut was loosened, the load was reapplied, and the pole was subsequently plucked. During the second test, a leveling nut was loosened and the top nut was tightened down to simulate the effect of improper leveling prior to tightening the top nuts. The third test at the Retrofit tower involved loosening two bolts while the load was applied, and subsequently plucking the pole.

The pluck tests with loose anchor bolts did not significantly alter the damping ratios. However, it appears that the 1st and 3rd modes were not excited, as determined by an FFT analysis of the raw data. At both towers, localized increases in stress were experienced near the base plate and in the vicinity of the loose anchor nuts, as shown in Table 2.6. During tests 4 and 9, the locking nut furthest from the load (tension side) was loosened.

Comparing the stresses from the properly (Table 2.5) and improperly (Table 2.6) tightened towers, it can be noted that the towers improperly installed are subjected to concentrated stress increases in the vicinity of the loose anchor bolts. Figure 2.6 also shows the localized effects of the stress increase due to poor installation (leveling nuts not level). Channel 1 is located on the pole wall 3 inches above the column-to-base plate weld toe near the improperly tightened anchor bolt. Channel 2 is on the opposite face from Channel 1. It can be seen that very high stresses were measured at Channel 1, over 60 ksi which may have resulted in local yielding in the tube wall. Notice that the stresses on the opposite side of the tower are not affected by the loose anchor bolts.

County	Pole Location	Material G or W	Pole Height (ft)	Pole Diameter at Base (in)	Number of Sides	Pole Wall Thickness at Base (in)	Base Plate Thickness (in)	Anchor Rod Pattern	Number of Anchor Rods	Comments
Story	I-35/US-30	W	100	22	12	--	1.75	S	4	Anchor Rod Stiffeners
		W	100	22	12	--	1.75	S	4	Anchor Rod Stiffeners
Polk	I-80/I-35/I-235 NW Interchange	W	140	29.5	12	1/2	2.75	C	12	
		W	145	30.1	12	1/2	3.00	C	12	
Polk	I-80/I-35/I-235 NE Interchange	W	140	--	--	--	--	C	6	
		W	140	--	--	--	--	C	6	
Warren	IA-5 & US65/US69	G	120	22	Round	1/4	1.50	C	6	
		G	120	22	Round	1/4	1.50	C	6	
Cerro Gordo	I-35/US18	W	148	28.5	12	5/16	1.75	C	6	Wind Pole
		W	148	28.5	12	5/16	1.75	C	6	

Notes:

W - Weathering Steel

G - Galvanized

C - Circular

S - Square

Table 2.1: High-Mast Lighting Towers Tested During Phase 1

Pole Location	Material G or W	Pole Height (ft)	Pole Diameter at Base (in)	Number of Sides	Pole Wall Thickness at Base (in)	Base Plate Thickness (in)	Anchor Rod Pattern	Number of Anchor Rods	Comments
I-29 and Exit 147B	G	140	24 7/8	16	3/16	1.25	C	8	As-built Tower Sioux City, Iowa
I-29 and Exit 147B	G	140	24 7/8	16	5/8	3	C	8	Retrofit Tower Sioux City, Iowa
I-29 and Hamilton Exit	W	140	27.51	12	1/4	2.75	C	12	Hamilton Tower Sioux City, Iowa

Notes:

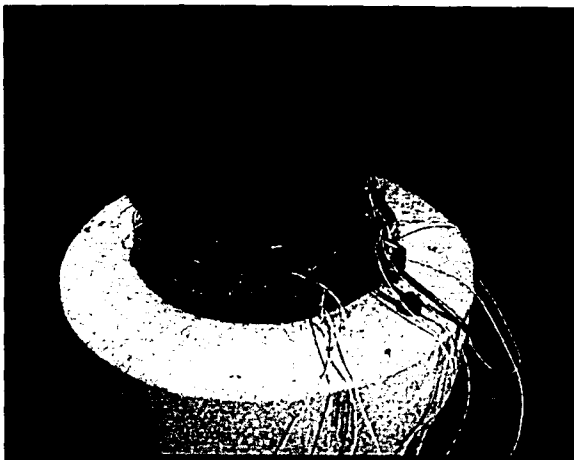
W – Weathering Steel

G – Galvanized

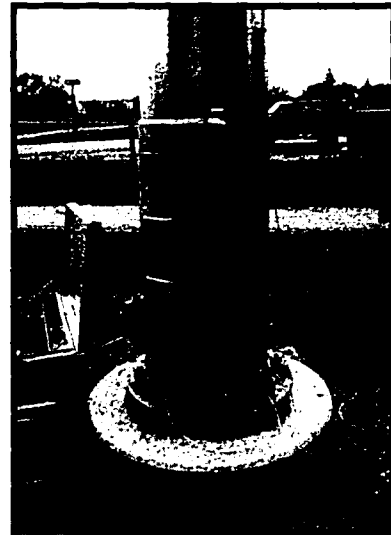
C - Circular

S – Square

Table 2.2: High-Mast Lighting Towers Tested During Phase 2



(a) As-Built Tower



(b) Retrofit Tower

Figure 2.1: High-Mast Lighting Towers in Sioux City, Iowa

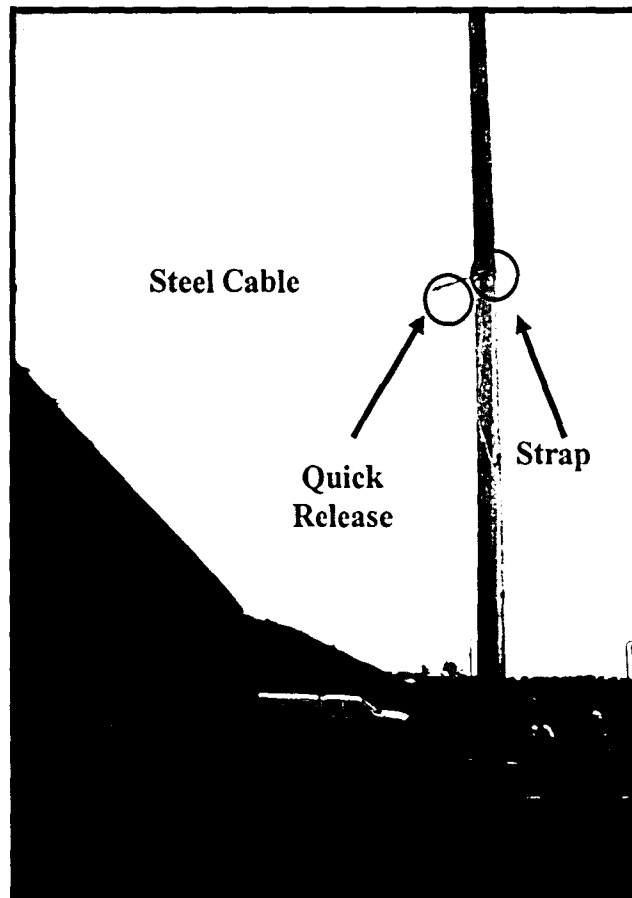
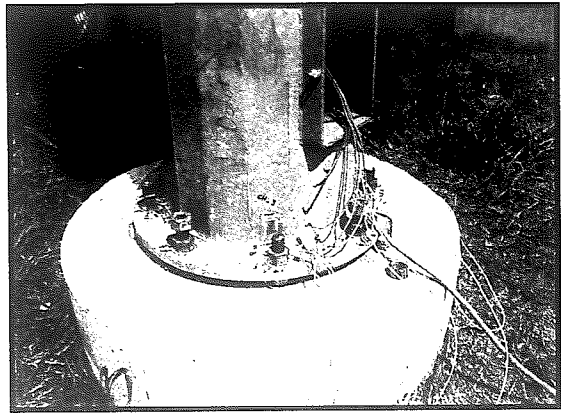
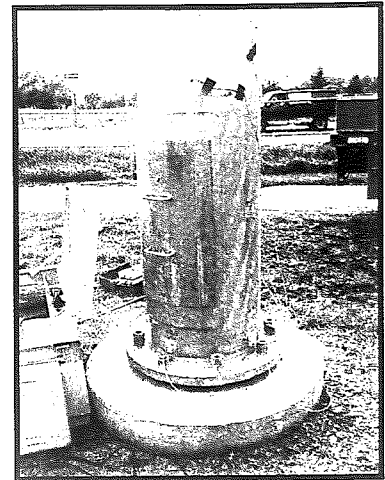


Figure 2.2: Pluck Test of a Pole in Sioux City, Iowa



(a) As-Built Tower



(b) Retrofit Tower

Figure 2.1: High-Mast Lighting Towers in Sioux City, Iowa

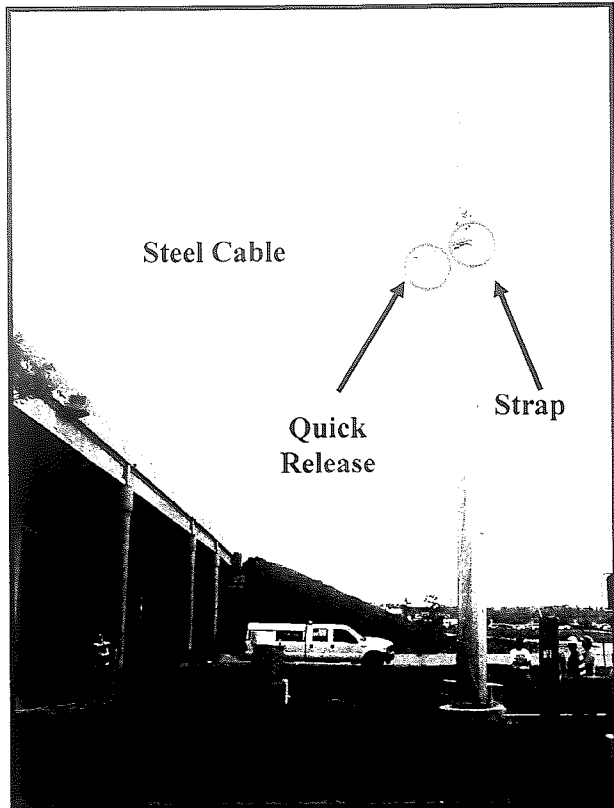


Figure 2.2: Pluck Test of a Pole in Sioux City, Iowa

Table 2.3: Natural Frequencies for the First Four Modes

Tower	Frequency			
	1 st Mode	2 nd Mode	3 rd Mode	4 th Mode
I-35/US18	0.32	1.34	3.41	6.46
I-35/US30 Tower 7	0.43	1.52	2.52	5.75
I-35/US30 Tower 6	0.46	--	2.14	6.00
NE Mixmaster Tower 8	0.27	1.14	3.04	6.11
NE Mixmaster Tower 7	0.28	1.18	3.02	6.05
US65-US69/SR-5 Tower 8	0.30	1.36	3.59	6.87
US65-US69/SR-5 Tower 2	0.31	1.40	3.61	6.79
West Mixmaster Tower 3	0.42	1.55	3.82	7.31
West Mixmaster Tower 7	0.41	1.54	3.82	7.30
Wind Pole - Clear Lake	0.32	1.29	3.34	6.40
As Built - Sioux City	0.25	1.14	3.03	5.99
Retrofit - Sioux City	0.30	1.38	3.20	5.65
Hamilton - Sioux City	0.33	1.37	3.51	6.90

Table 2.4: Damping Ratios of Each Tower Tested for the First Four Modal Frequencies

Tower	Damping Ratios			
	1 st Mode	2 nd Mode	3 rd Mode	4 th Mode
I-35/US18	1.20%	0.78%	0.23%	0.21%
I-35/US30 Tower 7	1.16%	--	0.45%	1.10%
I-35/US30 Tower 6	1.37%	--	1.07%	0.71%
NE Mixmaster Tower 8	1.01%	0.51%	0.16%	0.70%
NE Mixmaster Tower 7	1.92%	0.46%	0.14%	0.67%
US65-US69/SR-5 Tower 8	0.18%	0.50%	0.43%	0.60%
US65-US69/SR-5 Tower 2	0.10%	0.27%	0.04%	0.21%
West Mixmaster Tower 3	0.46%	0.23%	0.12%	0.28%
West Mixmaster Tower 7	0.74%	0.38%	0.11%	0.21%
Wind Pole - Clear Lake	0.60%	0.17%	0.27%	0.30%
As Built - Sioux City	2.60%	0.28%	0.26%	0.39%
Retrofit - Sioux City	3.15%	0.33%	0.52%	0.54%
Hamilton - Sioux City	2.74%	0.86%	0.60%	0.45%

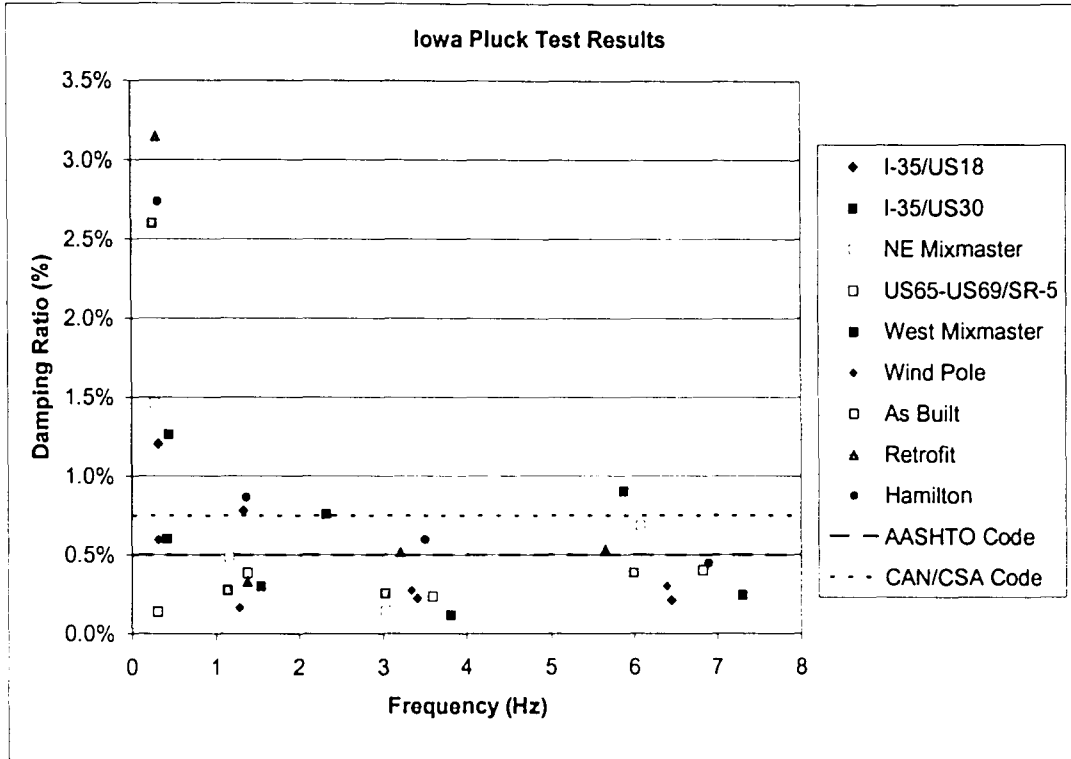


Figure 2.5: Damping Ratio vs. Frequency

Table 2.5: Maximum Measured Stresses at Critical Locations

	Test	Load (lb)	h = 3"		h = 5' 9"		h = 8"	
			CH_1 (ksi)	CH_2 (ksi)	CH_5 (ksi)	CH_6 (ksi)	CH_10 (ksi)	CH_11 (ksi)
As Built	1	592	3.89	-2.85	4.63	-4.36	-	-
	2	618	4.63	-3.51	5.51	-5.13	-	-
	3	561	3.77	-3.44	4.49	-4.92	-	-
Retrofit	6	563	1.85	-1.76	1.68	-1.66	1.35	-1.37
	7	602	1.90	-2.00	1.77	-1.78	1.63	-1.70
	8	656	2.01	-2.10	1.83	-1.89	1.68	-1.80

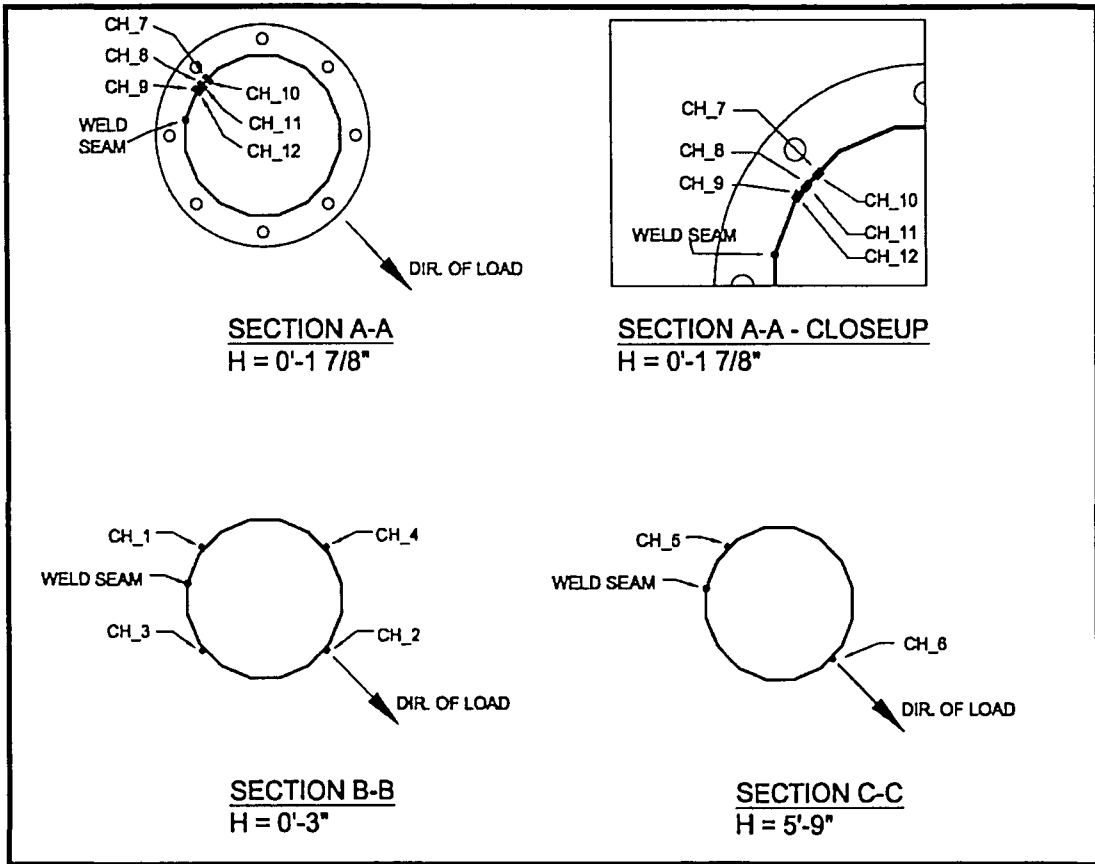


Figure 2.6 – Strain gage details for the As-built tower along I-29 in Sioux City, Iowa

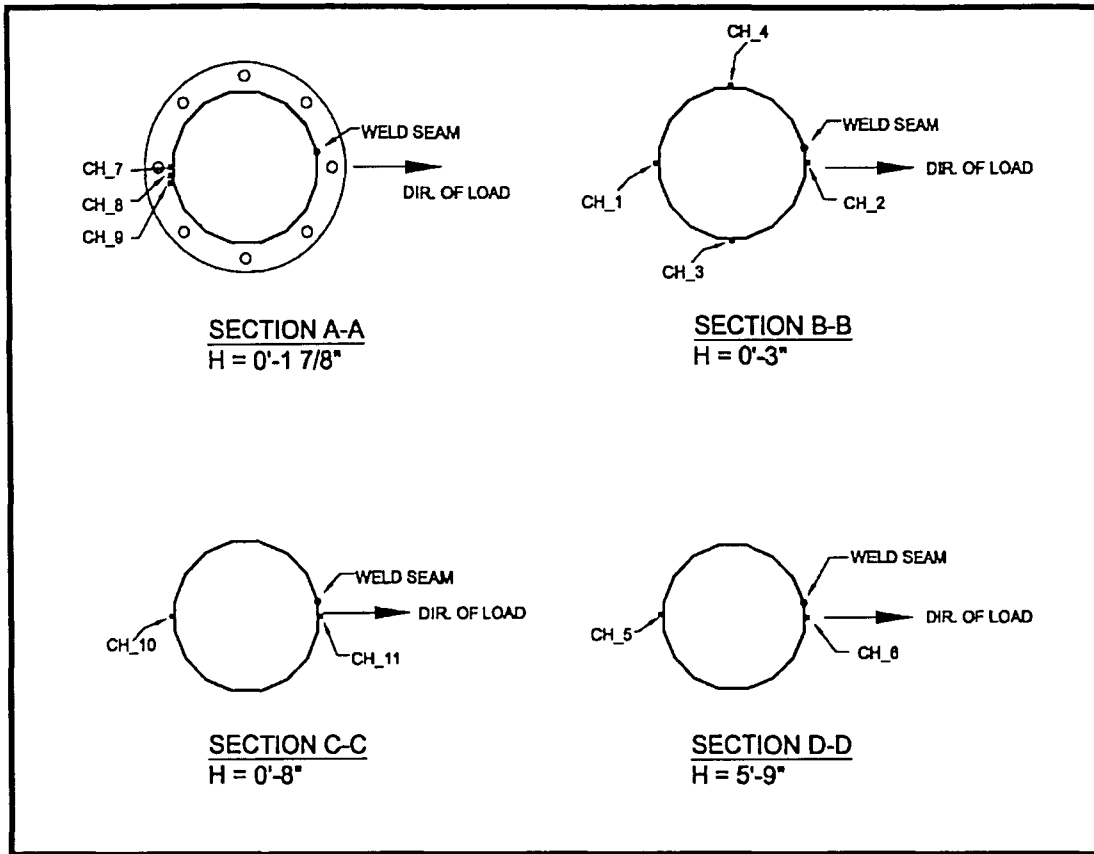


Figure 2.7 – Strain gage details for the Retrofit tower along I-29 in Sioux City, Iowa

Table 2.6: Maximum Measured Stresses at Critical Locations During Anchor Bolt Loosening Study

	Test	Load (lb)	h = 3"		h = 5' 9"		h = 8"	
			CH_1 (ksi)	CH_2 (ksi)	CH_5 (ksi)	CH_6 (ksi)	CH_10 (ksi)	CH_11 (ksi)
As Built	4	N/A	4.74	-2.84	4.09	-3.96	-	-
Retrofit	9	665	7.19	-2.67	1.67	-1.60	3.99	-2.08

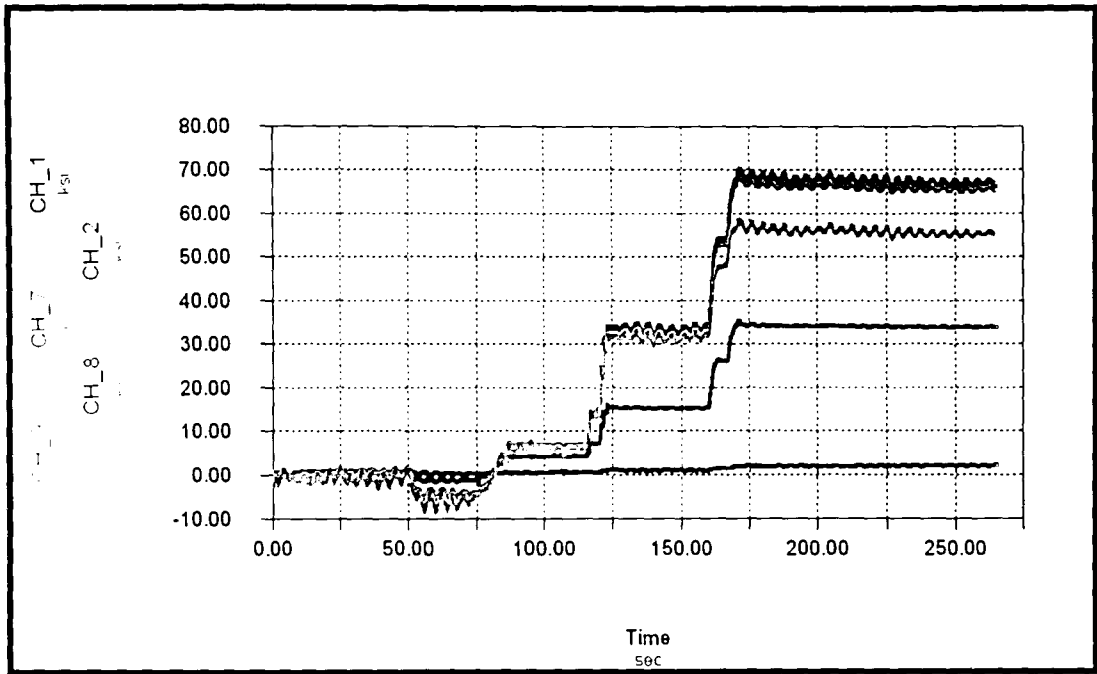


Figure 2.8: Localized Stress Changes Due to Poor Installation Techniques

Chapter 3 Finite Element Modeling

3.1 Introduction to Modeling

It may appear that high-mast lighting towers are simple cantilevers and can be modeled as such. However, upon closer examination there are several factors that make the modeling process complex. These features are a polygonal tapered tube (i.e., a non prismatic section), the base plate-to-tube wall connection, and the interaction between the leveling nuts and base plate. A pre and post-processor, FEMAP (Finite Element Mapping), enabled the complex features of the high-mast towers to be modeled relatively easily. Once built, the models were analyzed using ABAQUS, a very powerful, general purpose finite element analysis program. The purpose of Chapter 3 is to discuss the finite element modeling process of the Sioux City, Iowa high-mast tower. This model, referred to as the BASE model, will be described followed by the assumptions used to build the model.

3.2 BASE Finite Element Model

The BASE model, shown in Figure 3.1, is based on the as-designed tower in Sioux City, Iowa that collapsed in 2003. As discussed in Chapter 2, the tower is 140' tall and is composed of four hexdecagonal (16-sided) tube sections stacked on top of each other. The base plate thickness is 1 ¼" and the tube wall thickness of the lower tube section is 3/16". All dimensions are taken from the design plans for this high-mast tower. It is noted that the hand access hole detail and winch plate were

not included in the models in order to better study the effects of geometry changes on the tower. The BASE model is divided into four parts that correspond to the different types of elements (beams, shells, solids, and multi-point constraints).

3.2.1 Part 1 – Beam Elements

Part 1 of the BASE model is made up beam elements, as shown in Figure 3.2 and encompasses the top three tube sections of the high-mast tower. The tapered tube sections are made up of a series of constant diameter prismatic tube elements. Although the pre-processor, FEMAP, supports polygonal tube elements, ABAQUS does not, and prismatic tube elements were used instead. The choice of cylindrical tube elements will not affect the results of this study because the stresses in the tube wall in the upper sections are not being investigated. This portion of the model is intended to represent the global stiffness of the entire high-mast tower without the computational difficulty created and solution time required when modeling with shell or solid elements.

As shown in Figure 3.3, each tube section (a) is sub-divided into three portions of varying properties (b). The top portion represents the top third of the tube section and has a diameter equal to the average diameter of the top third. Similarly, the middle portion represents the middle third of the tube section, and the bottom portion represents the bottom third of the tube section. Each property portion is then sub-divided into two elements (six elements make up one tube section) each

69” long as shown in Figure 3.3(c). More elements would provide a better deflection profile for the entire structure, but are not necessary for this study.

Beam elements were also used to model seven of the eight anchor rods. Each anchor rod extended a distance of 10” below the base plate and was composed of 20 elements. The eighth anchor rod was modeled with solid elements (Section 3.2.3). The constraints (or boundary conditions) applied to the anchor rods will be discussed in Section 3.3.

3.2.2 Part 2 – Shell Elements

Part 2 of the BASE model is made up of 8-noded parabolic shell elements. This portion encompasses the bottom tube section (from a height of 0” to 441”) of the high-mast lighting tower and the base plate. The purpose of Part 2 is to accurately model the stresses around Part 3 (the solid elements), using elements that are less computationally taxing than solid elements. This section also serves to distribute the bending moment resulting from the point load applied at the top of the bottom section of tower to the base plate.

Only three typical shell sizes were used for Part 2 of the BASE model and are referred to as the “small”, “medium” and “larger” elements. This does not include the slight decrease in shell width due to the taper of the tower or the elements used in transition regions. The elements closest to the base plate are the smallest and they increase with increasing distance from the base plate. From the base plate ($Z=0$ ”) (excluding the solid elements of Part 3 to be discussed in Section 3.1.3) to a height of

Z=110.25” the vertical height of the “small” elements is 1.5”. There are 64 elements around the circumference of the tower; four elements make up each face of the multi-sided tower as shown in Figure 3.4. The average width of these elements is 1.1”. The base plate is also composed of shell elements with a width of approximately 1.1”. They are 1.2” long and are shown in Figure 3.5. The base plate is circular and has an outer diameter of 34.5”.

From a height of Z=110.25” to a height of Z=176.4” the vertical height of the “medium” elements is 2”. There are 32 elements around the circumference of the tower; two elements make up each face as shown in Figure 3.6. The average width of these elements is 2.2”. The vertical height of the “large” elements, from Z=176.4” to Z=441”, is 4”. The average width of these elements is 4.4”. There are 16 elements around the circumference of the tower, one element per face, as seen in Figure 3.6. The transition from one element size to a larger element size involved the use of quadrilateral elements also shown in Figure 3.6. The quadrilateral elements, or unequal sided elements are an effective way to reduce the mesh size while maintaining the use of four-sided elements.

To create Part 2, a 1/16th model that included the base plate and once face of the tube wall was built as shown in Figure 3.7. This small segment makes up one of the 16 sides of the tower and extends 441” up the tube wall to the termination of the shell portion. Utilizing the power of the pre-processor, FEMAP, the entire bottom section was built by revolving the 1/16th segment around the center line of the tower.

The model of the lower tube section of the high-mast tower was constructed entirely of shell elements before Part 3 was constructed, as discussed in Section 3.1.3.

Shell elements are simple two dimensional elements that represent the mid-surface of a plate. An area of overlap occurs when two elements do not lie in the same plane. Figure 3.8, which is an example of the intersection of the tube wall and the base plate, shows the overlap created when two elements perpendicular to each other share a common node. This is an inaccurate model of the socket connection as it can not account for the influence of the fillet welds. A high-mast tower model built entirely of shell elements will not produce accurate local stress results at this important connection. To produce better results, the area of interest was remeshed with solid elements as discussed in the next section.

3.2.3 Part 3 – Solid Elements

Part 3 makes up a small portion of the high-mast tower model as shown in Figures 3.9 and 3.10. Figure 3.9 shows an exploded view of the solid portion of the model and Figure 3.10 shows the front and profile views of the model. This part, composed of solid elements, is 10” high and includes three sides of the 16-sided tube. Part 3 is modeled with solid elements in order to accurately capture the effects of base plate flexibility and the base plate-to-tube wall connection on the vertical stress in the tube wall. It is the most important region of the entire model from a fatigue perspective which is why it has the highest mesh refinement. Part 3 is made

up of four sub-parts, the base plate, the tube wall, the weld, and the anchor rods and leveling nuts. It was constructed by extruding shell elements using FEMAP.

The meshing of Part 3 was very difficult and may not have been possible without the capabilities of the pre and post-processor, FEMAP. A brief description of the meshing process is as follows. The section to be extruded was identified and isolated from the rest of the model. The base plate and tube wall element meshes were refined so that each side of the tube wall is composed of 16 elements instead of the coarser four-element mesh used in the shell element region (Part 2). The base plate region was re-meshed in the vicinity of the anchor rod, as shown in Figure 3.11. This included removing a hole for the anchor rod. The base plate elements connected to the tube wall were then separated from the tube to allow for the extrusion of the tube wall elements. The base plate and tube wall were extruded along their own planes about their original centerlines to create a three dimensional, solid model. The nodes at the top of the base plate were joined to the tube wall to prepare for the addition of the fillet weld. Nodes were also joined at the bottom of the tube wall to the inside of the base plate cut out. A triangular weld was constructed along the base plate-to-tube wall connection. There is full connectivity between the base plate and the weld and full connectivity between the tube wall and the weld.

The transition region around the solid elements was added to transition the smaller elements to the larger elements, as shown in Figure 3.12. The solid anchor rod and the nuts were also built by extruding shell elements. There is full

connectivity between the nuts and the base plate to simulate a fully tightened anchor rod and nut system. Modeling the nuts as contact elements instead of providing full connectivity between the different sub-divisions is significantly more difficult and outside the scope of this study.

3.2.4 Part 4 – Multi-point Constraints

Multi-point constraints (MPCs), or rigid beam elements, are used to connect one element to another. MPCs transfer axial, shear, and bending forces and provide fully rigid continuity between separate nodes. MPCs were used at several different locations in this finite element model. The first set of MPCs was used at the beam-to-shell interface to connect the shell elements at the top of Part 2 ($Z=441''$) to the beam elements at the bottom of Part 1 as shown in Figure 3.13. This is also the location of the applied point load, to be discussed in Section 3.3. MPCs were placed around the entire solid-to-shell interface to rigidly connect the solid elements of Part 3 to the shell elements of Part 2 as shown in Figure 3.14. Because shell elements represent the mid-plane surface of a plate, the rotation and deflection of the outer most fibers of the plate are not translated correctly at a shell-to-solid interface. At a connection such as the base plate shell-to-solid interface, the rotations and deflections of the shells are translated to the nodes at the center of the base plate constructed of solid elements. The solid elements at the top fibers of the base plate will not rotate or deflect the same as the shell element. To avoid this problem of inconsistent rotation and deflection, MPCs are used to rigidly connect the shell to

multiple solid elements (i.e., through the entire base plate thickness). MPCs allow the edge of the base plate meshed with solids to deflect and rotate exactly the same as the shell.

3.3 Model Loading and Constraints

A 1 kip (1000 lb) point load was applied horizontally at the shell to beam interface, at a vertical height of $Z=441''$. The load was applied perpendicular the front side of Part 3, to induce tension in the solid region. Figure 3.15 is a plan view of the high-mast tower model and shows the direction of the load with respect to Part 3. The location of the applied load was chosen to match that used for the successful field tests and the given geometry of the tower. The connection between the termination of the bottom section of the tube (meshed with shell elements) and the beginning of the second tube section (meshed with beam elements) was an ideal location to place the point load because of the presence of a node on the centerline. The magnitude of the applied load was an arbitrary value. One kip was selected as the magnitude partly because it is a unit load. Another reason for the selected magnitude is that a 1 kip load applied at 441'' above the base plate creates a predicted simple beam theory nominal stress greater than 1 ksi.

Typically the base plate of a high-mast light tower does not make contact with the foundation, as discussed in Section 1.4; instead the nuts are responsible for transferring load from the tower to the anchor rods. This is a very difficult connection to model in finite elements and was closely investigated in a previous

finite element study that will be discussed in more detail in Section 3.5.3. Because the anchor rods can slip in the concrete foundation they can not be modeled as completely fixed to the foundation. Instead, the anchor rod is restrained by rollers in the horizontal directions for a length of 6” and fully restrained at the end. One major difference between the model and real behavior is that the rollers restraining the rod in the finite element model are rigid supports, whereas the concrete foundation is not rigid. (Refer to Section 3.5.2 for an investigation and discussion of the anchor rod length.)

The stand-off length as shown in Figure 3.16 is the distance between the bottom of the leveling nut and the top of the concrete foundation, or applied constraints in the finite element model. A stand-off length of 2.0” was used for this study and is reasonably consistent with the design plans for the Sioux City high-mast tower. Because tube wall stresses are not very sensitive to the stand-off length [Hall, 2005], the actual design value was used in the finite element model. A further discussion of the stand-off length is presented in Section 3.5.3. The anchor rods composed of beam elements had the same constraints and stand-off length as the solid anchor rod. One difference is that the beam elements were constrained at their center lines where as the solid anchor rod was constrained around the outer surface of the rod. Both methods of constraining anchor rods are acceptable as will be further discussed in Section 3.5.2. Both types of anchor rods are shown in Figure 3.17.

3.4 Submodel Study

Initially, it was thought that 10 to 12” of the bottom portion of the high-mast tower could be completely modeled with solid elements, similar to the method presented in Hall’s Masters’ Thesis [Hall, 2005]. However, the massive size of the high-mast lighting towers, specifically the diameter of the tube at the base, drastically increased the number of elements needed to model the entire bottom portion of the tower. This approach was abandoned for a more simplified approach was used that would meet the objectives of the study while remaining within the capabilities of the computer hardware.

Another approach was investigated that involved sub-modeling. For this second approach a “global model” built entirely of beam and shell elements was created. From the global model, the sub-model region was identified, separated from the global model, and extruded as an individual model. The submodel was built exactly the same way as Part 3, discussed in Section 3.2.3, with the exception that it was not connected to the rest of the model. Refer to Figure 3.18 for images of the global model (a) and the submodel (b). Nodes outlining the submodel, referred to as “driven nodes,” were selected as shown in Figure 3.19. The nodes are shown in this figure as dark black dots. The global model was analyzed separately from the submodel. The deflections and rotations of the global model at the location of the “driven nodes” were then applied to the submodel. This process is often referred to as “driving a model.”

Upon comparisons to the calculated nominal stresses, the stresses in the sub-model tube wall were significantly elevated. The submodeling technique using “driven nodes” was checked against a second sub-modeling technique in ABAQUS called “shell-to-solid” modeling for verification purposes. This type of submodeling has the analysis program analyze a sub-model made completely of solid elements, thus eliminating the need for MPCs. The deflections and rotations at specific points are selected and applied to solid elements within a predetermined tolerance, usually the thickness of the shell. Unfortunately, this method also produced the same results.

A third and final model was identified, referred to as the combined model, which combines the global shell model and the solid sub-model into one model. This combined model was used for this study. The vertical stress profile for the combined model was in much closer agreement to the predicted simple beam theory nominal stress profile than the submodel. Figure 3.20 presents the stress profiles of the global model, the submodel, the combined model, and the calculated simple beam theory nominal stress. Further detail regarding the stress profiles is provided in Chapter 4.

3.5 Model Verification

Several modeling variables have significant effects on the tube wall stresses while others do not. This section discusses modeling assumptions that were verified during this research, which includes the mesh refinement and the anchor rod constraint details. Several assumptions from a previous finite element study on traffic support signal structures, as described in [Hall, 2005], were very helpful

during the construction of the high-mast tower model. Hall's extensive calibration studies answered many of the modeling concerns that arose when modeling cantilevered, socket connection structures.

3.5.1 Mesh Refinement

As with all finite element models, it is necessary to verify that the mesh refinement of the BASE model is adequate. Finer meshes are typically used in regions of high stress gradients, such as the base plate-to-tube wall connection. This was performed with a simple convergence test. Two refined models were constructed from the base model, with different levels of refinement. The models were refined by increasing the number of elements in a specific location. If the BASE model refinement is accurate, the refined models will have nearly indistinguishable results from the coarser-meshed models. The only type of mesh refinement investigated was increasing the number of elements. It is possible that a coarser mesh would provide the same results and reduce the computation time, however this was not investigated.

The first model analyzed involved refining only the shells of the model by splitting each element into four elements. These new shell elements are twice the size of the solid elements, which retained their original size. This model, referred to as Refined 1 is shown in Figure 3.21(a). The second model, Refined 2, as shown in Figure 3.21(b), involved splitting the first refined model a second time. In this model, the shell elements are exactly the same size as solid elements. Figure 3.22

presents the results of the refinement models and the BASE model. The mesh refinement study shows a very small variation between the BASE model and the models with finer meshes. Because the difference is so small, the BASE model is acceptable for this parametric study. The finite element models used in the parametric studies were not directly compared to field investigation results. This further justifies the use of a less computationally difficult model, the BASE model.

Previous finite element studies determined that two solid elements through the tube wall thickness and a minimum of four elements through the base plate thickness are acceptable for modeling cantilevered signal structures [Hall, 2005]. These guidelines were used when the solid portion of the high-mast tower model was constructed. Two elements were used through the tube wall thickness and eight elements were used through the base plate thickness.

3.5.2 Anchor Rod Studies

Studies of the anchor rod were conducted to determine the appropriate length that the anchor rod is restrained in the concrete. Additional studies investigated two constraint methods for the solid anchor rod. In the first study, several finite element models were created to determine if the 6" restraint length was acceptable. The first model, termed Anchor Rod 1 increased the constrained length from 6" to 18". The second model, termed Anchor Rod 2 increased the constrained length to 30". Based on Figure 3.23, the difference in normalized outer, inner, and mid-plane vertical stresses in the tube wall between the two anchor rod models and the original model

was not significant. The slight increase in tube wall stress at the connection does not justify using a model with longer anchor rods because of the increased computation time that accompanies the increased length. Therefore, the original restraint length of 6" was deemed acceptable.

A small study investigating the location of the applied constraints was carried out to confirm that the method of restraining the surface nodes is acceptable. This study focused on the solid anchor rod. A modified model was evaluated in which the nodes along the centerline of the solid anchor rod were braced laterally instead of along the outer surface. This study showed that the location of the applied constraints has a small effect on the vertical tube wall stresses, as shown in Figure 3.24. The original model with restrained surface nodes is referred to as the Surface Constraint model and the model restrained along the centerline is referred as the Centerline Constraint model. Because the method of restraining the outer surface produces slightly higher stresses in the tube wall, it is a conservative technique to use for modeling. Furthermore, the centerline constraint approach is a simplification used for structural analysis and may not produce accurate results. Based on this small study, the technique of restraining the surface nodes used in the BASE model is sufficient for modeling the solid anchor rod.

3.5.3 Previous Calibration Studies

Several calibration studies carried out for Hall's Masters' Thesis [Hall, 2005] were very helpful in modeling the high-mast lighting towers in this study. The areas

closely studied were the fillet weld, the stand-off length, and the connection between the leveling nuts and the base plate. The previous finite element studies determined that the weld profile for a specimen with a thick base plate (3") had less of an effect on the tube wall stresses than a specimen with a thin base plate (3/4"). Both differences are not significant enough to include an accurately modeled profile in the final model. These results justified the use of a triangular weld profile, thus simplifying the model. A brief study of the effect of the vertical fillet weld leg on the tube wall stresses showed practically no difference in the stresses at locations above the weld. There was however a slight difference in the hot spot stresses, although relatively small. Another brief study investigated the importance of the lower fillet weld connecting the bottom of the tube wall to the base plate. It was determined that this weld is not very important to the tube wall stresses. For this reason, and the fact that the weld is not intended to be a structural connection, the weld was omitted from the BASE model. The tube wall and the base plate simply share common nodes to account for the presence of the weld.

Because the anchor rod to the concrete foundation is highly simplified, the stand-off length used for modeling was investigated. Varying the stand-off length to accommodate for the simplified boundary conditions did not prove to affect the vertical tube wall stresses and it was concluded that the actual length specified in design plans was acceptable for modeling purposes.

Perhaps the most important feature of the high-mast lighting tower model is the contact between the leveling nut and the base plate. The leveling nuts provide

for the transfer of load from the base plate to the anchor rods. Contact elements are a highly complex element type which can be used to model this phenomenon. However they are beyond the scope of this project, and would present significant difficulties because information such as the preload force applied during tightening of the nuts is unknown. For this finite element study, the nut-to-base plate connection is modeled as fully preloaded and completely in contact. As such, full continuity was provided between the anchor nuts and the base plate. In previous calibration studies, a partial leveling nut technique was implemented for the purpose of obtaining data agreement between a finite element model and an experimental test. It involved modeling the nuts as partial leveling nuts. Material was removed from portions of the leveling nuts that were non-load bearing locations. This method is only valid for specimens with thinner base plate thicknesses and had no significant effect on specimens with thicker base plates [Hall, 2005].

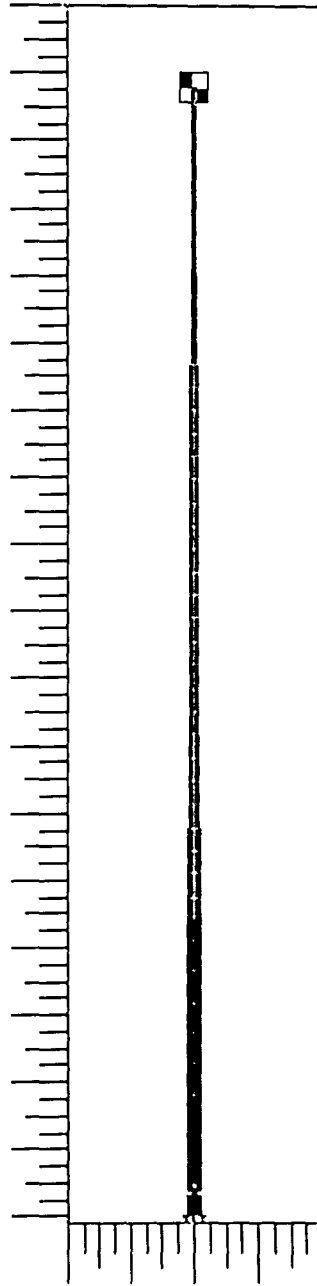


Figure 3.1: Front View of the High-mast Lighting Tower Model

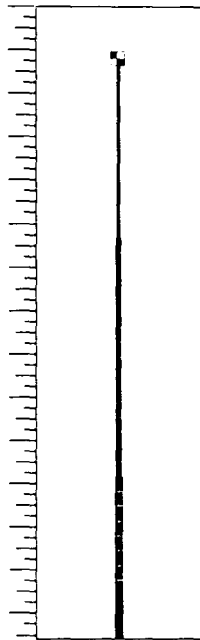


Figure 3.2: Part 1 of the BASE Model, Constructed of Beam Elements

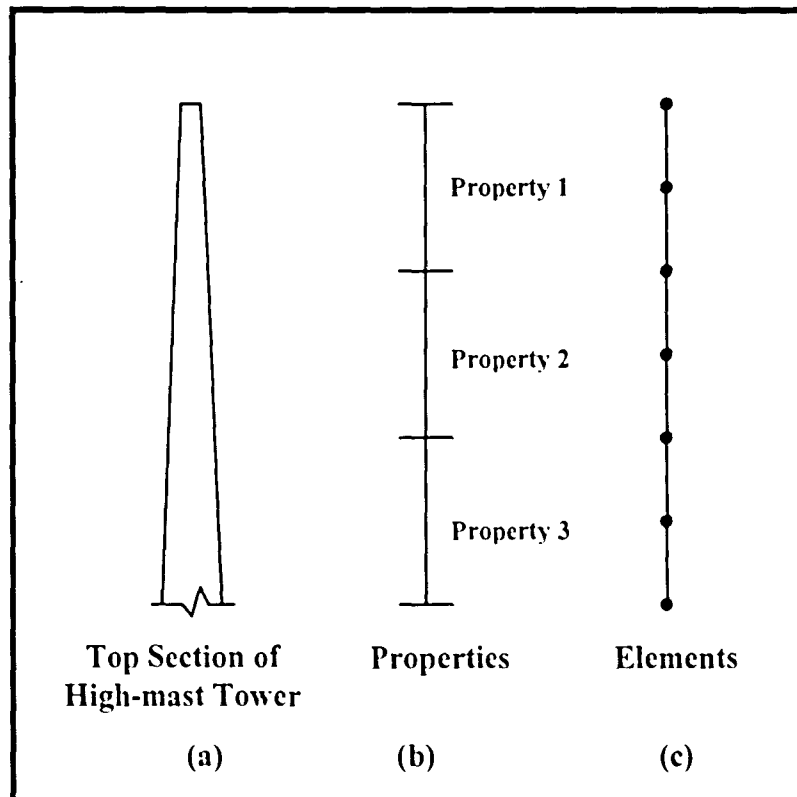


Figure 3.3: Part 1 - Beam Section Sub-Division into Properties and Elements

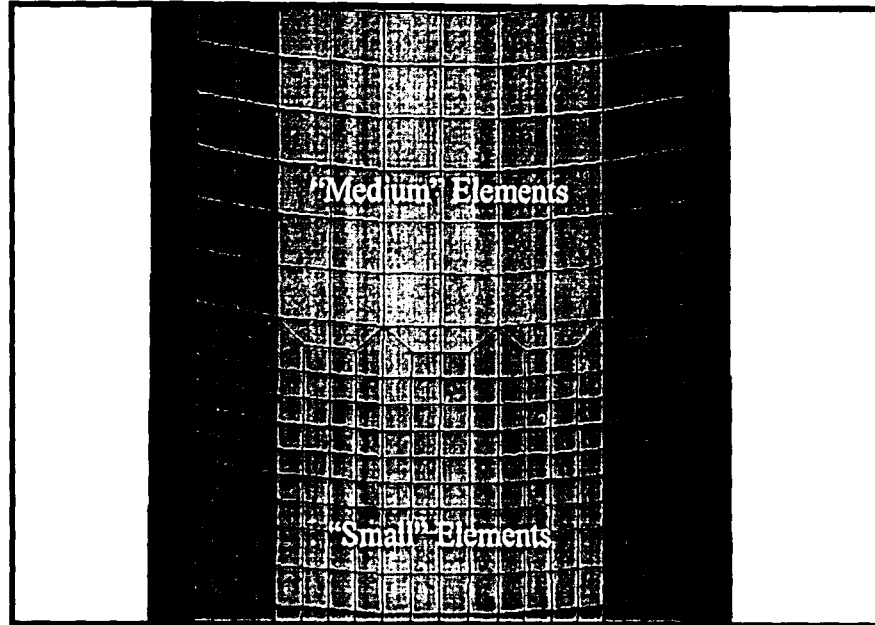


Figure 3.4: Part 2 - Lower Transition - 1" shell elements to 2" shell elements

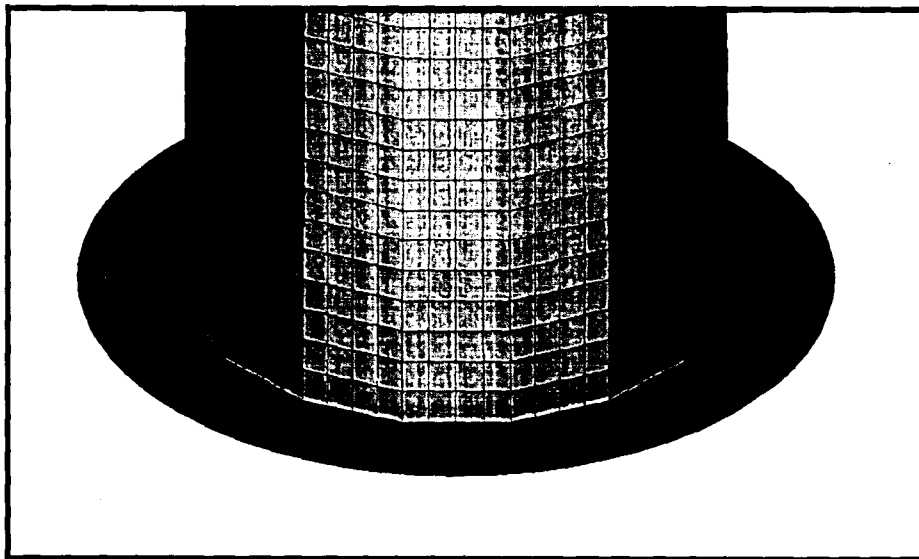


Figure 3.5: Part 2 - Base Plate and Tube Wall Mesh

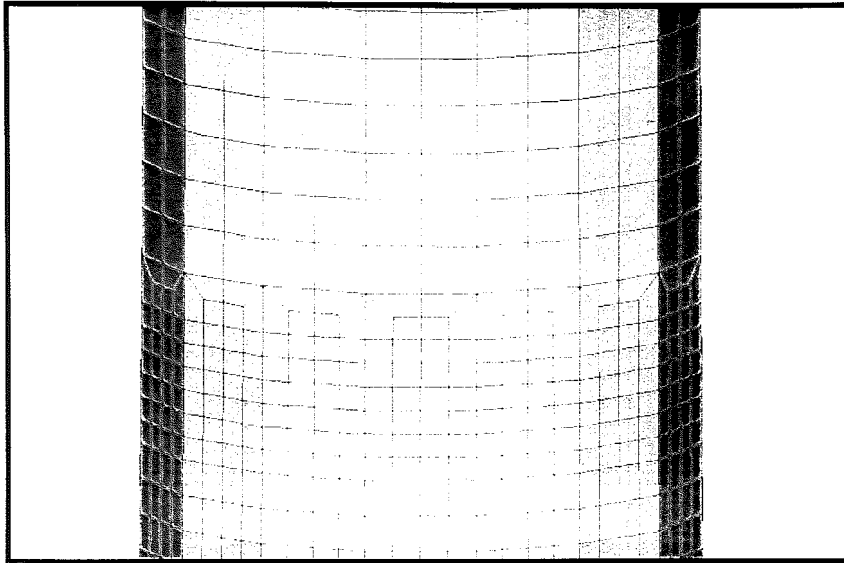


Figure 3.4: Part 2 - Lower Transition - 1" shell elements to 2" shell elements

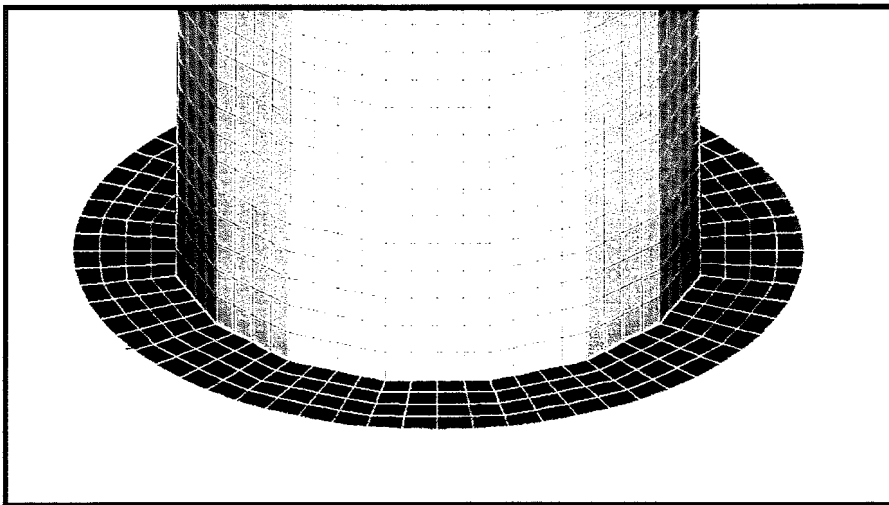


Figure 3.5: Part 2 - Base Plate and Tube Wall Mesh

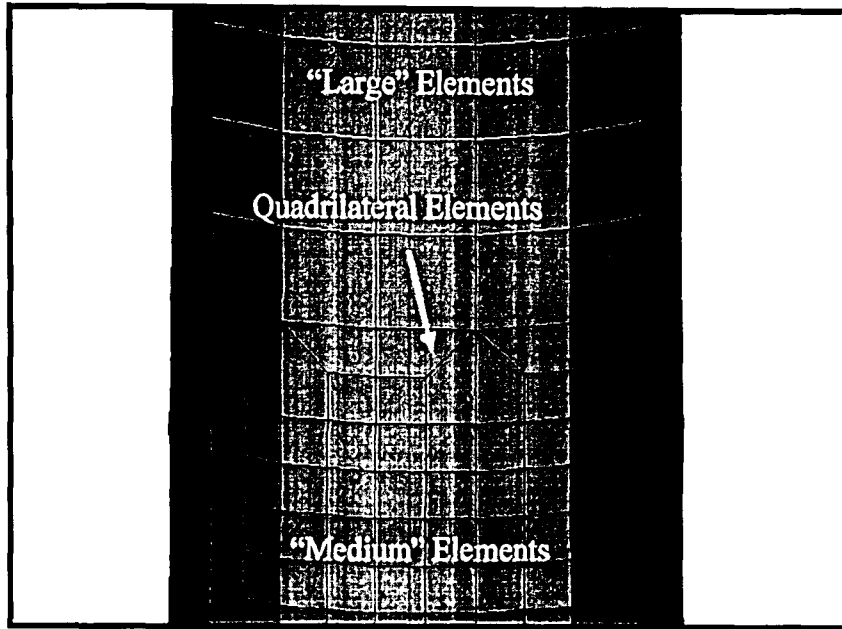


Figure 3.6: Part 2 - Upper Transition – 2” Shell Elements to 4” Shell Elements

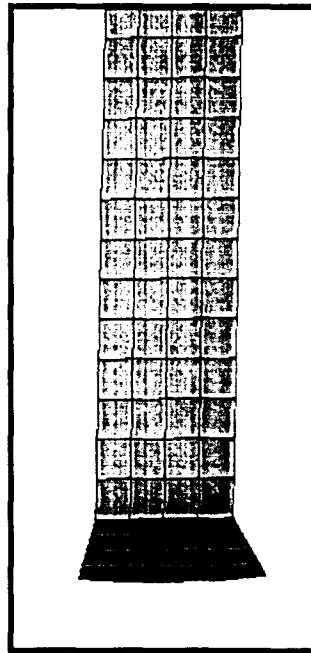


Figure 3.7: Part 2 - 1/16th Section Used to Create the Entire Shell Model

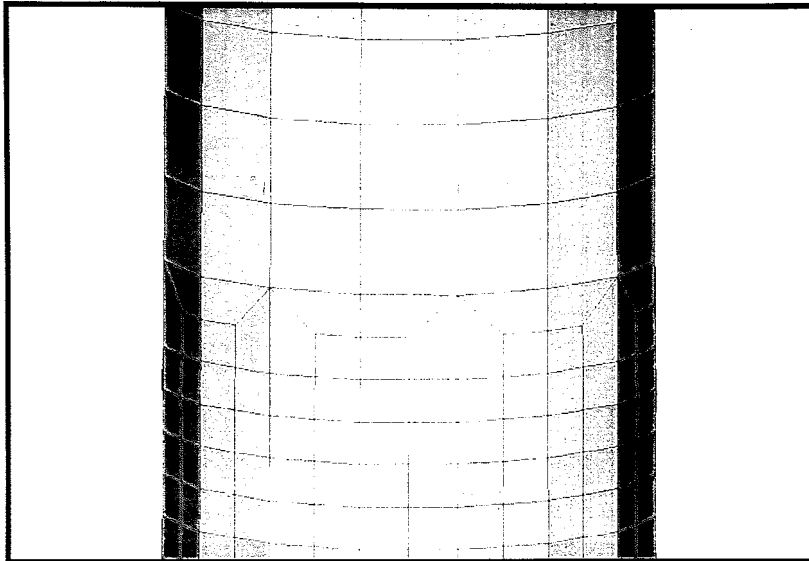


Figure 3.6: Part 2 - Upper Transition – 2” Shell Elements to 4” Shell Elements

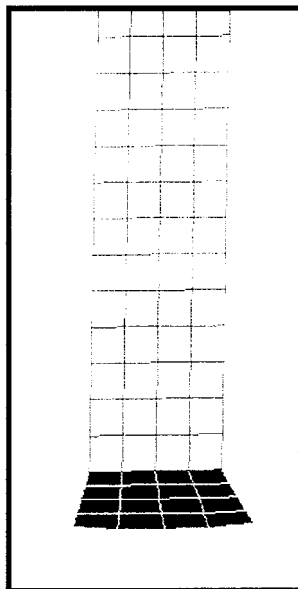


Figure 3.7: Part 2 - 1/16th Section Used to Create the Entire Shell Model

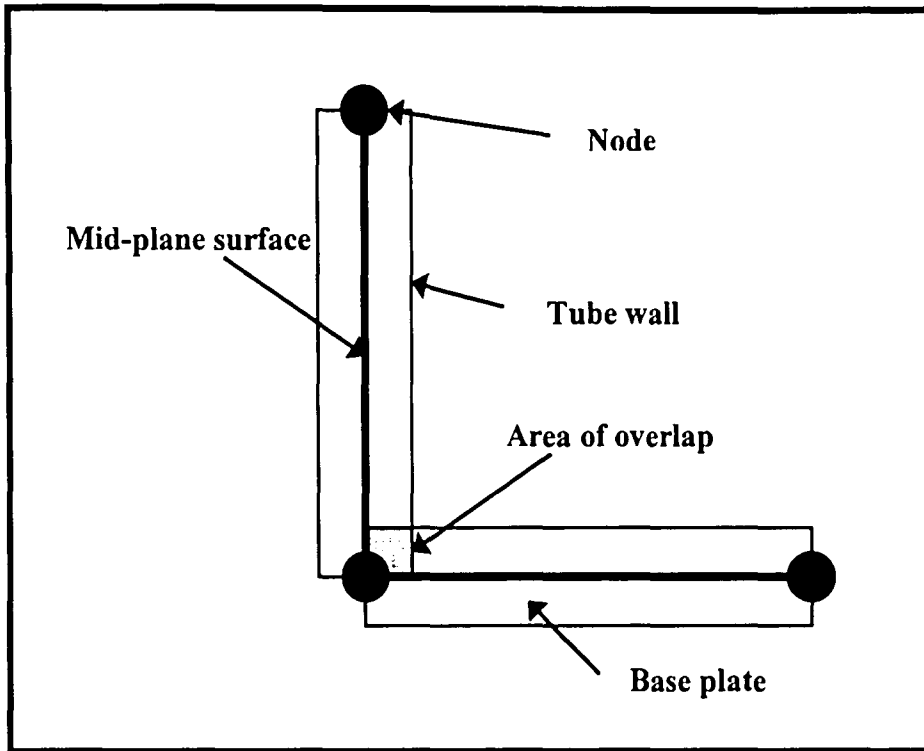


Figure 3.8: Area of Overlap When Using Shell Elements

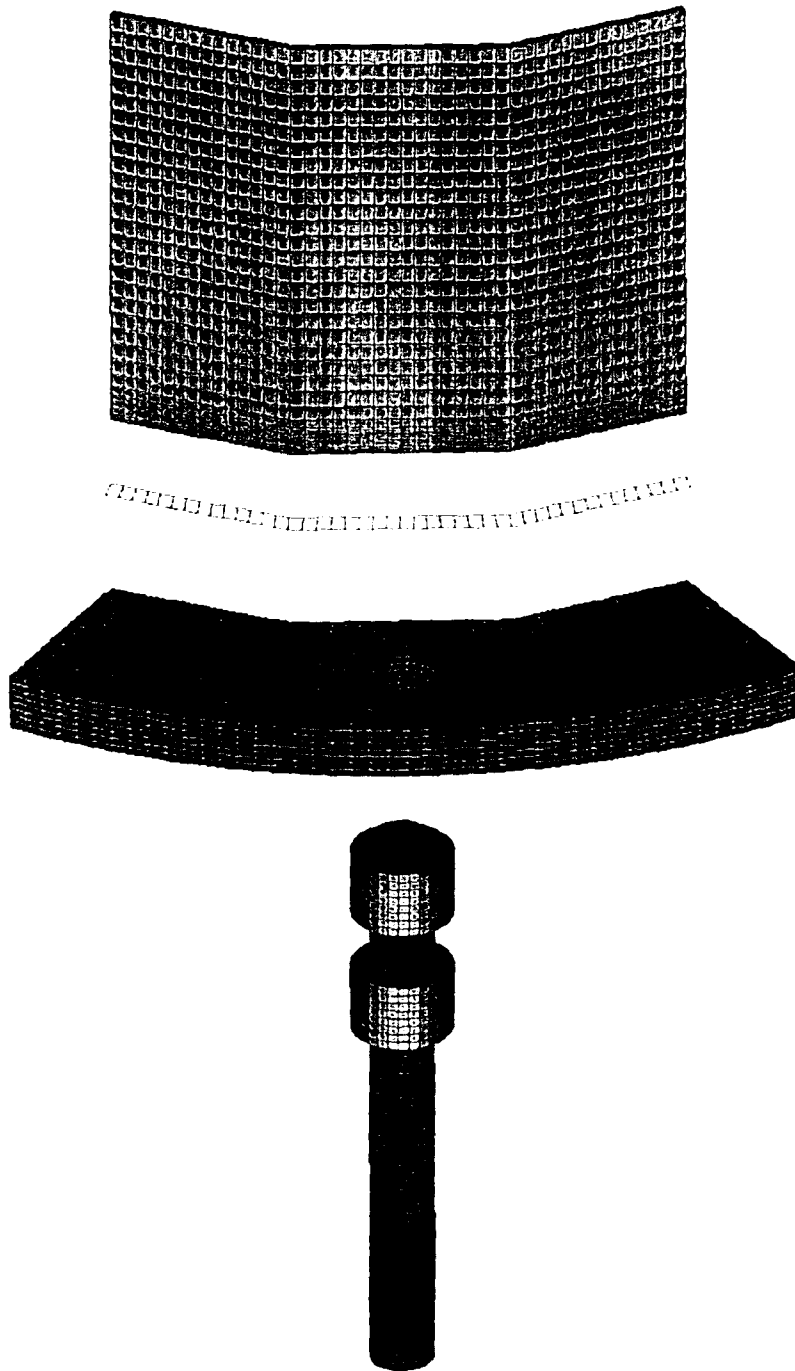


Figure 3.9: Part 3 – Solid Finite Element Model, Lower Tube, Weld, Base Plate, Leveling Nuts, and Anchor Rods

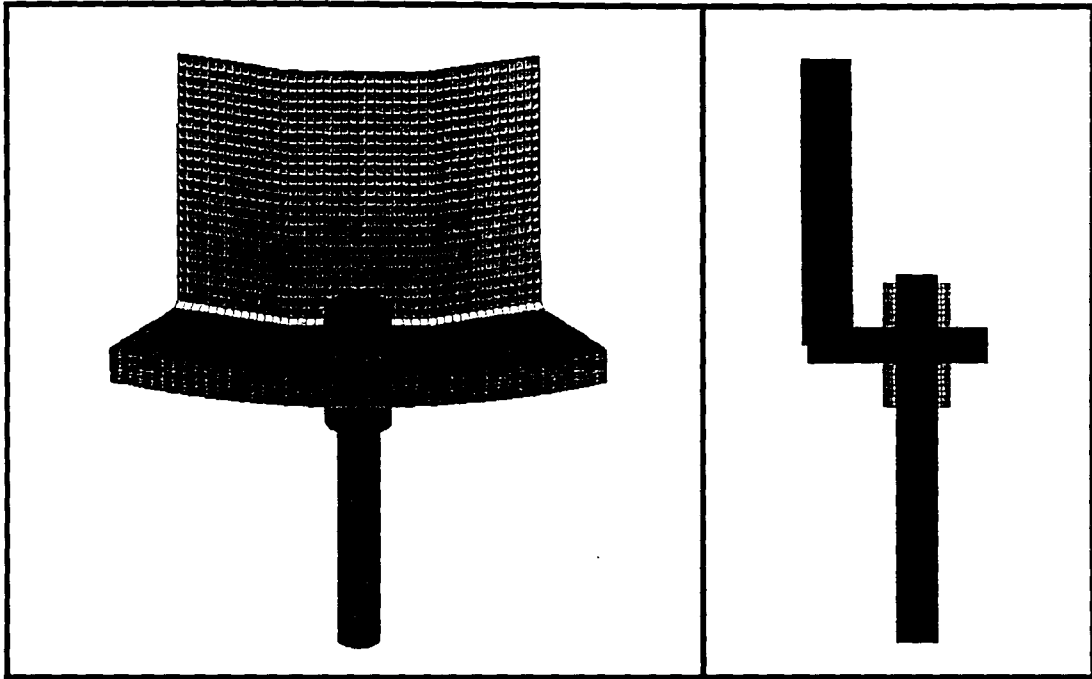


Figure 3.10: Part 3 – Solid Finite Element Model

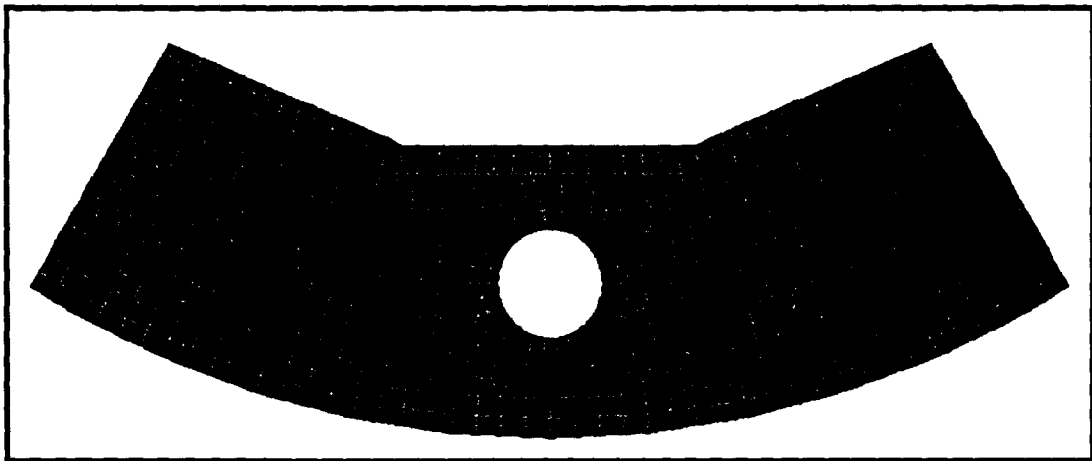


Figure 3.11: Part 3 - Remeshed Region of the Base Plate to Allow for the Anchor Rod and Leveling Nuts

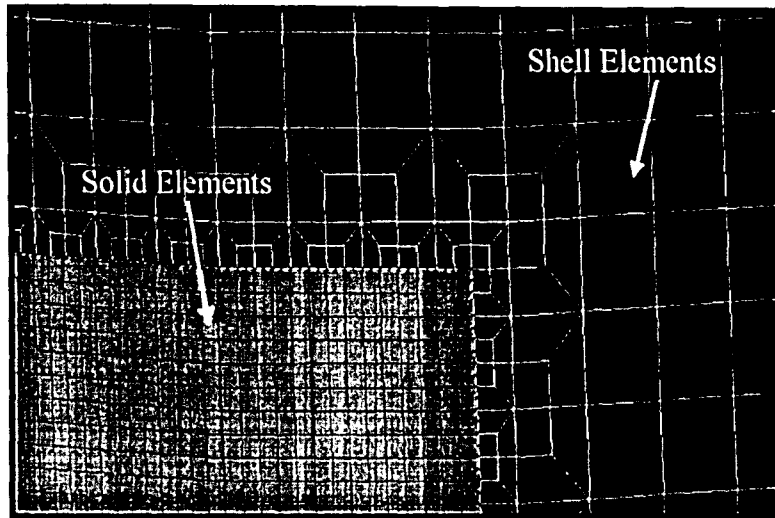


Figure 3.12: Shell to Solid Transition Region Around Part 3

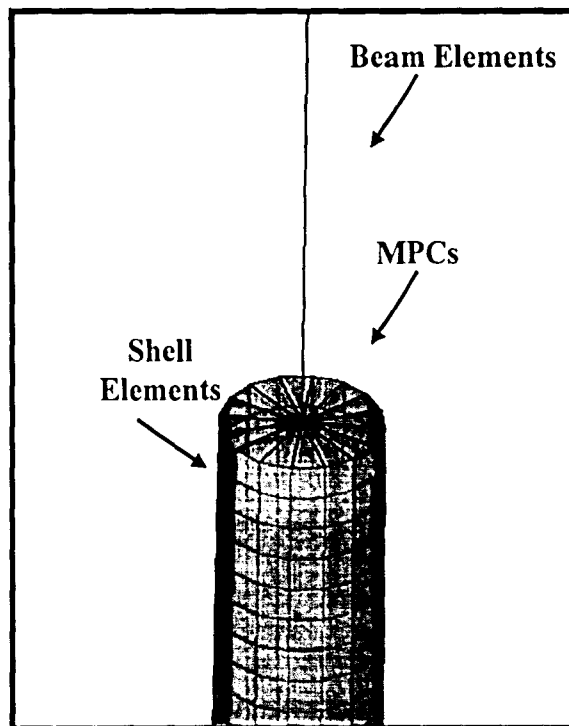


Figure 3.13: Part 4 - Multi-Point Constraints at the Beam-to-Shell Interface

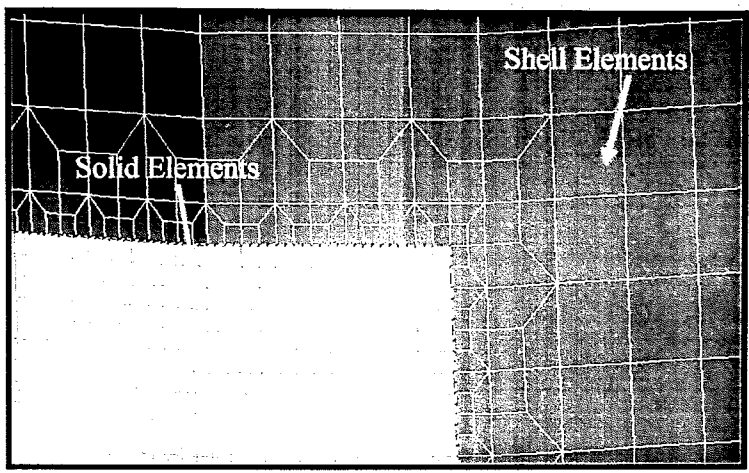


Figure 3.12: Shell to Solid Transition Region Around Part 3

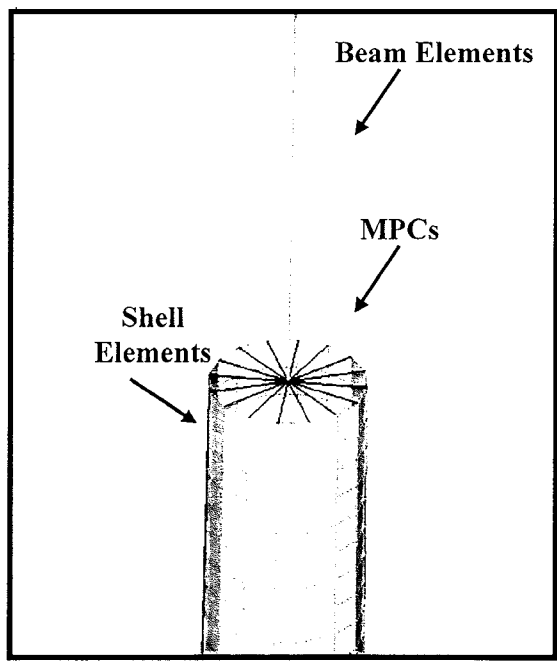


Figure 3.13: Part 4 - Multi-Point Constraints at the Beam-to-Shell Interface

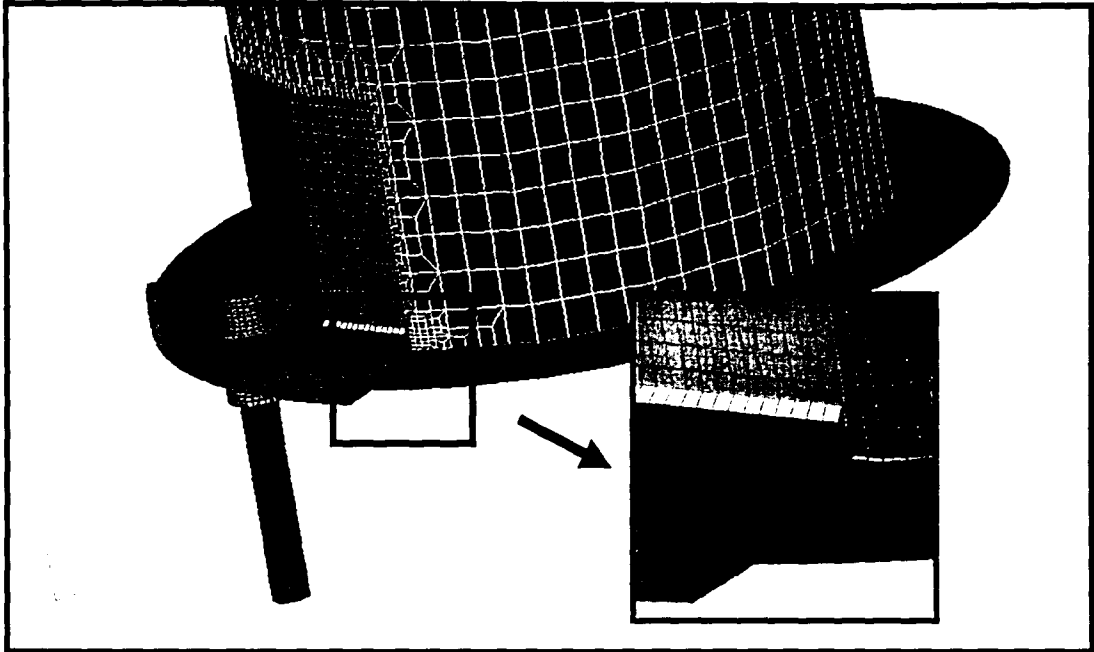


Figure 3.14: Part 4 - Multi-Point Constraints at the Shell-to-Solid Interface

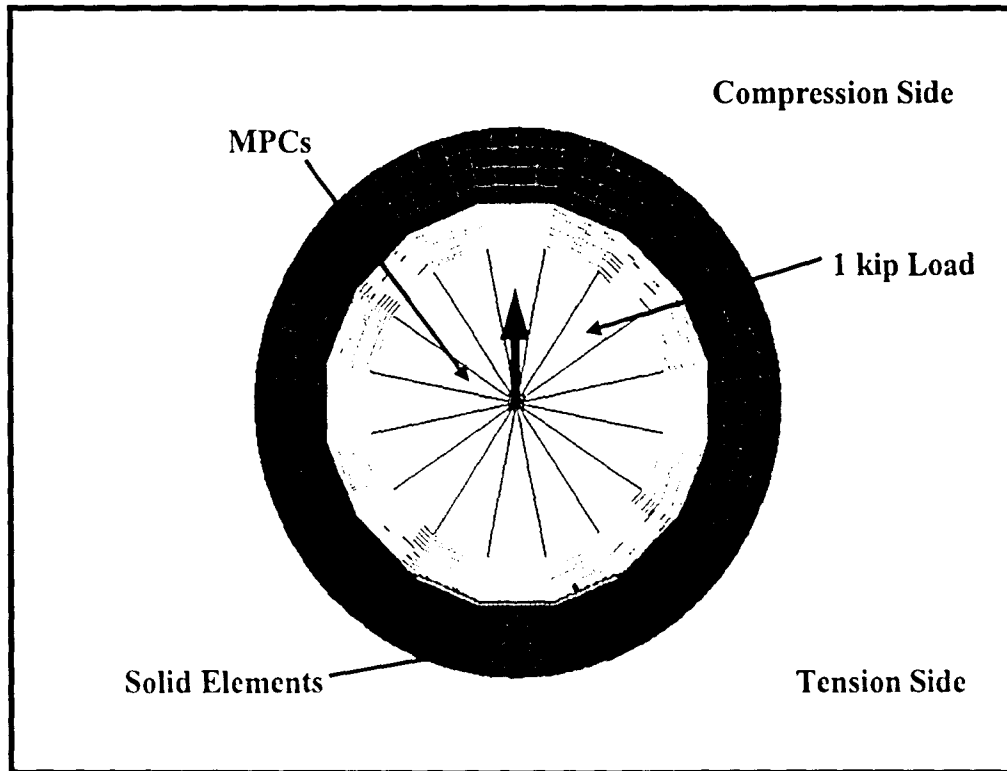


Figure 3.15: Plan View of Point Load Applied to the High-mast Lighting Tower

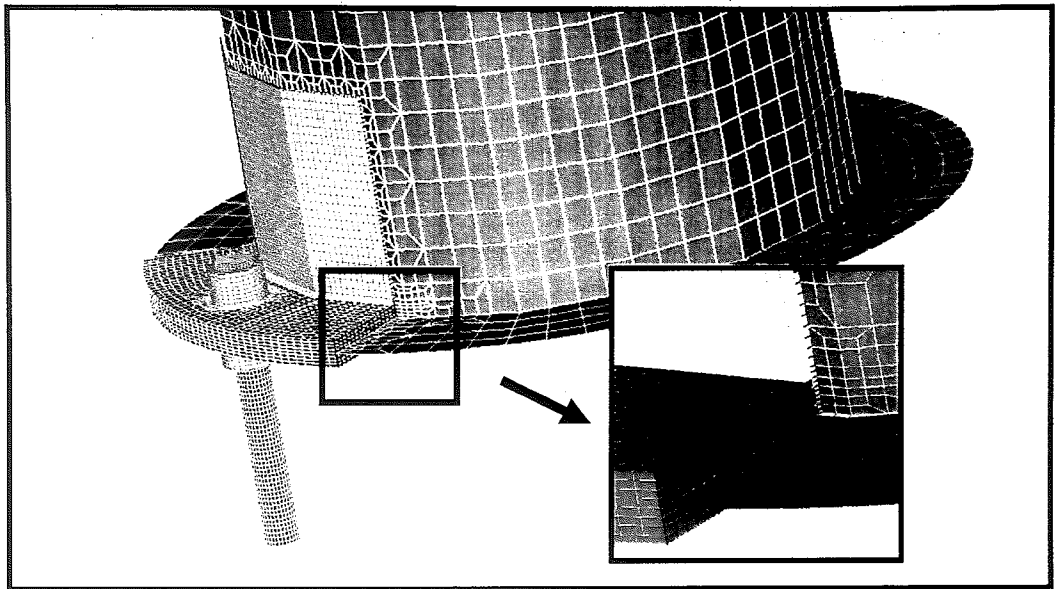


Figure 3.14: Part 4 - Multi-Point Constraints at the Shell-to-Solid Interface

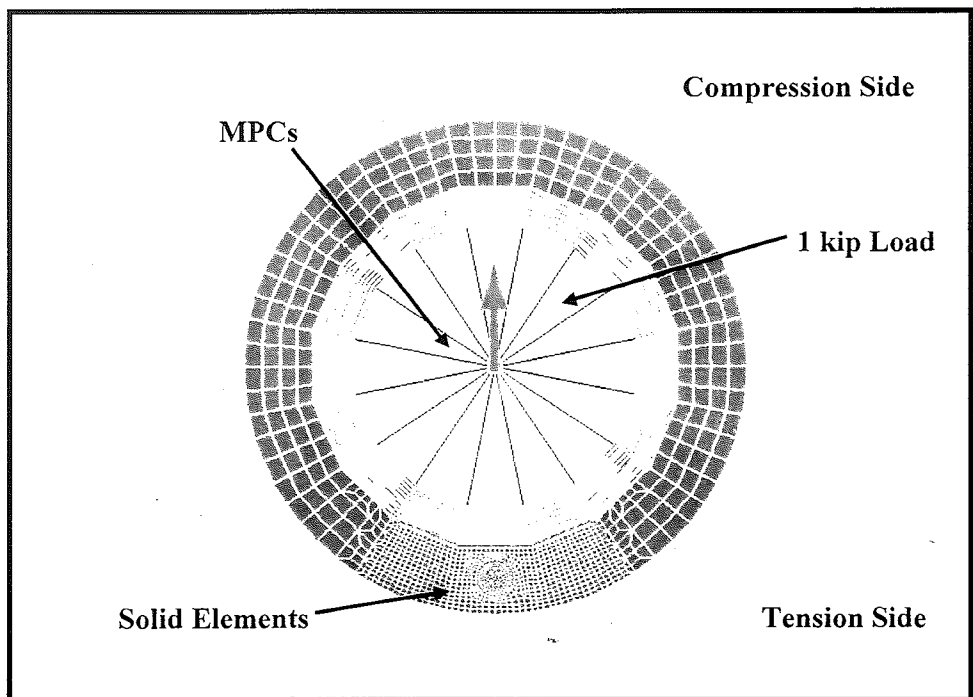


Figure 3.15: Plan View of Point Load Applied to the High-mast Lighting Tower

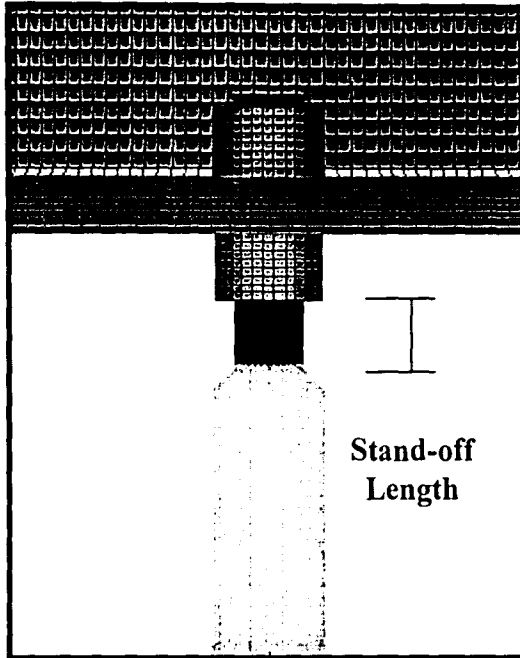


Figure 3.16: Stand-off Length

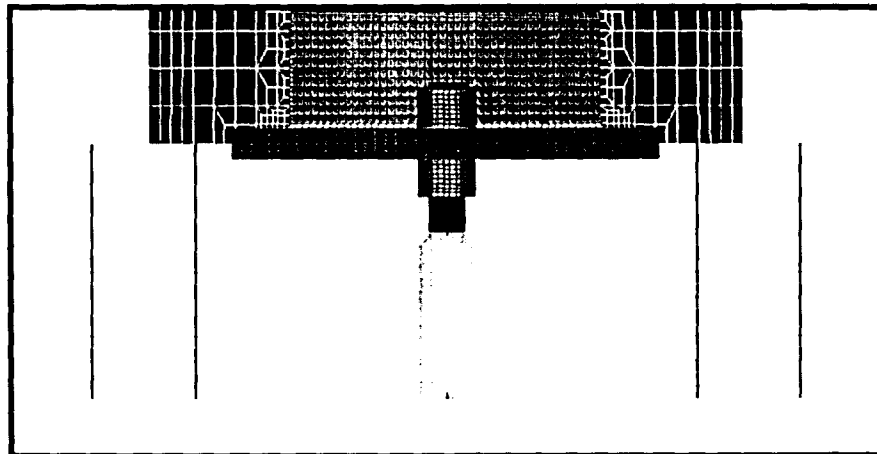


Figure 3.17: Anchor Rods Built of Bar Elements that are Constrained at the Center Line and Anchor Rod Built of Solid Elements that is Constrained along the Outer Surface

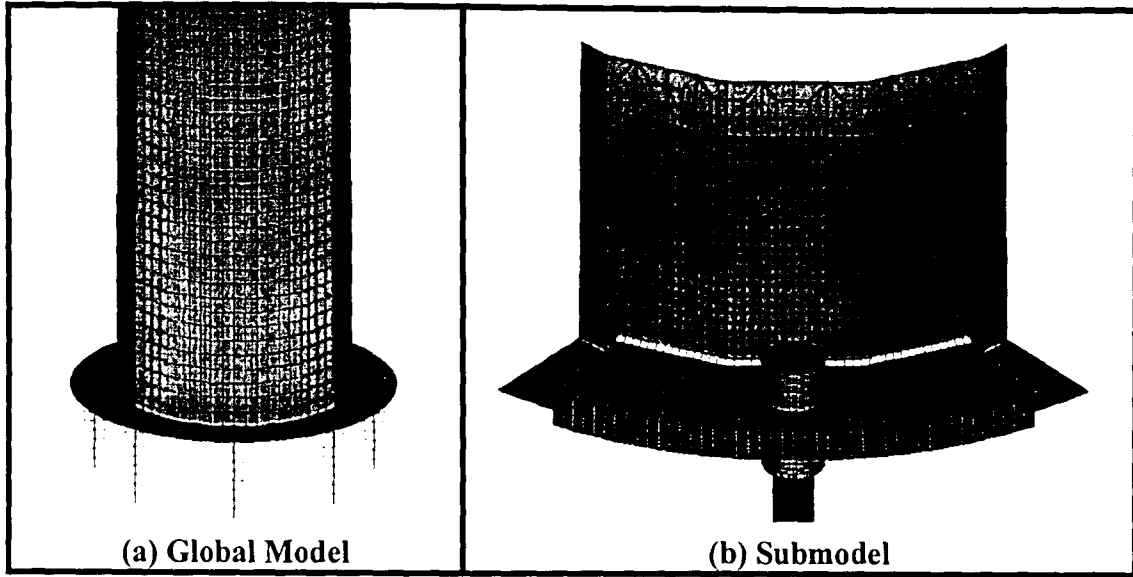


Figure 3.18: Global Model and Submodel

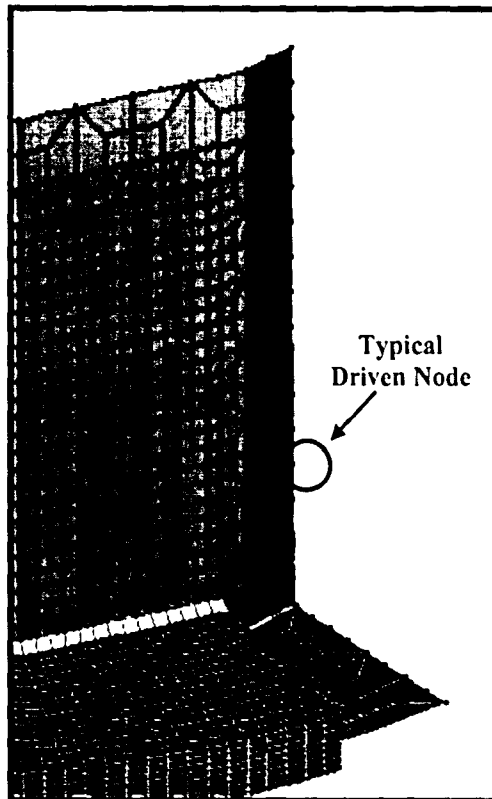


Figure 3.19: Driven Nodes

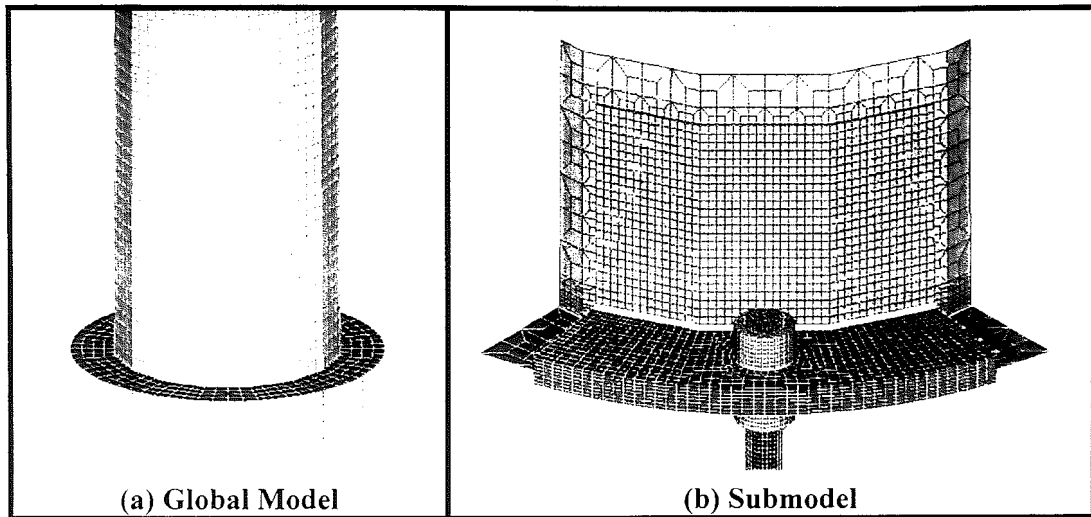


Figure 3.18: Global Model and Submodel

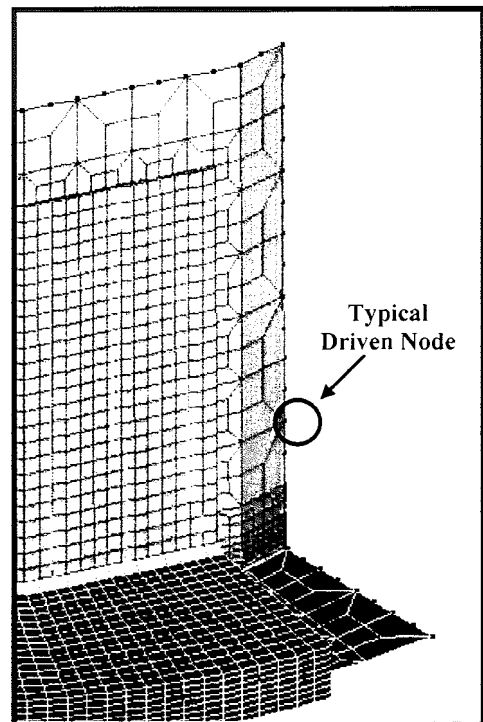


Figure 3.19: Driven Nodes

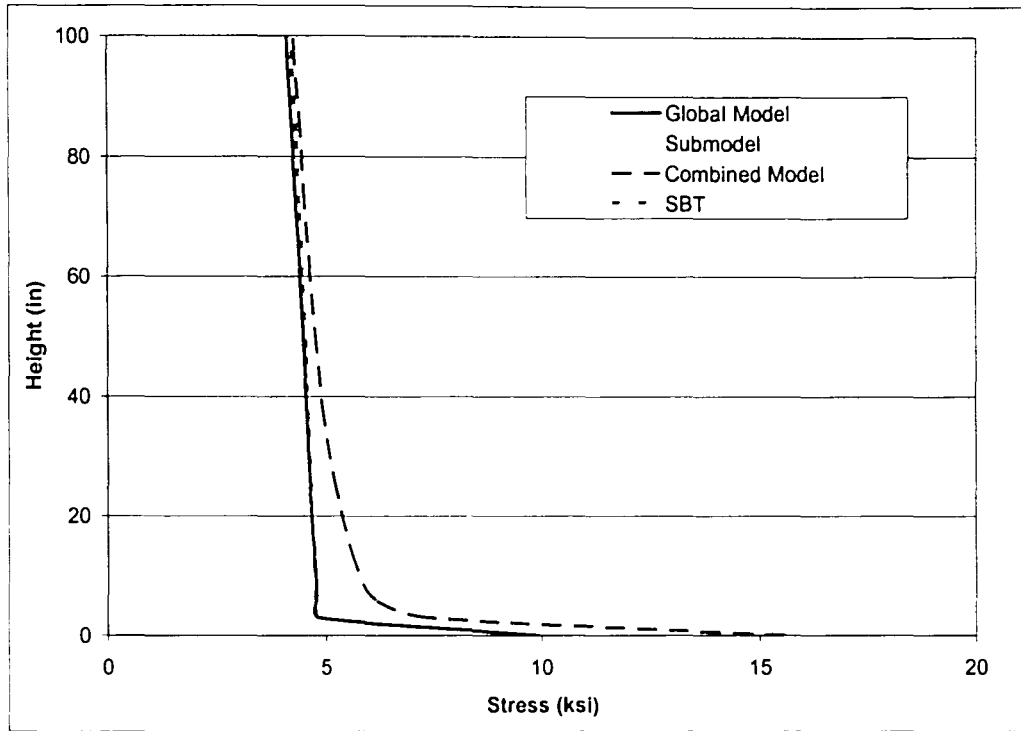


Figure 3.20: Comparison of Results for the Global Model, the Submodel, and the Combined Model

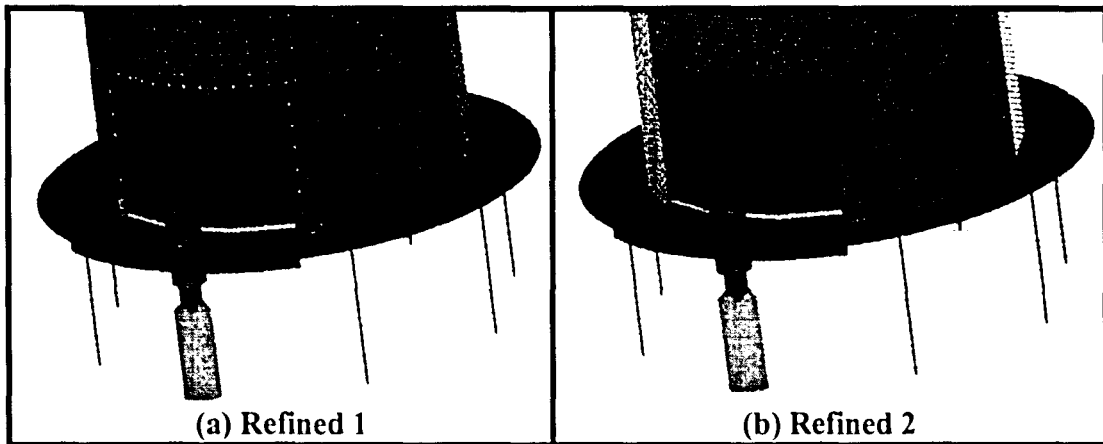


Figure 3.21: Mesh Refinement Studies

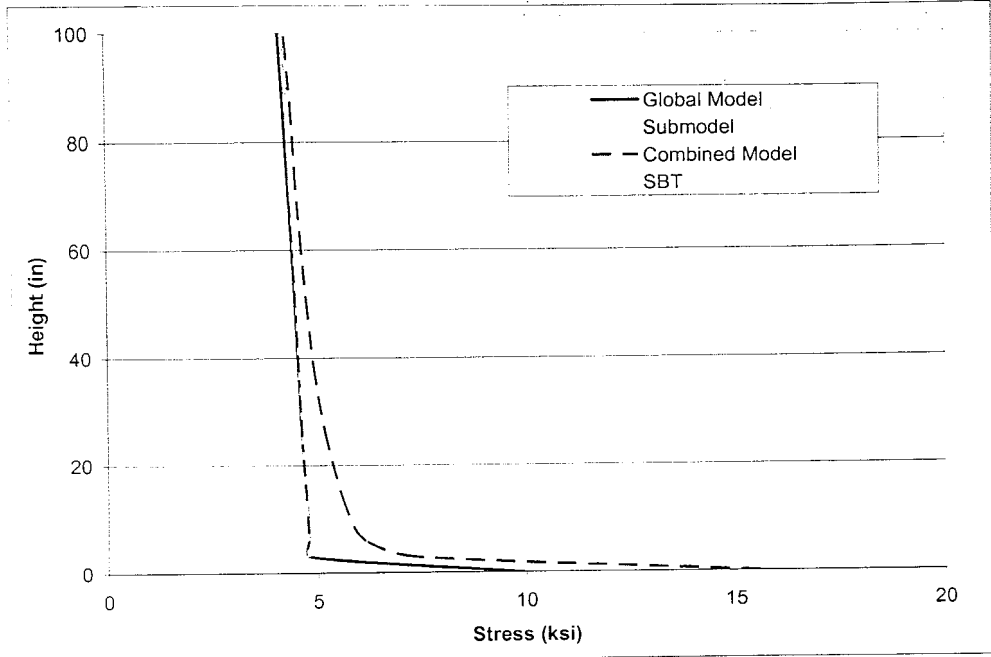


Figure 3.20: Comparison of Results for the Global Model, the Submodel, and the Combined Model

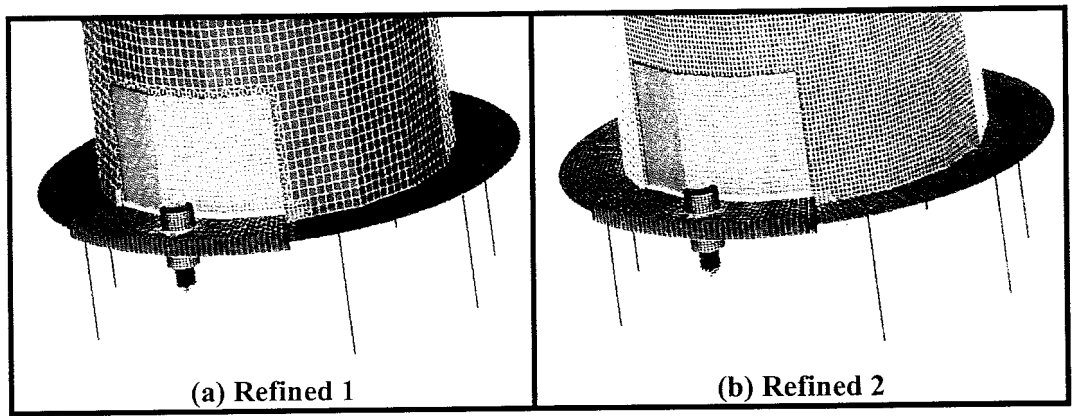


Figure 3.21: Mesh Refinement Studies

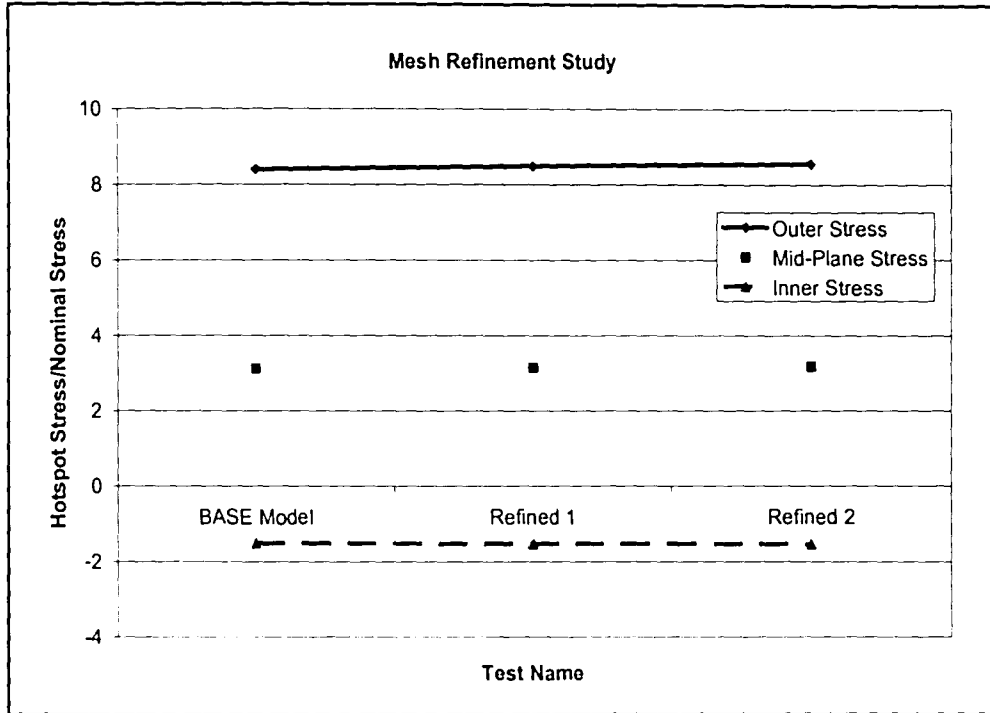


Figure 3.22: Mesh Refinement Study

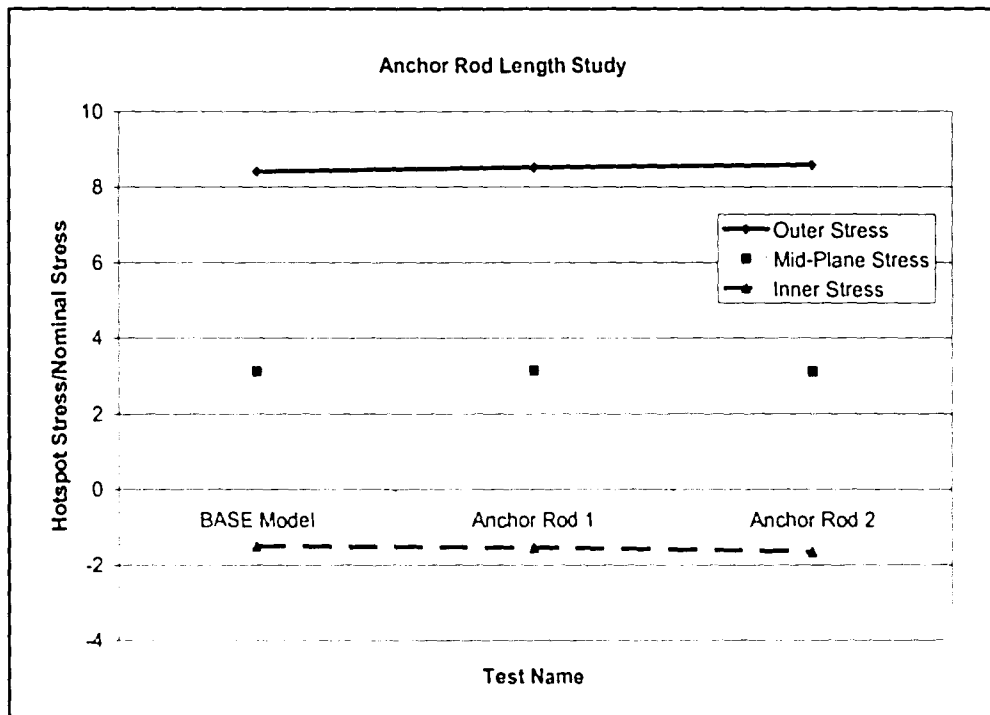


Figure 3.23: Study of the Length that the Anchor Rod is Restrained in the Concrete Foundation

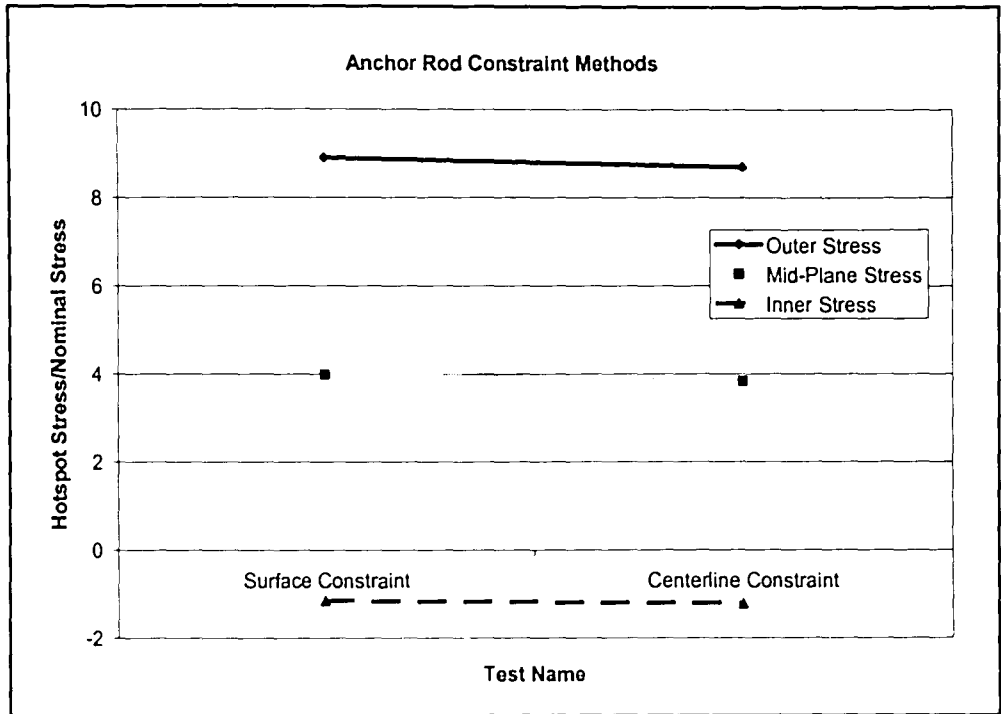


Figure 3.24: Anchor Rod Constraint Study

Chapter 4 Finite Element Parametric Study

4.1 Introduction to the Parametric Study

The purpose of this study is to assess the fatigue performance of high-mast lighting towers based on finite element parametric studies. The performance of the towers with several geometric variations will be evaluated.

It has been found that there are three variables that are important to the design of high-mast lighting towers that are evaluated in this parametric study. They are the base plate thickness, the tube wall thickness, and the number of anchor rods. For the parametric studies, the BASE model was modified to create new models or Cases (as they will be referred to for the remainder of this paper). There are many geometric variables that remain constant during the modeling process and include tower height, tube diameter at the base plate, taper, the number of sides, and the mass of the luminary. This is done in order to isolate the effects of changing any one parameter on the overall stress distribution near the connection. Other variables include the location, magnitude and direction of the applied point load, material properties, the section properties of the top three segments of the tower (modeled as beam elements), and the degree of tightening of the anchor rods and leveling nuts. Table 4.1 lists the values for many of the constant variables. Furthermore, the assumptions made during the creation of the BASE model are the same for this parametric study, including the mesh refinement, the anchor rod constraints, the weld

profile and the stand-off length. Table 4.2 presents the finite element parametric study matrix.

In current fatigue design practice, high-mast lighting towers are designed according to a nominal stress approach presented in the AASHTO code [AASHTO, 2001], as discussed in Section 1.5.1. The towers are designed so that the calculated nominal stress range at the base due to a specified fatigue loading is less than the constant-amplitude fatigue limit (CAFL). For this study, the maximum vertical stress in the tube wall at the weld toe is the area of interest. This region is important because the abrupt change in the cross-section creates an area of high localized stress. As expected, the stresses located at the base plate-to-tube wall connection are higher than the calculated nominal stress from simple beam theory. Because elastic theory can not accurately determine the stresses in this region, experimental tests and more recently finite element analyses, are methods relied upon. Many of the results in this chapter will be presented in terms of a stress amplification factor, which is actually the normalized stress. The stress amplification factor is the maximum hotspot stress, located at the socket connection, for a specific finite element Case normalized to its calculated nominal stress. The amplification factor is simply a multiplier of the nominal stress that can be used for direct comparisons between models with different tube wall thicknesses. Changes in base plate thickness and the anchor rod pattern do not alter the calculated simple beam theory nominal stress.

The maximum hotspot stress will be taken as the stress located at the toe of the vertical weld leg on the tube wall. Based on previous experience, the weld toe is

the best location for comparisons between models. One reason for this decision is that the variation in stress at a set location above the toe of the weld may be different between the models. This occurs because the models have different outer stress gradients. A flexible tower will have a higher stress gradient than a stiffer tower, which means the stress increase a short distance from the weld toe is more significant for the flexible tower. Of interest is the observation that the stress one node above the weld toe is some times slightly larger than the stress at the weld toe. This will be discussed in more detail at the end of this Section. Due to the slight difference in stress gradients, the location of maximum vertical stress obtained from the models will be taken at the weld toe.

The maximum hotspot stresses in multi-sided towers occur at the fold in the tube wall because of the abrupt change in cross-section. The location of the hotspot stress in a circular tube section is different, it varies as the geometric parameters change [Hall, 2005]. There are two regions of interest in this parametric study. The first is the folds on the front side (or tension side) of the tube. For consistency, results will always be taken from the fold on the left when facing the tension side. The second area of interest is the center of the front side. The reason for extracting results from this region is to assess the distribution of stress between the fold and the front side as the geometric parameters are altered. Figure 4.1 is a plan view of the tension side of the multi-sided high-mast tower used in this parametric study. This fold and the center of the front side are identified.

Presented in Figures 4.2 and 4.3 are vertical stress profiles extending up the tube wall several inches for Case 1, the BASE model. Case 1 has a base plate thickness of 1.25" and a tube wall thickness of 3/16". The first Figure presents the vertical stress along the fold and the second Figure presents the vertical stress along the center of the front face. Both profiles are plots of stress on the tension side of the high-mast tower beginning at the tip of the weld toe. The outer, inner, mid-plane, and local bending stresses in the tube wall presented. The outer stress, as its name would imply is the stress on the outer surface of the tube. Similarly, the inner stress is the stress on the inside surface of the tube. The mid-plane stress is the stress in the center of the tube wall. The stress in the tube wall varies linearly, which means that the mid-plane stress is actually the average of the outer and inner stresses. The bending stress is the difference between the mid-plane stress and either the outer or the inner stress. Both differences are the same value. The sign convention used for this study is that a positive bending stress corresponds to the outer wall experiencing tension while the inner wall is in compression. Also included in the figures is the calculated outer nominal stress predicted by simple beam theory.

There are three distinctive locations along the stress profiles that are typical features in all Cases. They have been labeled as (a), (b), and (c) on Figures 4.2 and 4.3. Location (a) is the location at the weld toe. At this point, the outer and inner stresses vary greatly. This is the location of the greatest stress concentration, or in other words the location in which the actual measured stress varies drastically from the predicted simple beam theory nominal stress. Location (b) has been referred to

as the valley stress by Hall and Koenigs [Hall, 2005] [Koenigs, 2003]. At this point, the outer stress is at its most compressive and the inner stress is at its most non-compressive value. Location (c) is the region where the stress begins to converge with the predicted simple beam theory nominal stress.

A general observation made from a direct comparison between the two stress profiles is that the stress near the weld toe on the fold is much higher than the stress on the center of the front side face at the same vertical height. The stress profile along the fold has a much higher stress gradient and rapidly approaches the simple beam theory stress. The outer valley stress along the fold occurs at a height of 2" above the base plate. The stress profile along the center of the front face has a lower gradient and does not reach the valley stress until a height of 4" above the base plate.

Of particular interest is that the stress slightly above the weld toe at the center of the front face, as shown in Figure 4.3, is higher than the stress at the weld toe. This trend is also present in other Cases. The lower stress at the weld toe may be due to the increase geometric properties at this location. Although the stress is elevated in this region, it is not the location of maximum vertical stress. It is possible that the increased stress directly above the weld toe is due to the distribution of stress in the tube wall away from the folds. The vertical stress profiles for Cases 2 through 18 are presented in Appendix A. Profiles are presented for both locations of interest, i.e., along the fold and along the center of the front side.

Figures 4.4 and 4.5 are contour plots of vertical stress in the tube wall. Figure 4.4 presents the results for Case 1 (1.25" base plate and 3/16" tubewall) and

Figure 4.5 presents the results for Case 13 (1.25" base plate, 1/2" tubewall). Figure 4.4 clearly shows the distribution of high stress away from the folds and towards the center of the front face. An arched elevated stress region is formed at the center of the front side. At a height of one inch above the base plate, the stress at the fold is lower than the stress at the center of the front side. Note that the center of the front side is also the side of maximum tension. The stress increases along the outer edges of the solid model should be disregarded as they are due to the shell to solid transition. This stress distribution is also apparent in Case 13 (Figure 4.5), although not as prominent. The maximum vertical stresses located at the intersection of the fold and the weld toe are lower for a model with a thicker tube wall or base plate. Therefore, the stress distribution to the center is not as great and the arch is not as steep.

Figure 4.6 shows a general radial plot of outer vertical stresses for a typical multi-sided high-mast tower at several heights, 0.75", 1.5" and 6.0" above the top of the base plate. Also included in this plot is the calculated simple beam theory nominal stress. The stresses are presented in absolute values for clarity and the tension and compression sides are labeled. There is symmetry of the stress distribution about the bending axis and about the neutral axis. This symmetry is expected because the multi-sided tower is symmetric about the same axes. Note that the four folds, two on the tension side and two on the compression side, have the highest stress values at 0.75" above the base plate. At a height of 1.5", the stress in the tube wall decreases. Of interest is that the stresses located on those four folds

have drastically decreased and are now lower than the stresses at the center of the front (tension) and back (compression) sides. The stress in the tube wall is even lower at a height of 6.0" above the base plate. At this point, the stresses are approaching the predicted simple beam theory nominal stress. Figure 4.7 is a radial plot of the outer stress at 6.0" and the predicted simple beam theory nominal stress. Although simple beam theory can accurately predict the maximum tube wall stresses a good distance away from the base plate-to-tube connection, it can not account for the multi-sided tube and over-estimates the stress at locations 45 degrees on either side of the maximum tension and compression sides.

Figure 4.8 shows the radial distribution of the outer vertical stress in the solid portion of the Case 1 model at the intersection of the vertical weld leg and the tube wall. The stresses at the fold are higher than the stresses at the center of the front side at the socket weld connection which was previously determined from the stress profiles at the two locations. The radial graphs are another way to compare the stresses at different locations around the tube wall and they will be used in the next couple of sections.

4.2 Base Plate Thickness Study

The first parametric study performed was the base plate thickness study. Its purpose was to evaluate the effect of altering the base plate thickness on the vertical tube wall stress. Two base plate thickness studies were conducted. Study A varied the base plate thickness of a model with a tube wall thickness of 3/16". The base plate thicknesses ranged from 1.0" to 6.0" and the list of Cases is presented in Table

4.3. (It is recognized that a base plate thickness of 6 inches is unreasonable, but it provides a good upper bound for the parametric study in order to fully characterize the influence of this parameter) The second study, Study B, varied the base plate thickness of a model with a 1/2" tube wall thickness. It was analyzed with varying base plate thicknesses as shown in Table 4.4. In addition to evaluating the vertical tubewall stress as a function of the base plate thickness, the two trends from the base plate studies can be compared. This comparison shows the effect of tube wall thickness on the vertical tube wall stress. This Section will first look at the stresses at the fold location. Results from Studies A and B will be presented and then a comparison will be made between the two. After presenting the results from the fold, the results at the center of the front side will be the focus of discussion. The results from both studies will then be presented followed by a comparison of Studies A and B.

The results of Study A are presented in Figures 4.9 and 4.10. Figure 4.9 is a plot of the outer, inner, and mid-plane maximum (also called the hotspot stress) stresses as a function of base plate thickness. This plot shows the hotspot stress decreasing with increasing base plate thickness. The outer hotspot stress of a model with a 1.0" thick base plate can be decreased from approximately 45 ksi to approximately 15 ksi by increasing the base plate thickness to 6.0". However, that drastic of a change may not be necessary. It is observed that the effect of changing the base plate thickness begins to level off at a thickness of 3.0", which would suggest that 3.0" is an optimum thickness for these high-mast lighting towers and

that further increase in base plate thickness does not offer significant additional reduction in stress.. Figure 4.10 is the same plot as Figure 4.9, with the exception that the hotspot stress is normalized with the predicted simple beam theory nominal stress. The nominal stress for a tower with a 3/16" tubewall thickness is 4.8 ksi.

Figures 4.11 and 4.12 are plots of the hotspot stress and the normalized stress, respectively, as a function of the base plate thickness for Study B (i.e., models with a 0.50" tube wall thickness). The results for this study are similar to Study A, as they both have similar trends of decreasing tube wall stress with increasing base plate thickness. These Figures also show that the benefit of increasing base plate thickness begins to diminish at a base plate thickness of 3.0". The calculated nominal stress for Study B is 1.8 ksi. The trend shown in Figures 4.9 through 4.12 would suggest that drastically increasing the base plate thickness would decrease the localized stress in the high-mast towers and thus improve the fatigue life.

Figure 4.13 is a comparison of the maximum outer tube wall stresses for both Study A and B at the fold in the tube. As expected, a thicker tube wall decreases the stress concentration at the fold and would support increasing the tube wall thickness. Although the magnitude of the stress is lower for the thicker tube wall, the amplification factor is increased, as shown in Figure 4.14. This figure may suggest that a lower ratio of tube wall thickness to base plate thickness would be ideal. As discussed by Hall, this increase in amplification factor may be caused by a stiff tube wall that sheds load to the adjoining base plate [Hall, 2005]. Hall also concluded that changes in tube wall thickness do not have as significant effect as does altering

the base plate thickness. These findings were confirmed in this parametric study and will be discussed in more detail in Section 4.3, the Tube Wall Thickness Study.

Shifting the focus to the center of the front side, Figures 4.15 to 4.18 present the results of Studies A and B at this particular location. Again, the results are presented in terms of the actual observed hotspot stresses and the normalized hotspot stresses. Figure 4.19 is a comparison of the hotspot stresses for Studies A and B, at the center of the front face, versus the base plate thickness. The maximum stresses in Studies A and B fall in the same region for flexible base plates (thicknesses less than 3.0"). However, the stresses in the tube wall in the 3/16" model (A) are higher than the 1/2" model (B) when the base plate is more rigid (thickness greater than 2 1/2 inches). Figure 4.20 presents this same comparison with the exception that the maximum vertical stresses are normalized with the predicted simple beam theory nominal stresses. As previously seen in Figure 4.14, the normalized vertical stresses in Study B (thickness of 1/2") are higher than Study A (thickness of 3/16"). Once again, this seems to suggest that the tube wall thickness is not the geometric parameter with the greatest influence, and that a lower ratio of tube wall to base plate thickness is desirable.

Comparisons of the two normalized maximum vertical stress locations, at the fold and at the center of the front side, are presented in Figure 4.21. Only the results from Study A are presented, as the trends are similar. As predicted, the maximum stresses at the fold are significantly higher than at the center of the front side. The difference in stress between the two locations can also be observed in contour plots

from Case 1 (Study A) and Case 13 (Study B). The contour plots, as previously discussed, are shown in Figures 4.4 and 4.5.

The differences in stress at the two locations of interest for different base plate thicknesses are also presented in the form of radial plots. Figure 4.22 presents a comparison of the outer vertical stresses in the solid portion of the tube wall for Cases 1 (1.25" base plate) and 6 (3.0" base plate). This plot demonstrates the benefit of increasing the base plate thickness. The vertical stresses around the front portion of the tube wall in Case 6 are simply scaled down from Case 1. There is no change in the general shape of the curve (i.e., there is no change in general behavior).

4.3 Tube Wall Thickness Study

Several parametric studies addressed the effect of the tube wall thickness on the maximum vertical stress in the tube wall. The first studies, as mentioned in the previous section, compare the maximum stress trend due to changing base plate thicknesses for high-mast towers with two different tube wall thicknesses (Study A and Study B). The third study, Study C, varies the tube wall thickness of a model with a constant base plate thickness of 1.25". Table 4.5 is a summary of Study C, the tube wall thickness study. This study consists of four models with tube wall thicknesses of 3/16", 5/16", 1/2" and 5/8".

The purpose of the tube wall thickness study was to determine if altering the tube wall thickness would reduce the flexibility of the base plate and alter the stress distribution. A thicker tubewall will always reduce the stress in the tubewall because

the moment of inertia is increased, thus the nominal stresses are decreased. Figure 4.23 shows the relationship between the measured hotspot stress and the tube wall thickness at the fold in the tube wall. As expected, the stress in the tube wall decreases with increasing tube wall thickness, however the decrease is not as drastic as was seen in the base plate thickness studies (Studies A and B). Conversely, Figure 4.24, which presents the relationship between the normalized hotspot stress and tube wall thickness at the fold in the tube wall, shows that the amplification factor is increased as the tube wall thickness is increased. Figures 4.25 and 4.26 present the results for Study C at the center of the front side. Figure 4.25 presents the stress in the tube wall as a function of tube wall thickness. Figure 4.26 presents the normalized hotspot stress as a function of the tube wall thickness and demonstrates the same trend seen in Figure 4.24. Note that each Case was normalized with its respective nominal stress. The trend of increasing amplification factor with increasing tube wall thickness was previously observed in the base plate thickness study as shown in Figures 4.14 and 4.20 and discussed in Section 4.2.

Figures 4.27 and 4.28 present the effects of increasing the tube wall thickness with radial plots. The first plot, Figure 4.27, graphs the stresses for Cases 1 (3/16" tube wall) and 13 (1/2" tube wall). Figure 4.28 graphs the ratio of localized stress at the weld toe to the predicted simple beam theory nominal stress (also called the amplification factor) for Cases 1 and 13. Once again, the stresses in the tube wall decrease with increasing tube wall thickness and the amplification factors increase. Note that the shape of the radial stress profile between the two Cases is different.

This did not happen when the base plate thickness was increased, as presented in Figure 4.22. It is believed that this change in profile shape is due to the fact that the thicker tube wall more evenly distributes the stress in the tube wall away from the folds and towards the center of the front side.

There are several ways of looking at the tube wall thickness phenomenon. First, a thick, rigid tube wall applies more load to the base plate than a thin, flexible tube wall. Secondly, the base plate is not able to resist the increased load due to a stiffer tube and the deformation of the base plate increases [Hall, 2005]. Larger deformations cause larger stresses in the base plate and reduce the fatigue resistance. Although the stresses in the tube wall have been decreased, the base plate flexibility has not been decreased. When the tube wall is thick, stresses are distributed to the base plate, which effectively decreases the stress in the tube wall, but increases the stress in the base plate and the deformations. Proportionately increasing the base plate thickness as the tube wall is increased would decrease the flexibility of the high-mast tower. Previous finite element studies had similar results and suggested that the tube wall thickness does not have a significant effect on the flexibility of the base plate.

4.4 Anchor Rod Studies

The purpose of the anchor rod studies is to assess the number of anchor rods used to attach the high-mast towers to the concrete foundation and to determine if the 8 rod combination used for the Sioux City, Iowa tower is adequate. Several anchor

rod patterns are used in current practice, including 4, 6, and 8 rod combinations. This study evaluates anchor rod patterns with 4, 8, and 16 anchor rods. Two anchor rod studies were performed. Study D, described in Table 4.6, varies the number of anchor rods for a model with a 1.25" thick base plate and a 3/16" thick tube wall. Study E, presented in Table 4.7, varies the number of anchor rods for a model with a 3.0" thick base plate and a 3/16" tube wall thickness. Similar to the previous parametric studies, the results for the parametric studies are presented by location. First the normalized hotspot stresses at the fold are presented for Studies D and E, and then the normalized hotspot stresses at the center of the front side are presented.

Figure 4.29 presents the normalized hotspot stresses at the fold for Studies D and E. All of the models have a predicted simple beam theory nominal stress of 4.8 ksi. As expected, increasing the number of anchor rods on the tower with a base plate thickness of 1 1/4" decreases the normalized vertical tube wall stress, or the amplification factor, as presented in this figure. However, the opposite effect is observed for the tower with a base plate thickness of 3.0", though the increase is relatively small. It is believed that the trend of increasing hotspot stress (at the fold) with increasing number of anchor rods for the tower with a 3.0" base plate is due to the decreased flexibility of the base plate. Note that the added benefit of doubling the number of anchor rods from 8 to 16 is not very significant and there is a greater difference in the fold region between the 4 anchor rod and 8 anchor rod configurations for both base plate thicknesses.

Figure 4.30 presents the normalized hotspot stress at the center of the front side for both studies. In this Figure, the normalized hotspot stress decreases as the number of anchor rods is increased for Studies D and E. It appears that increasing the base plate thickness does not have an adverse effect on the hotspot stresses in this region of the tower. It can also be observed that the difference between the 4 and 8-rod configurations is reduced as the base plate thickness is increased. This is also believed to be caused by the increased rigidity of the thicker base plate.

Both studies validate the 8 anchor rod configuration currently in use. Although a 16 anchor rod configuration may slightly decrease the tube wall stresses, the added cost of this configuration is not justified. Additionally, for a tower with a thicker base plate, even though the maximum tube wall stress along the fold increases as the number of anchor rods increases, this increase is minimal and a more significant decrease occurs at the center of the front face. Therefore the use of a 4 rod configuration is not recommended.

Table 4.1: Constant Variables for the Finite Element Parametric Study

Parameter	Value
Tower Height	140'
Diameter at Base	24.75"
Taper	0.001173 in/in
Number of Sides	16
Load	1 kip
Direction of Load	Perpendicular To Front Face
Luminary Mass	1.911917 lbm

Table 4.2: Finite Element Parametric Study Matrix

Case	Base Plate Thickness (in)	Tube Wall Thickness (in)	Number of Anchor Rods
1 – BASE Model	1.25	0.1875	8
2	1.00	0.1875	8
3	1.50	0.1875	8
4	2.00	0.1875	8
5	2.50	0.1875	8
6	3.00	0.1875	8
7	6.00	0.1875	8
8	1.00	0.50	8
9	2.00	0.50	8
10	3.00	0.50	8
11	6.00	0.50	8
12	1.25	0.3125	8
13	1.25	0.50	8
14	1.25	0.625	8
15	1.25	0.1875	4
16	3.00	0.1875	4
17	1.25	0.1875	16
18	3.00	0.1875	16

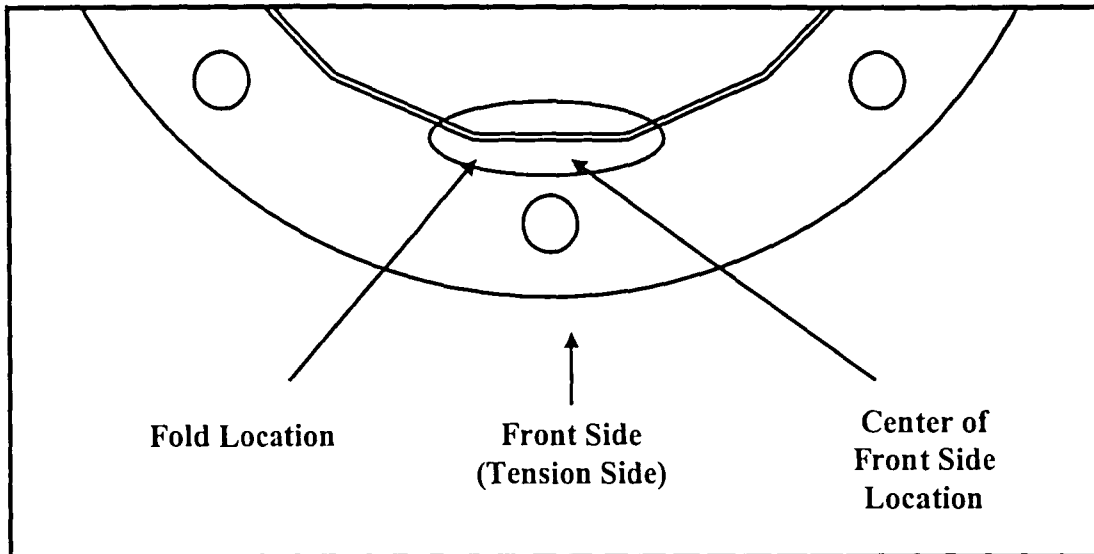


Figure 4.1: Plan View of High-Mast Tower Base Including the Direction of the Applied Load

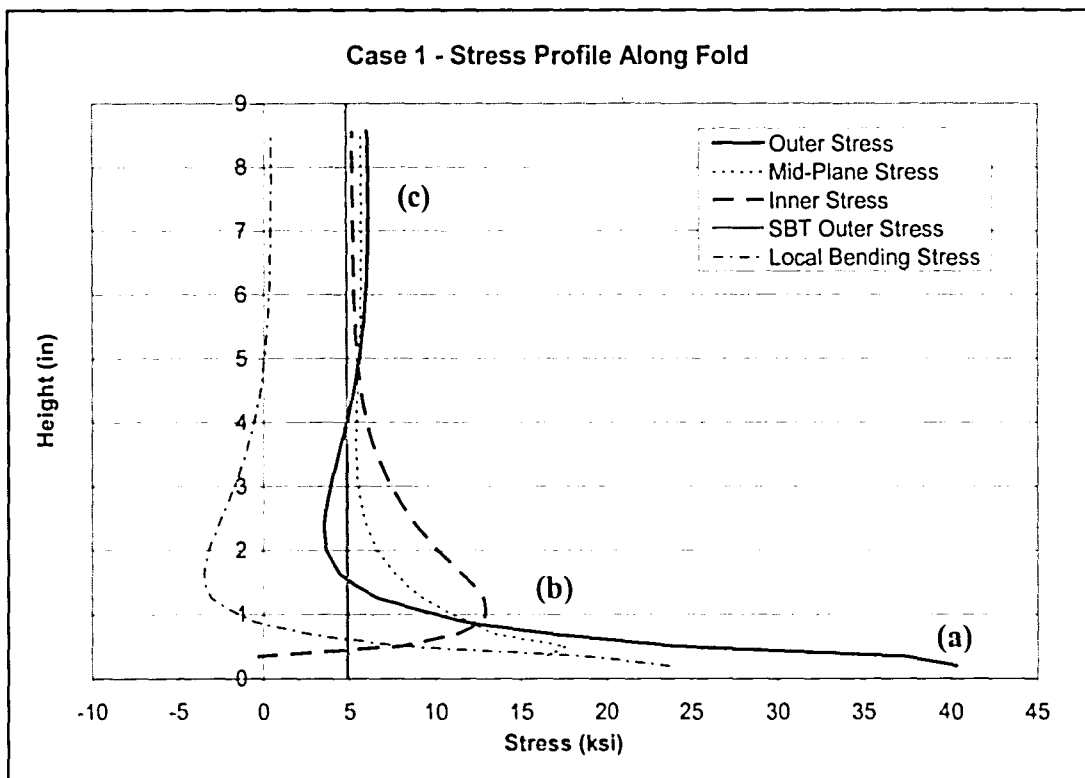


Figure 4.2: Case 1 Vertical Stress Profile Along Tube Wall Fold

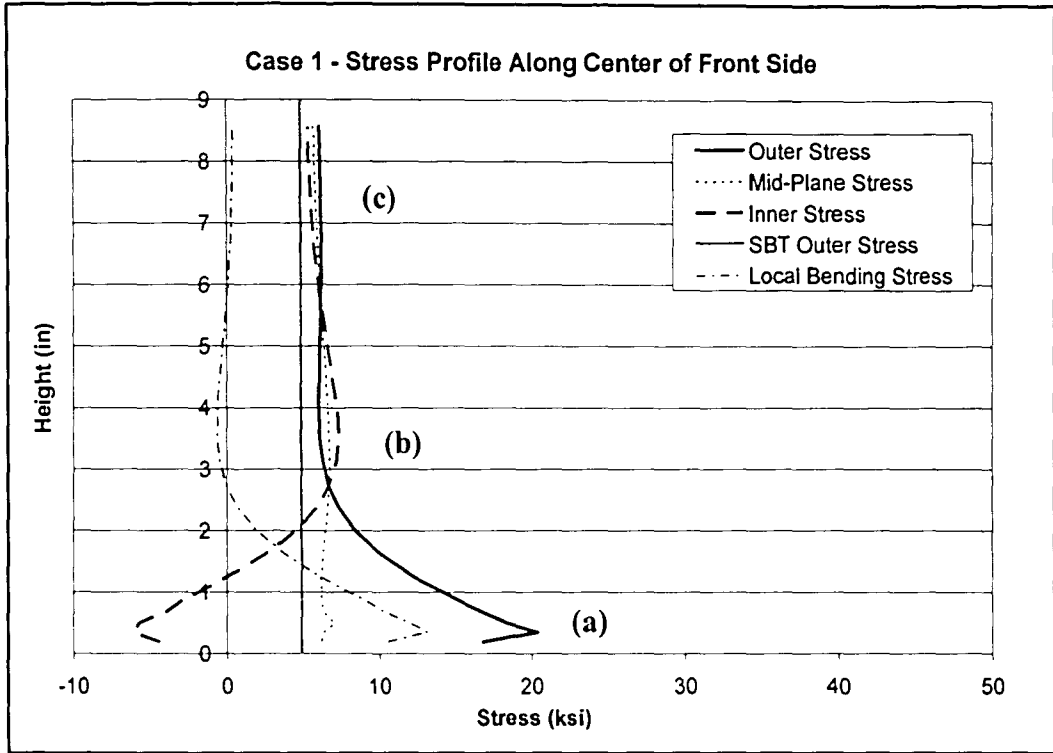


Figure 4.3: Case 1 Vertical Stress Profile Along The Center of the Front Face of Tube Wall

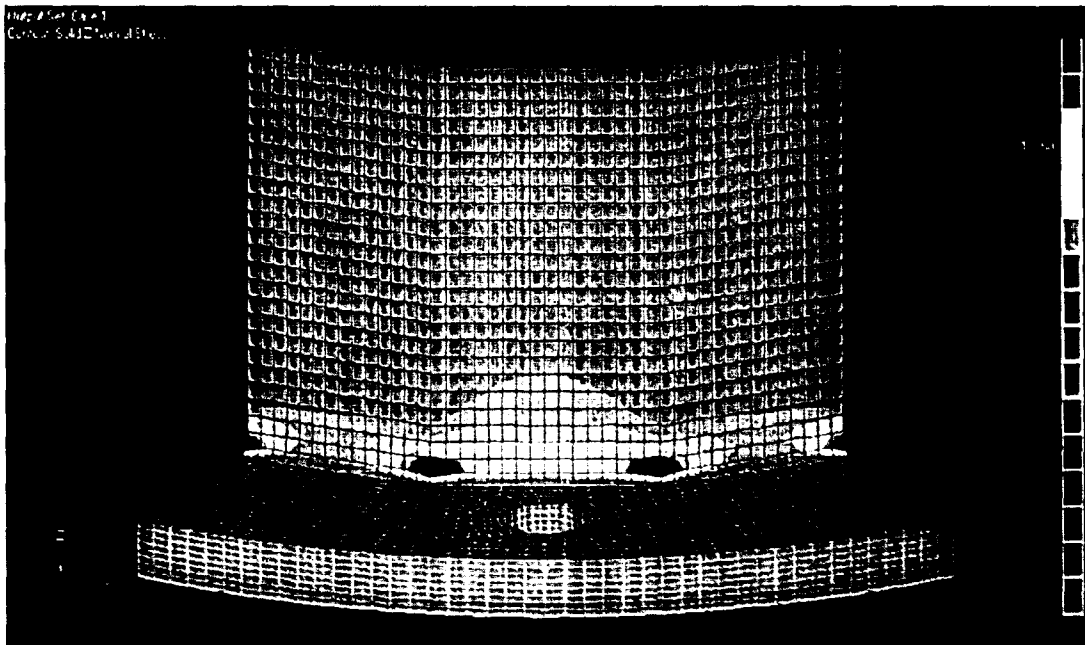


Figure 4.4: Case 1 Vertical Stress Contour Plot

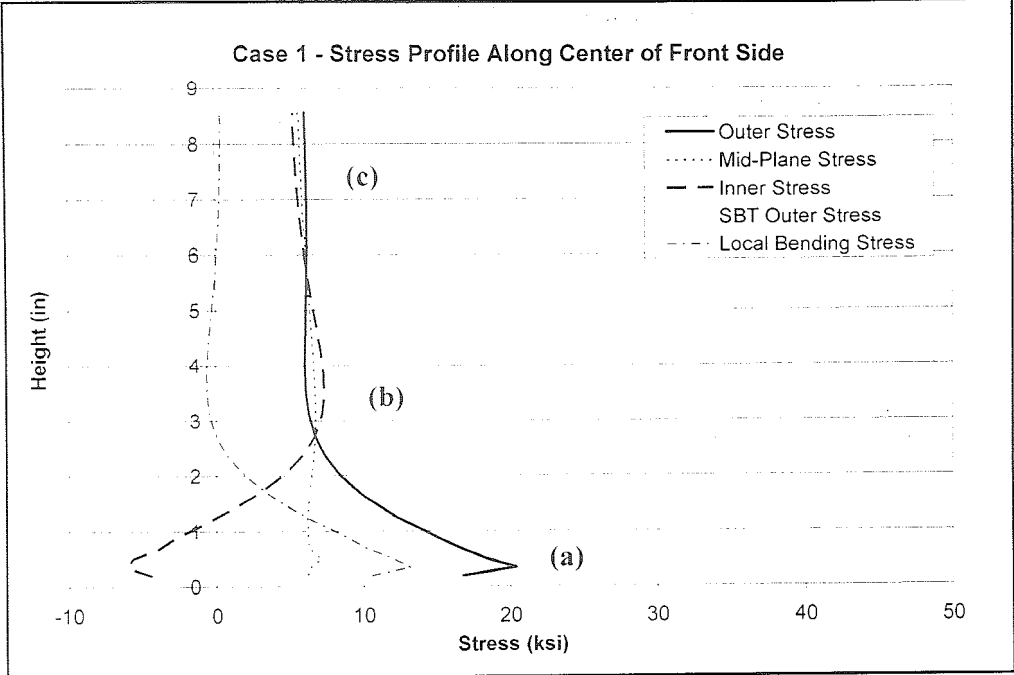


Figure 4.3: Case 1 Vertical Stress Profile Along The Center of the Front Face of Tube Wall

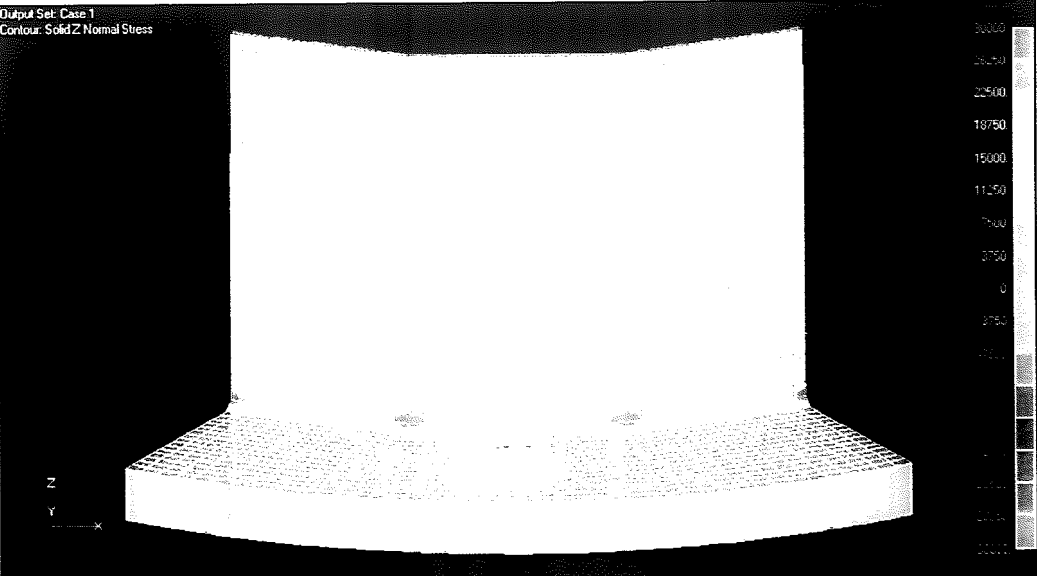


Figure 4.4: Case 1 Vertical Stress Contour Plot

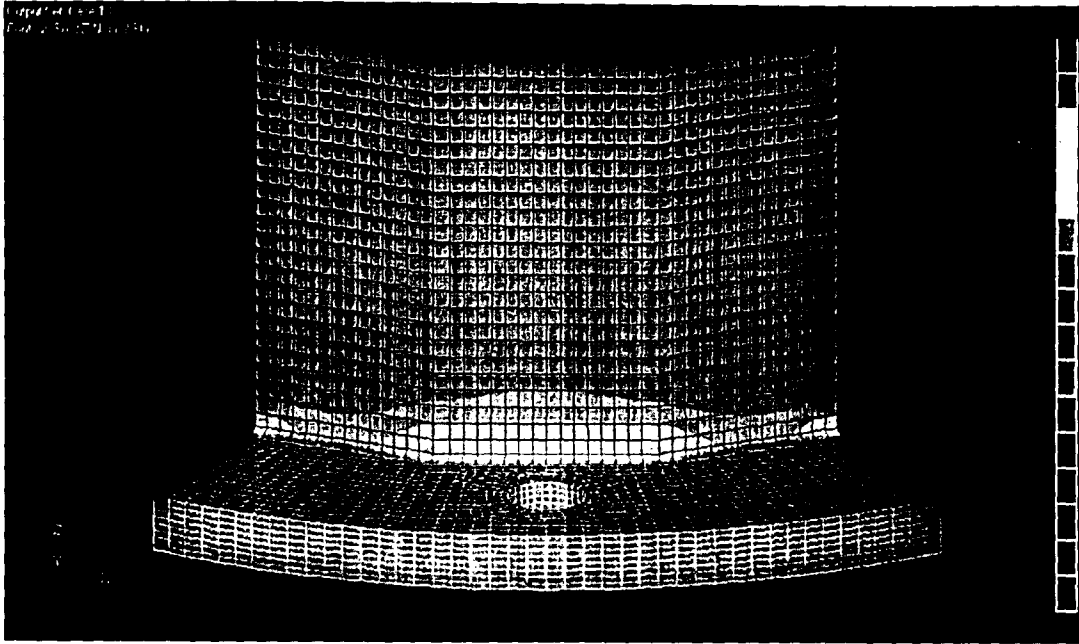


Figure 4.5: Case 13 Vertical Stress Contour Plot

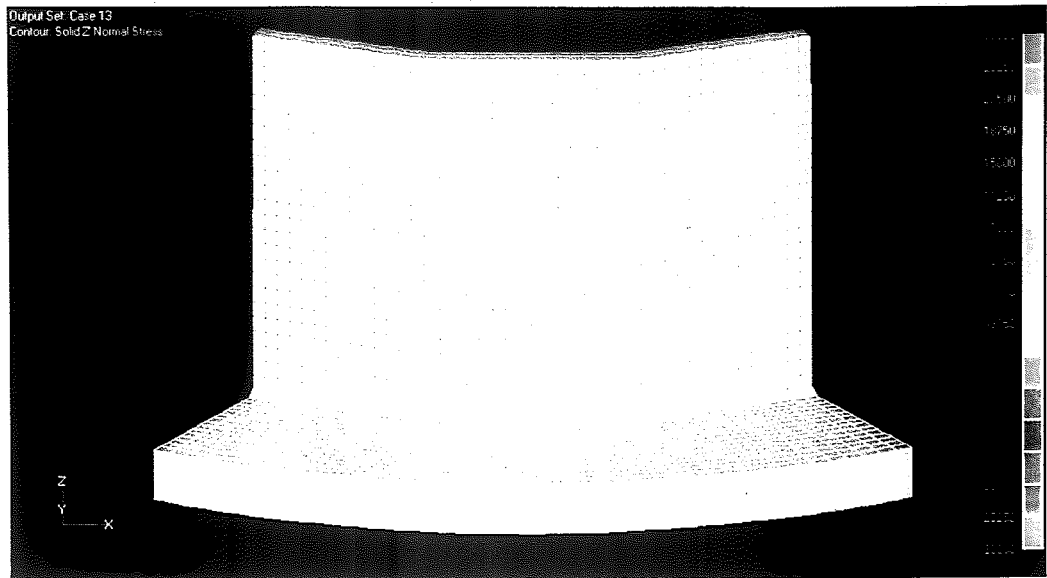


Figure 4.5: Case 13 Vertical Stress Contour Plot

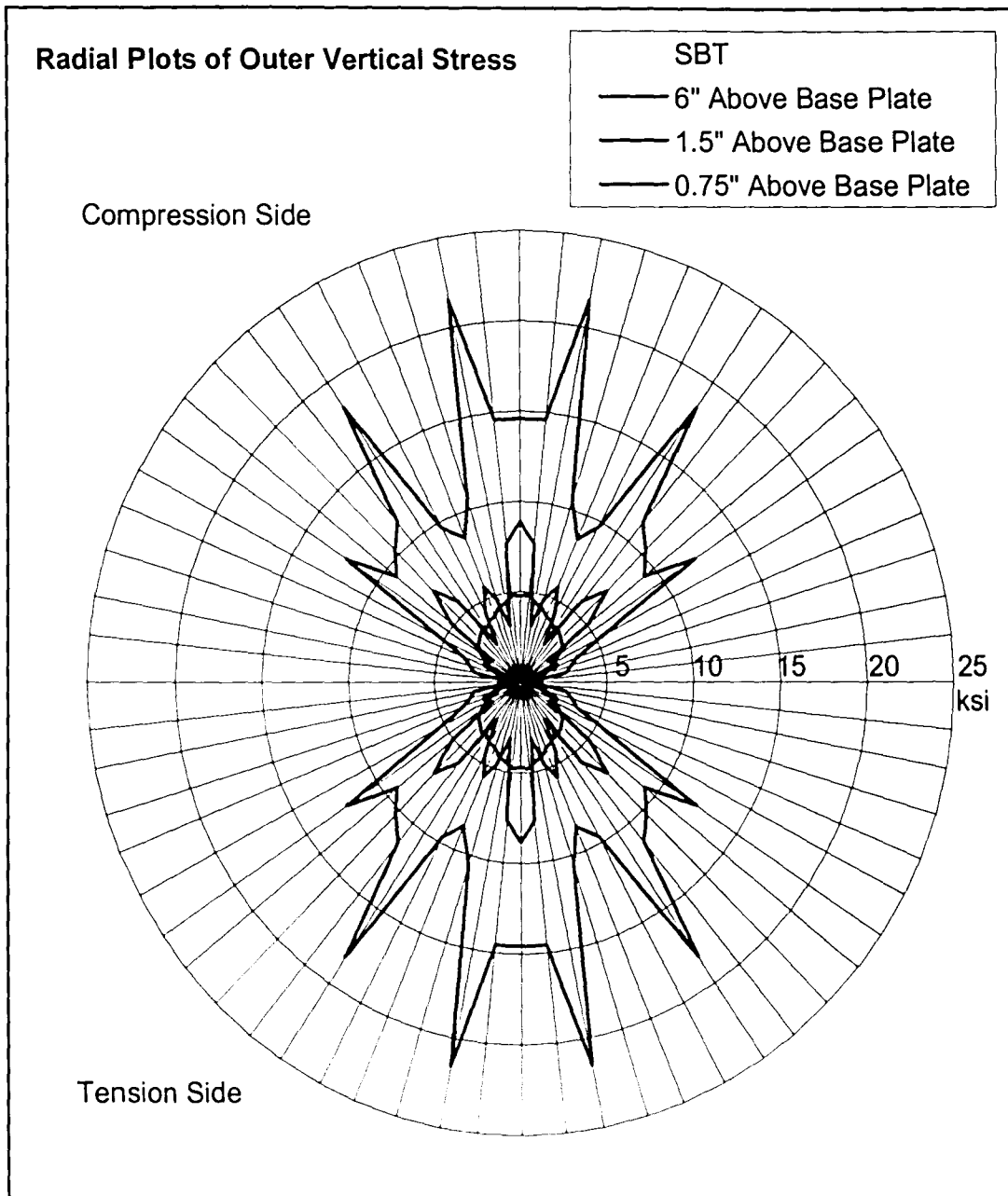


Figure 4.6: General Radial Plot of Vertical Tube Wall Stress in a Multi-Sided Tower and the Predicted Simply Beam Theory Nominal Stress

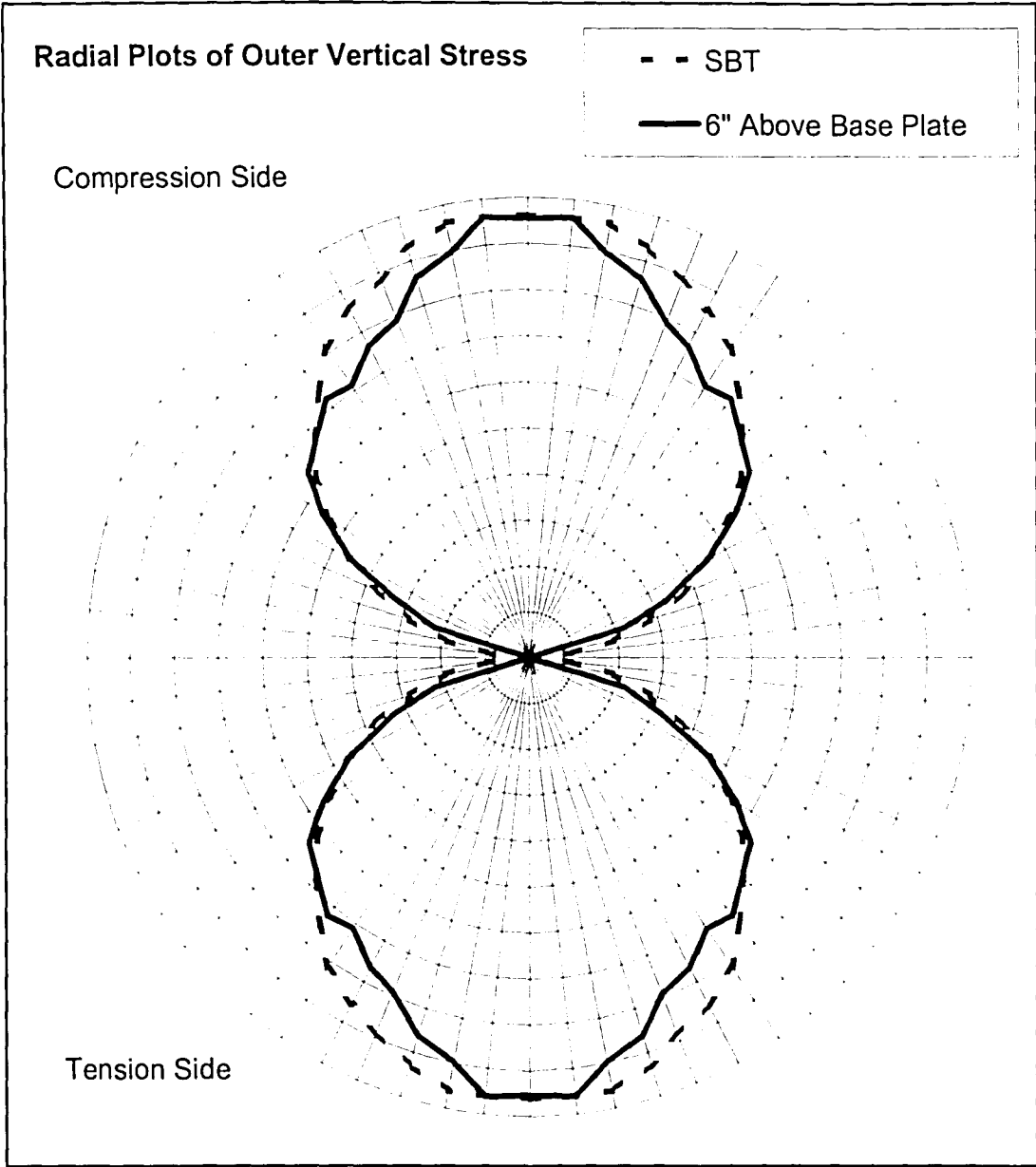


Figure 4.7: General Radial Plot of Vertical Tube Wall Stress in a Multi-Sided Tower at a Height of 6" Above the Base Plate and the Predicted Simply Beam Theory Nominal Stress

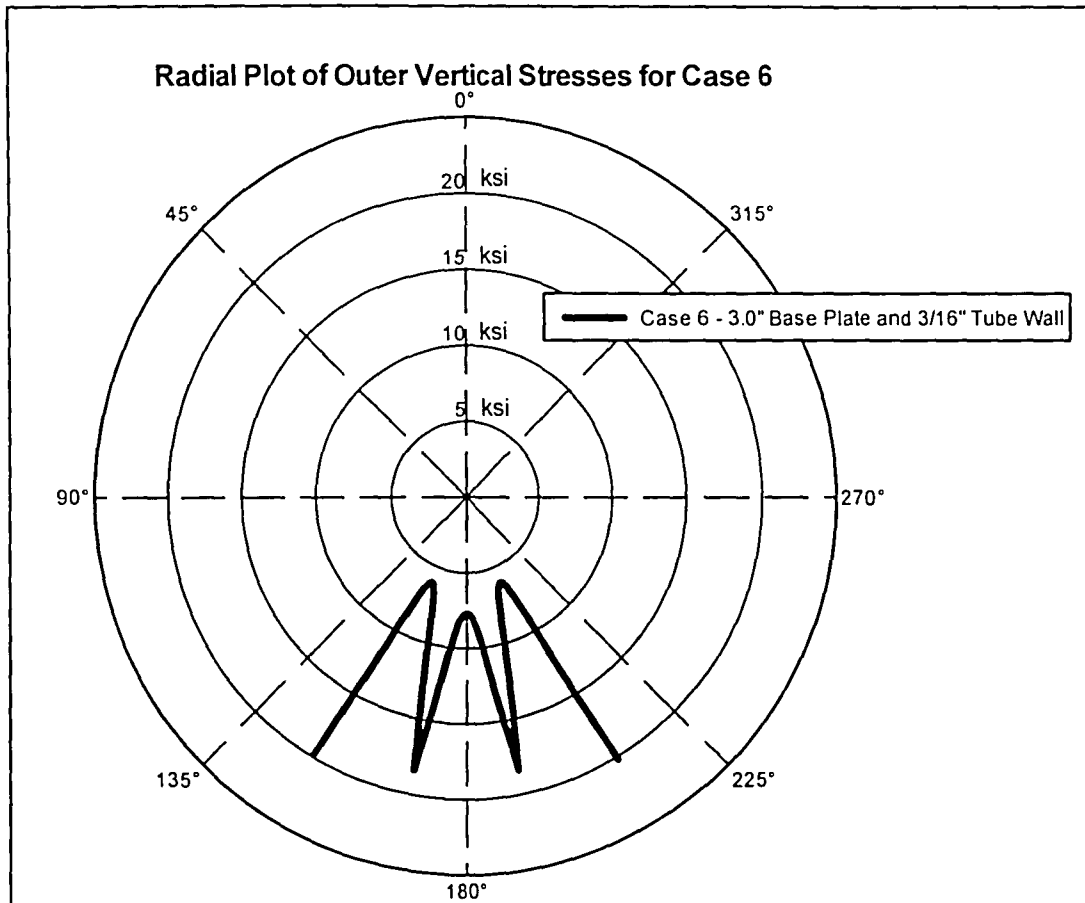


Figure 4.8: Radial Plot of Outer Vertical Tube Wall Stress at the Weld Toe for Case 6 at the Weld Toe

Table 4.3: Study A - Base Plate Thickness Parametric Study with a Tube Wall Thickness of 0.1875"

Case	Base Plate Thickness (in)	Tube Wall Thickness (in)	Number of Anchor Rods
2	1.00	0.1875	8
1 - BASE Model	1.25	0.1875	8
3	1.50	0.1875	8
4	2.00	0.1875	8
5	2.50	0.1875	8
6	3.00	0.1875	8
7	6.00	0.1875	8

Table 4.4: Study B - Base Plate Thickness Parametric Study with a Tube Wall Thickness of 0.5"

Case	Base Plate Thickness (in)	Tube Wall Thickness (in)	Number of Anchor Rods
8	1.00	0.50	8
13	1.25	0.50	8
9	2.00	0.50	8
10	3.00	0.50	8
11	6.00	0.50	8

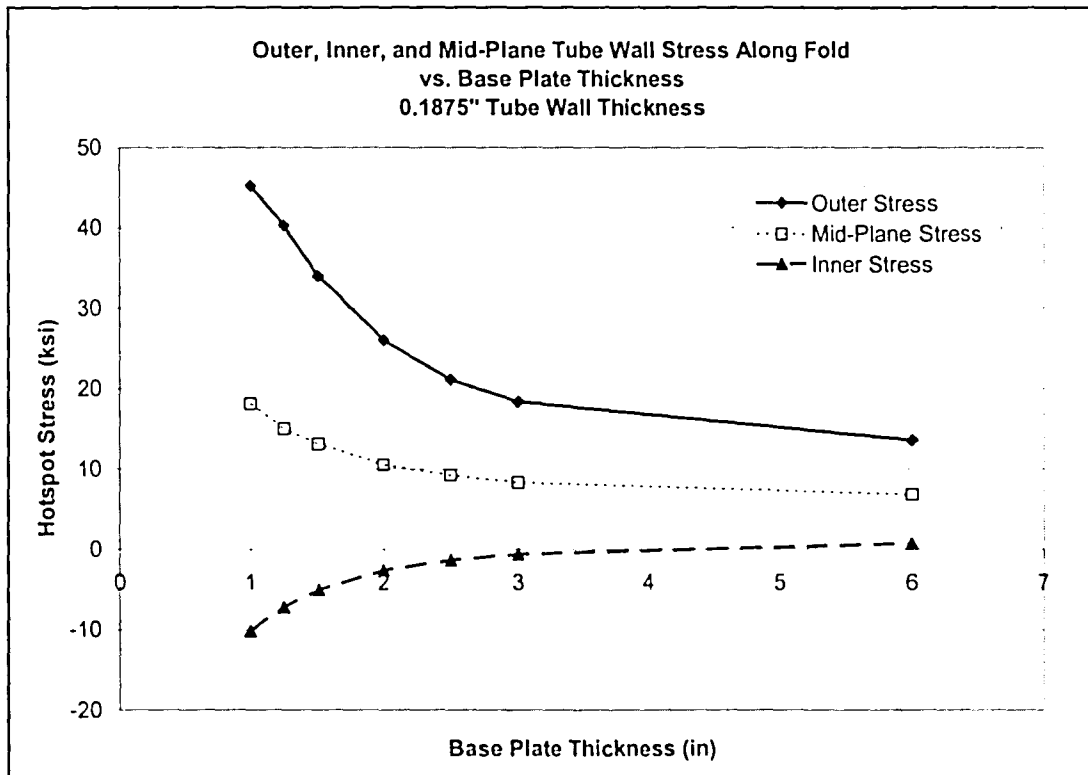


Figure 4.9: Study A Results - Vertical Stress at the Tube Wall Fold vs. Base Plate Thickness for a Tube Wall Thickness of 3/16"

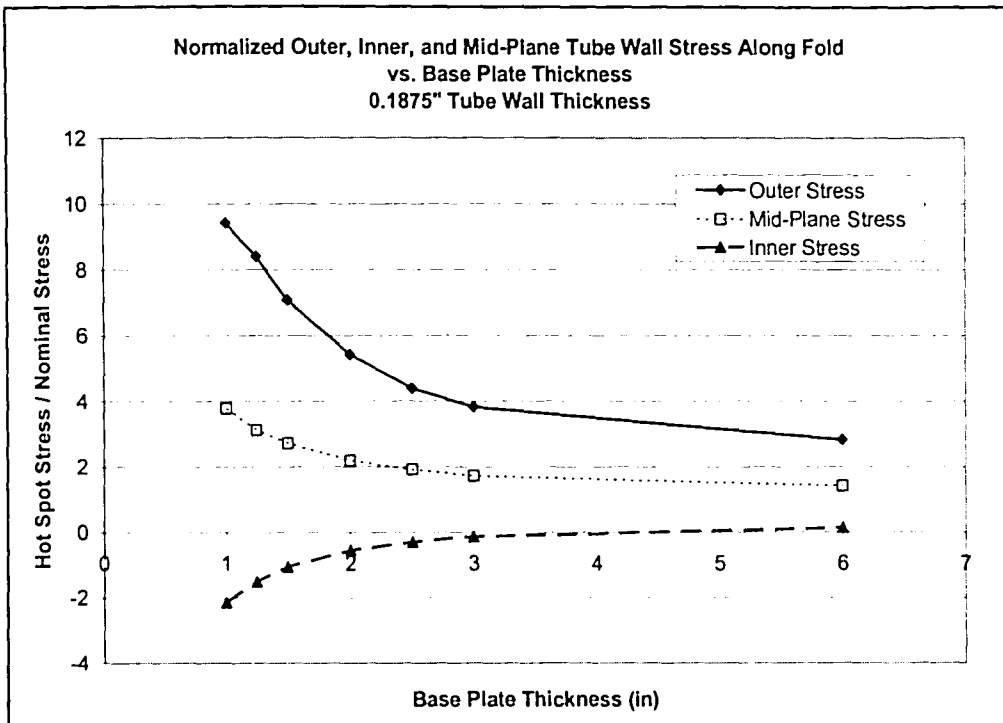


Figure 4.10: Study A Results - Normalized Vertical Stress at the Tube Wall Fold vs. Base Plate Thickness for a Tube Wall Thickness of 3/16"

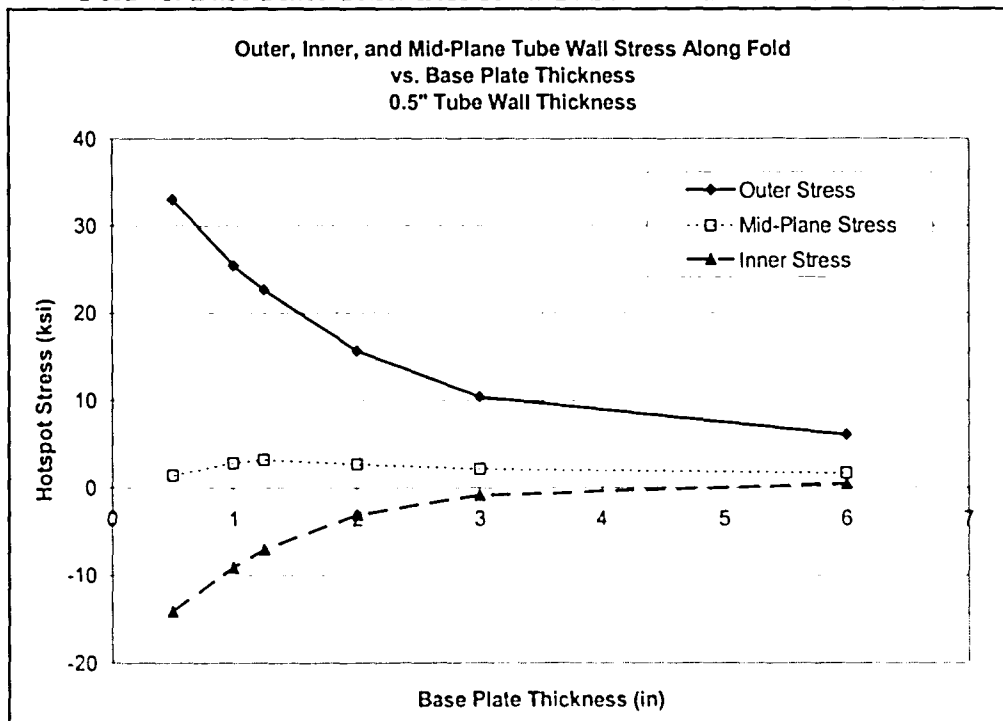


Figure 4.11: Study B Results - Vertical Stress at the Tube Wall Fold vs. Base Plate Thickness for Tube Wall Thickness of 1/2"

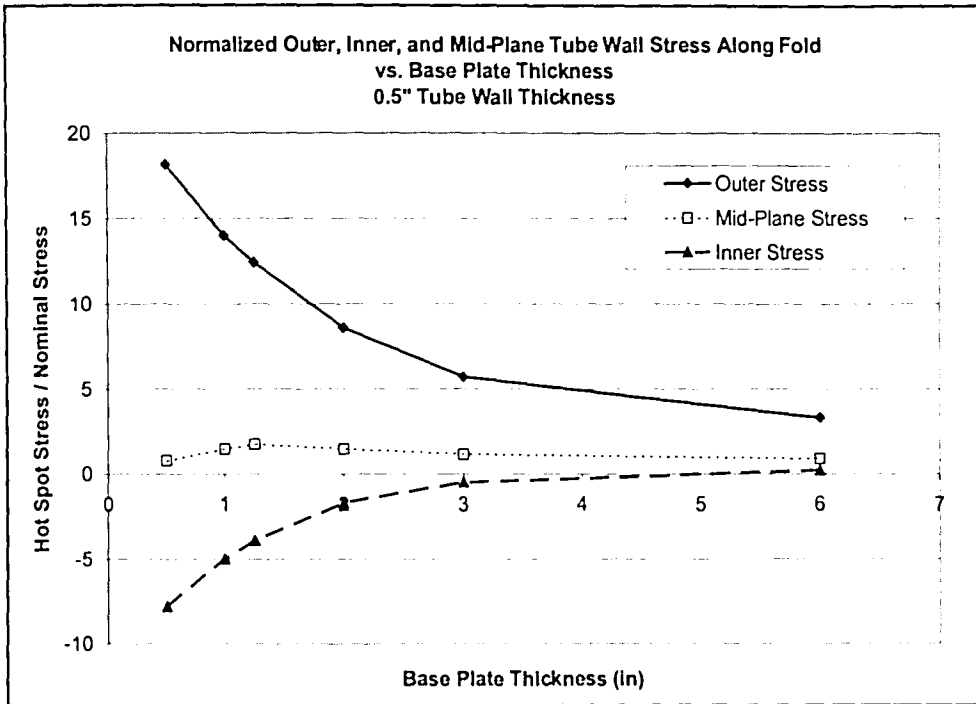


Figure 4.12: Study B Results - Normalized Vertical Stress at the Tube Wall Fold vs. Base Plate Thickness for Tube Wall Thickness of 1/2"

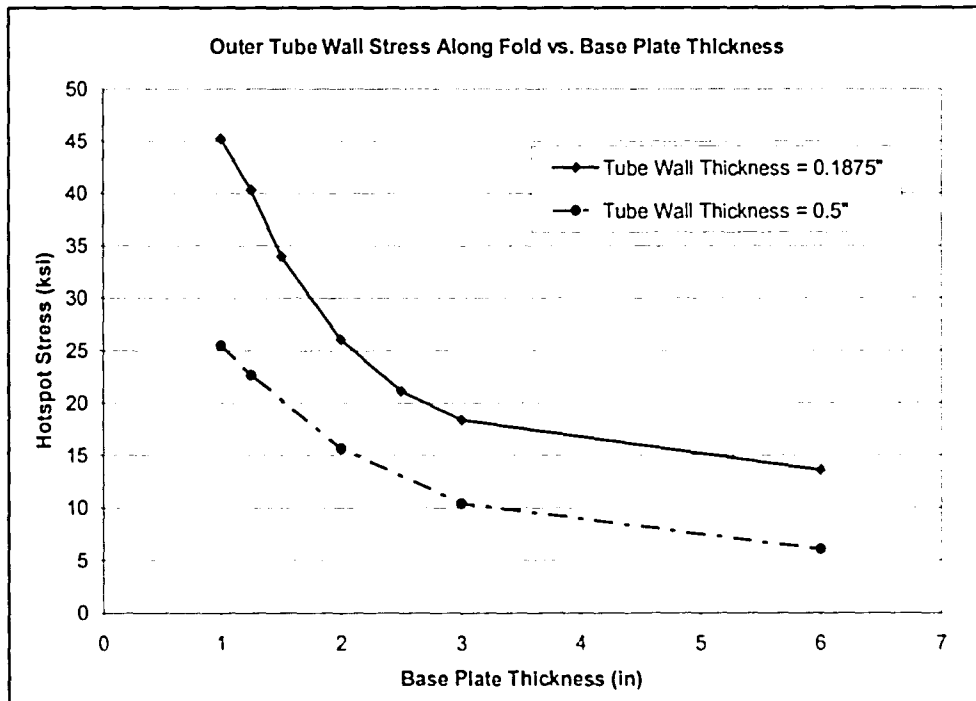


Figure 4.13: Results of Studies A and B - Maximum Vertical Tube Wall Stress at the Tube Wall Fold vs. Base Plate Thickness for Tube Wall Thicknesses of 3/16" and 1/2"

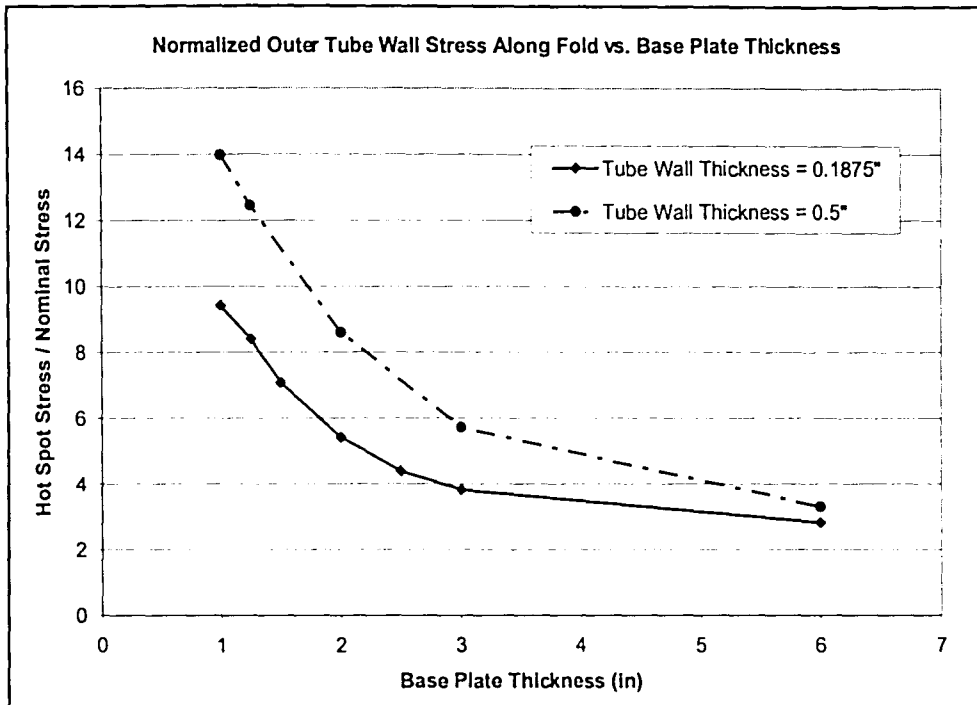


Figure 4.14: Results of Studies A and B - Normalized Maximum Vertical Tube Wall Stress at the Tube Wall Fold vs. Base Plate Thickness for Tube Wall Thicknesses of 3/16" and 1/2"

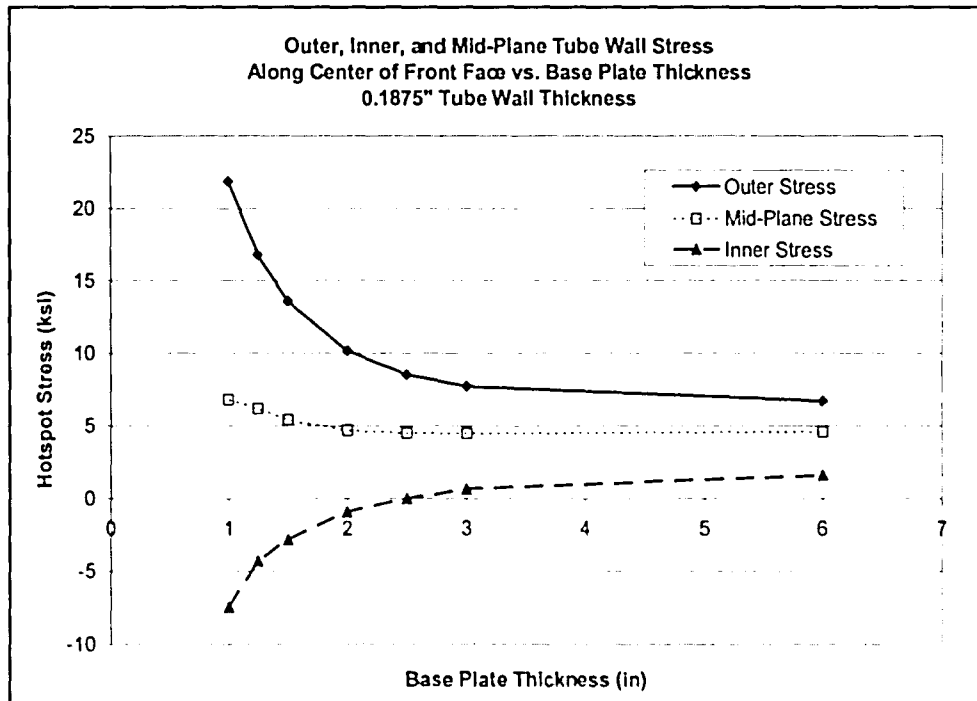


Figure 4.15: Study A Results - Vertical Stress at the Center of the Front Side of Tube Wall vs. Base Plate Thickness for a Tube Wall Thickness of 3/16"

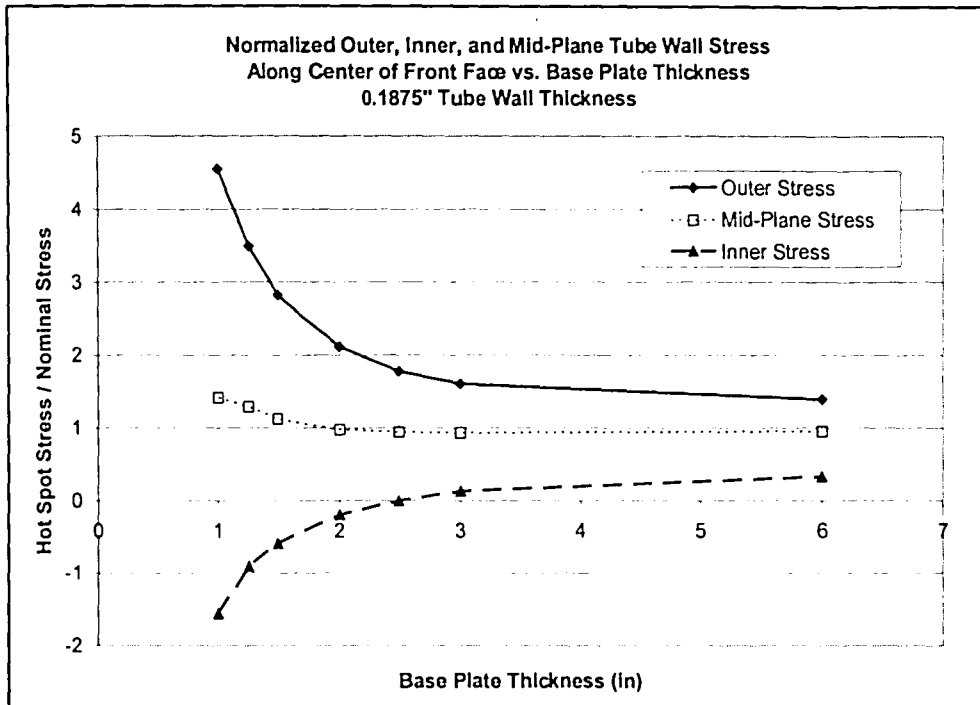


Figure 4.16: Study A Results - Normalized Vertical Stress at the Center of the Front Side of Tube Wall vs. Base Plate Thickness for a Tube Wall Thickness of 3/16"

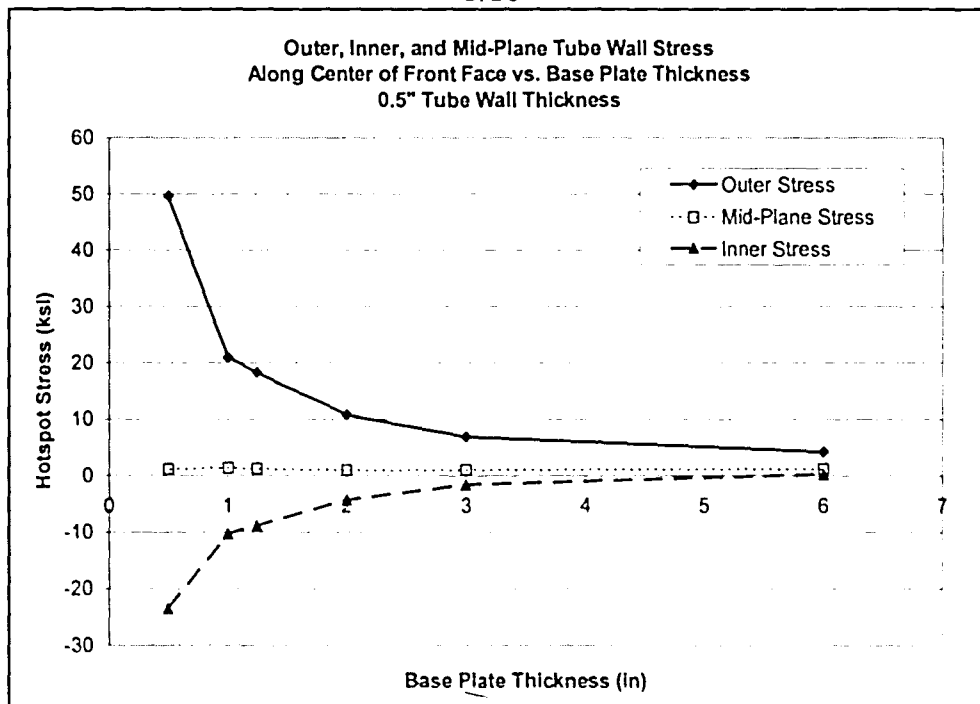


Figure 4.17: Study B Results - Vertical Stress at the Center of the Front Side of the Tube Wall vs. Base Plate Thickness for a Tube Wall Thickness of 1/2"

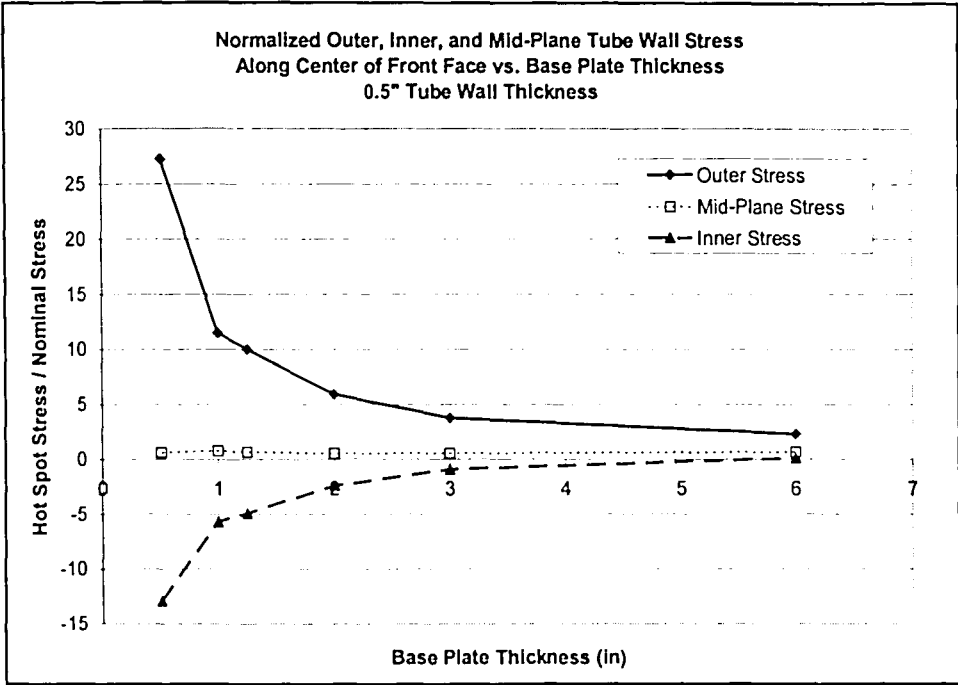


Figure 4.18: Study B Results - Normalized Vertical Stress at the Center of the Front Side of the Tube Wall vs. Base Plate Thickness for a Tube Wall Thickness of 1/2"

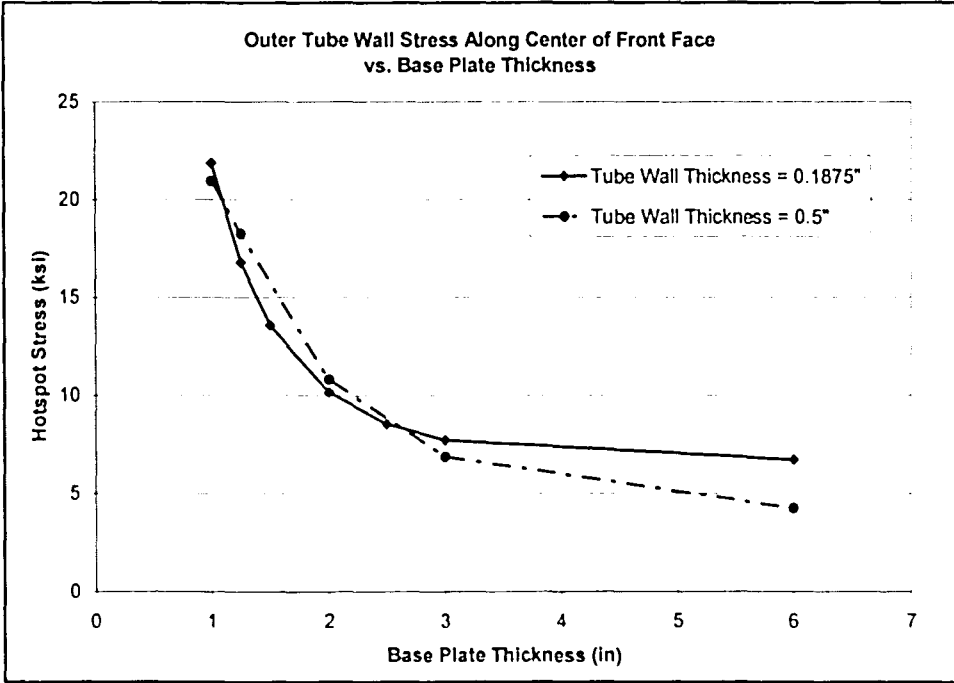


Figure 4.19: Results for Studies A and B - Maximum Vertical Tube Wall Stress at the Center of the Front Side vs. Base Plate Thickness for Tube Wall Thicknesses of 3/16" and 1/2"

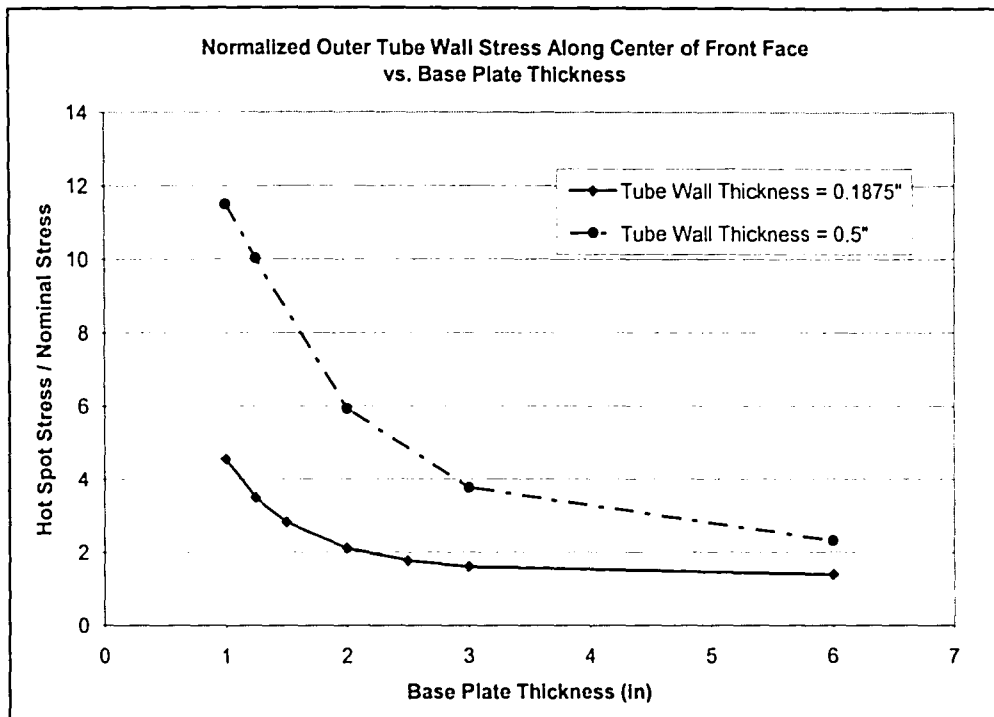


Figure 4.20: Results of Studies A and B - Normalized Maximum Vertical Tube Wall Stress at the Center of the Front Side vs. Base Plate Thickness for Tube Wall Thicknesses of 3/16" and 1/2"

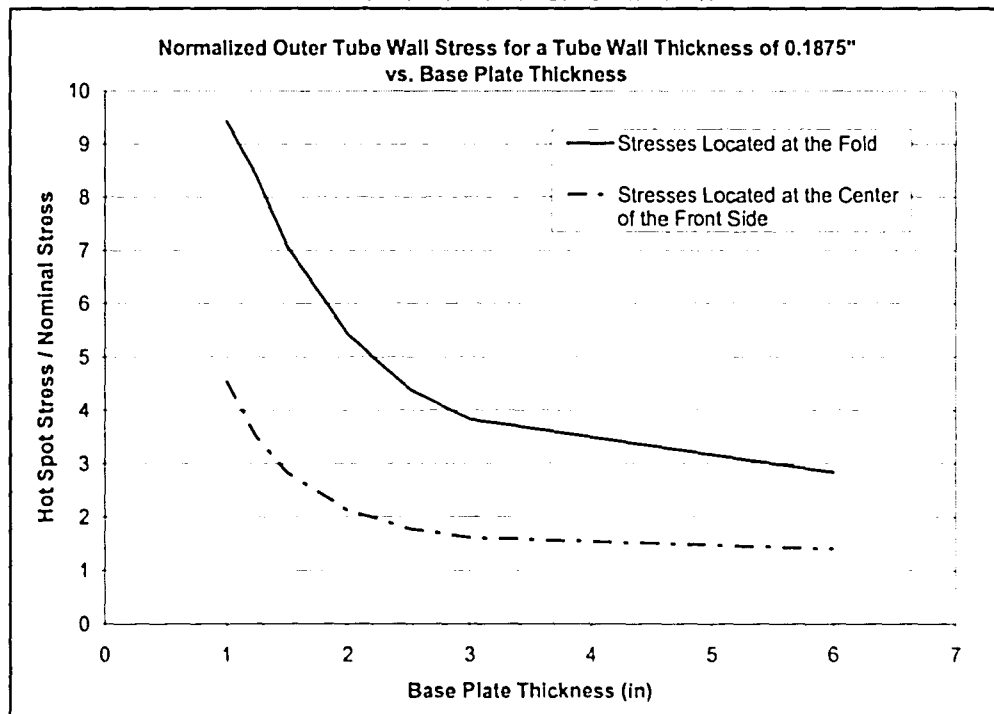


Figure 4.21: Study A Results - Comparison Between Stress Locations

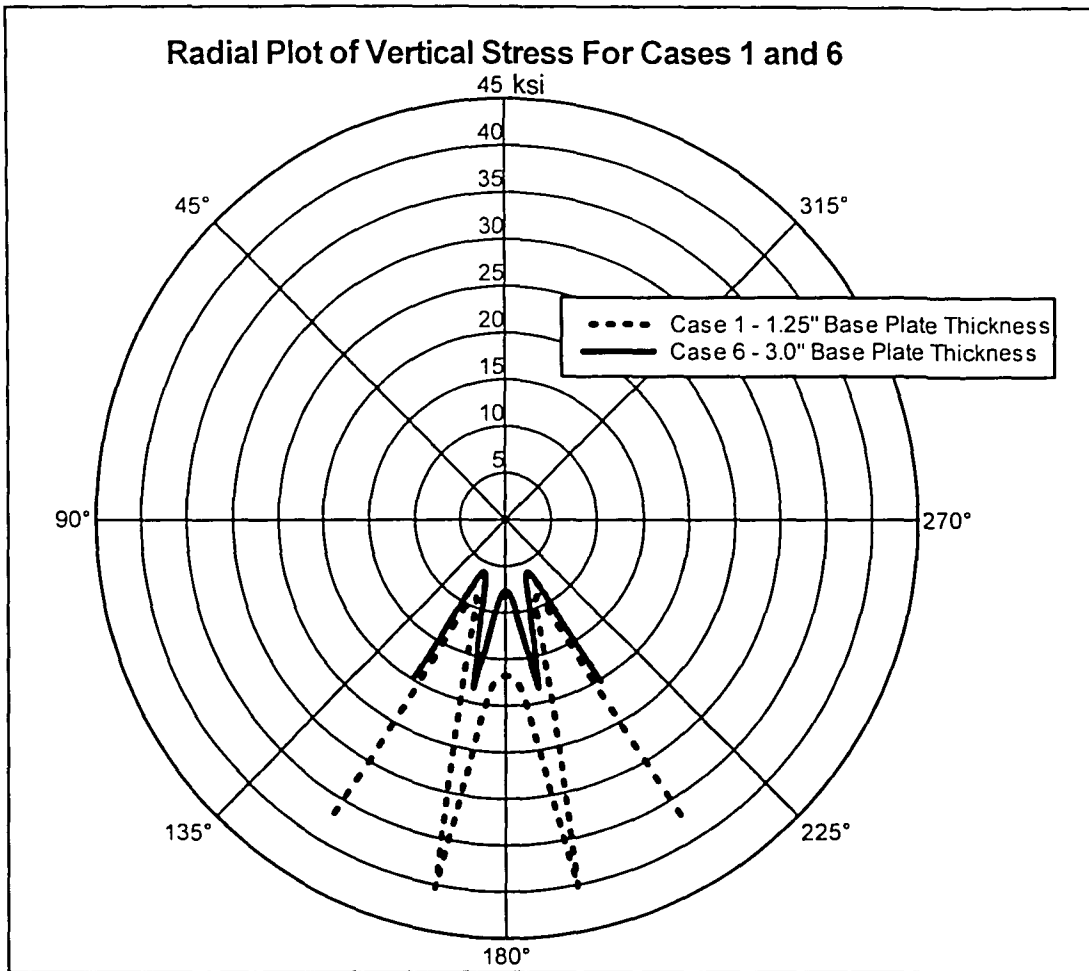


Figure 4.22: Radial Plot of Outer Vertical Stress for Cases 1 and 6 at the Weld Toe

Table 4.5: Study C - Tube Wall Thickness Parametric Study with a Base Plate Thickness of 1.25"

Case	Base Plate Thickness (in)	Tube Wall Thickness (in)	Number of Anchor Rods
1 - BASE Model	1.25	0.1875	8
12	1.25	0.3125	8
13	1.25	0.50	8
14	1.25	0.625	8

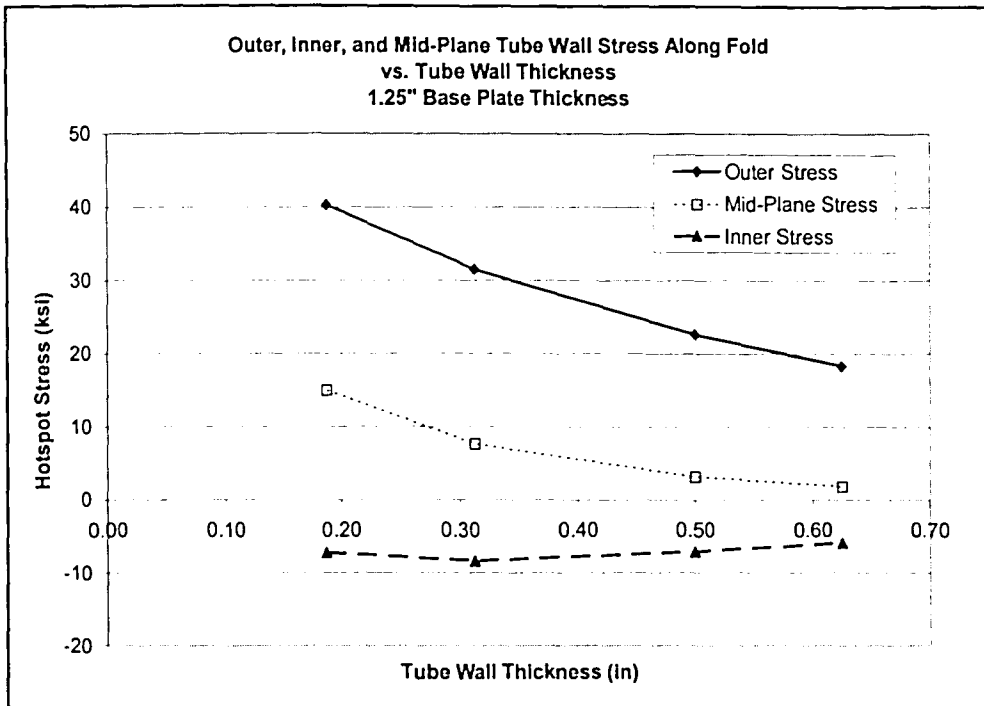


Figure 4.23: Results of Study C - Vertical Tube Wall Stress Along the Fold With A Base Plate Thickness of 1.25" vs. Tube Wall Thickness

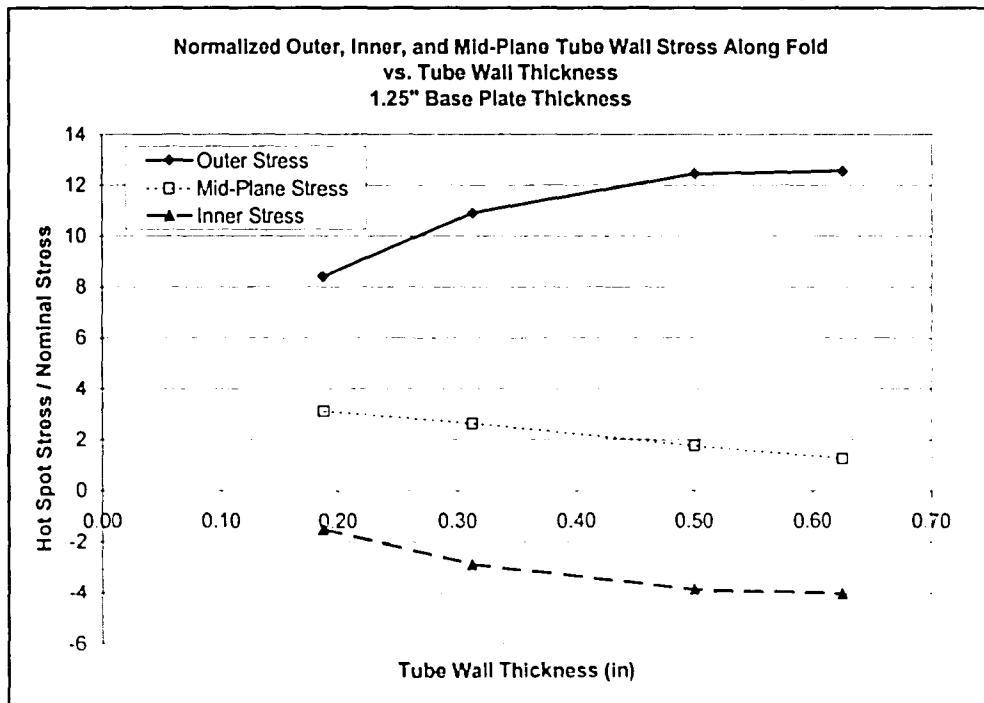


Figure 4.24: Results of Study C - Normalized Vertical Tube Wall Stress Along the Fold With a Base Plate Thickness of 1.25" vs. Tube Wall Thickness

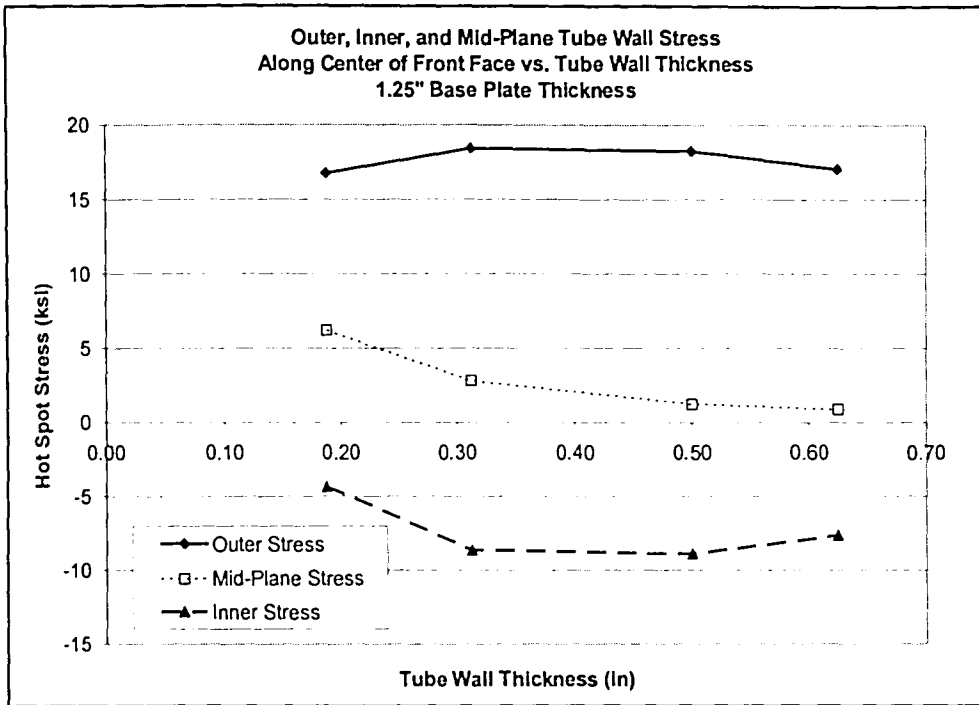


Figure 4.25: Results of Study C - Vertical Tube Wall Stress Along the Center of the Front Side With a Base Plate Thickness of 1.25" vs. Tube Wall Thickness

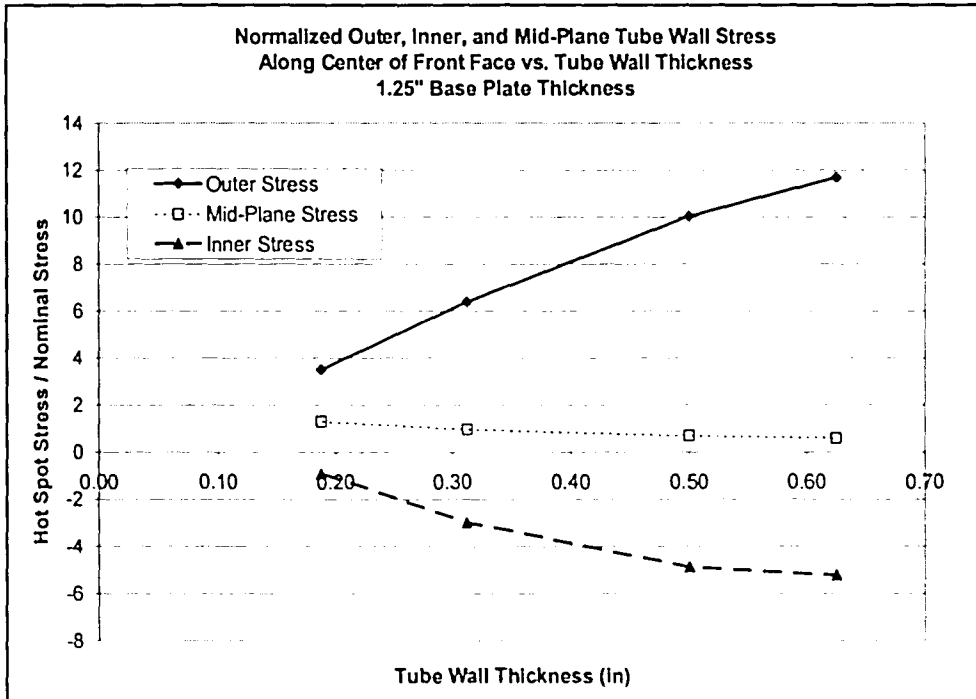


Figure 4.26: Results of Study C - Normalized Vertical Tube Wall Stress Along the Center of the Front Side With a Base Plate Thickness of 1.25" vs. Tube Wall Thickness

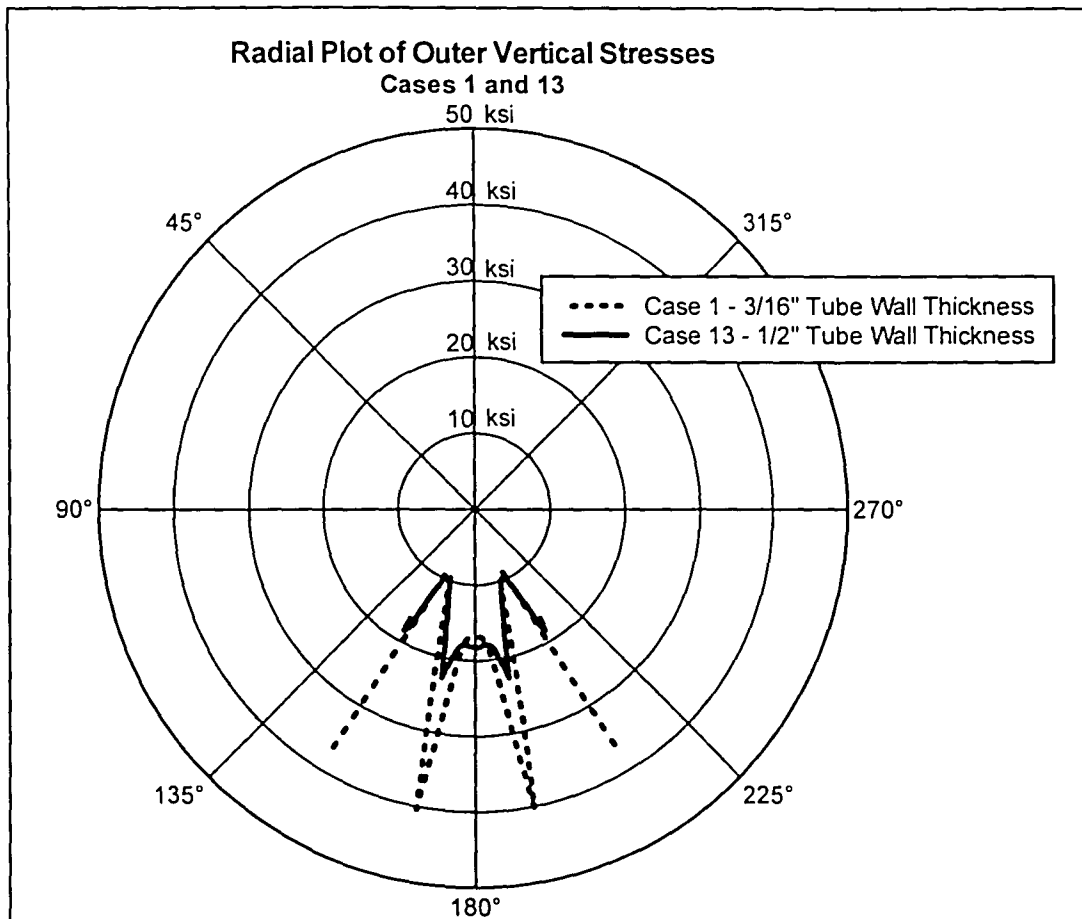


Figure 4.27: Radial Plot of Outer Vertical Stresses for Cases 1 and 13 at the Weld Toe

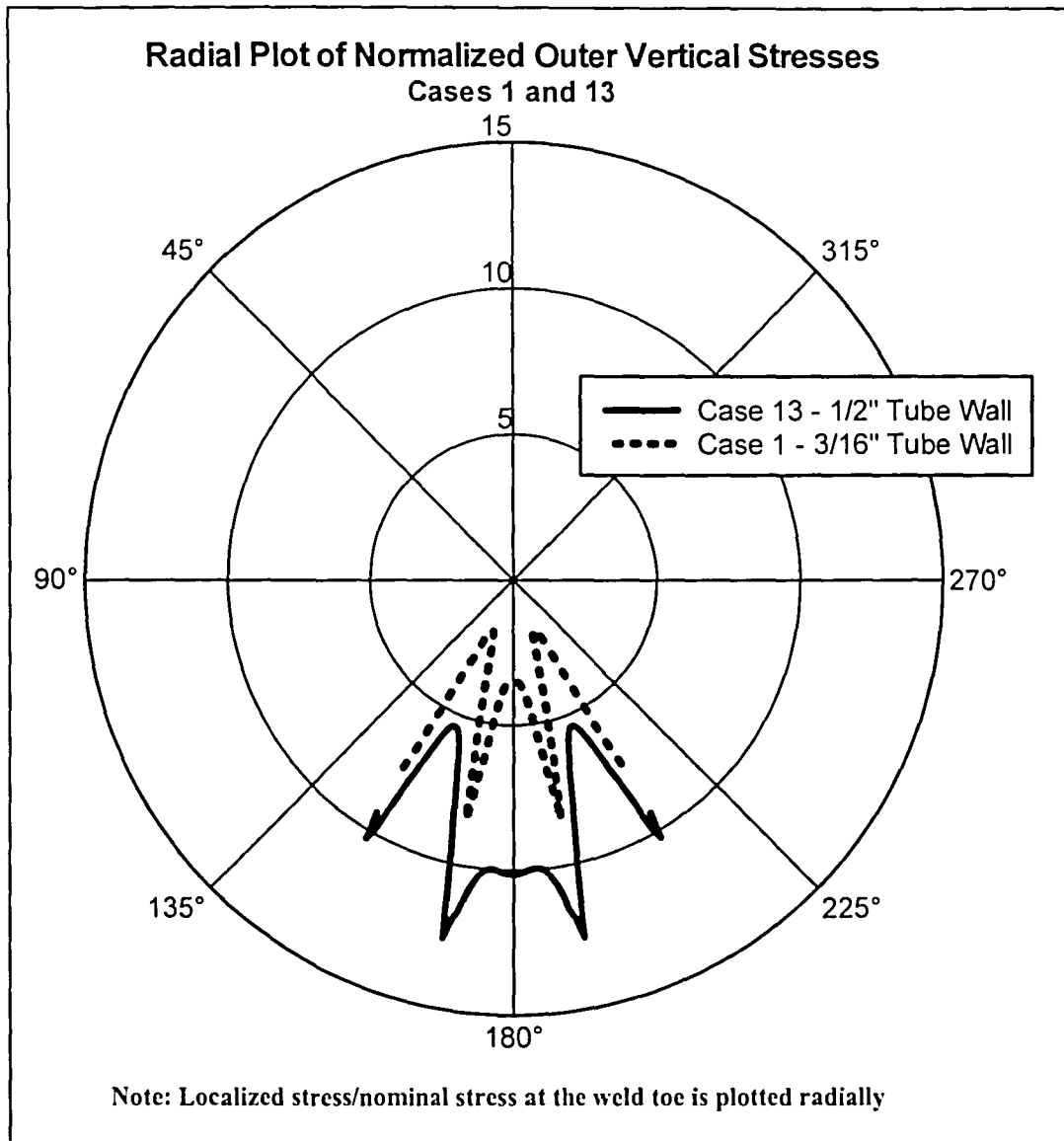


Figure 4.28: Radial Plot of Normalized Outer Vertical Stresses for Cases 1 and 13 at the Weld Toe

Table 4.6: Study D - Anchor Rods Parametric Study with a Base Plate Thickness of 1.25"

Case	Base Plate Thickness (in)	Tube Wall Thickness (in)	Number of Anchor Rods	Tube Diameter at Base (in)
15	1.25	0.1875	4	24.75
1 - BASE Model	1.25	0.1875	8	24.75
17	1.25	0.1875	16	24.75

Table 4.7: Study E - Anchor Rods Parametric Study with a Base Plate Thickness of 3.0"

Case	Base Plate Thickness (in)	Tube Wall Thickness (in)	Number of Anchor Rods	Tube Diameter at Base (in)
16	3.0	0.1875	4	24.75
6	3.0	0.1875	8	24.75
18	3.0	0.1875	16	24.75

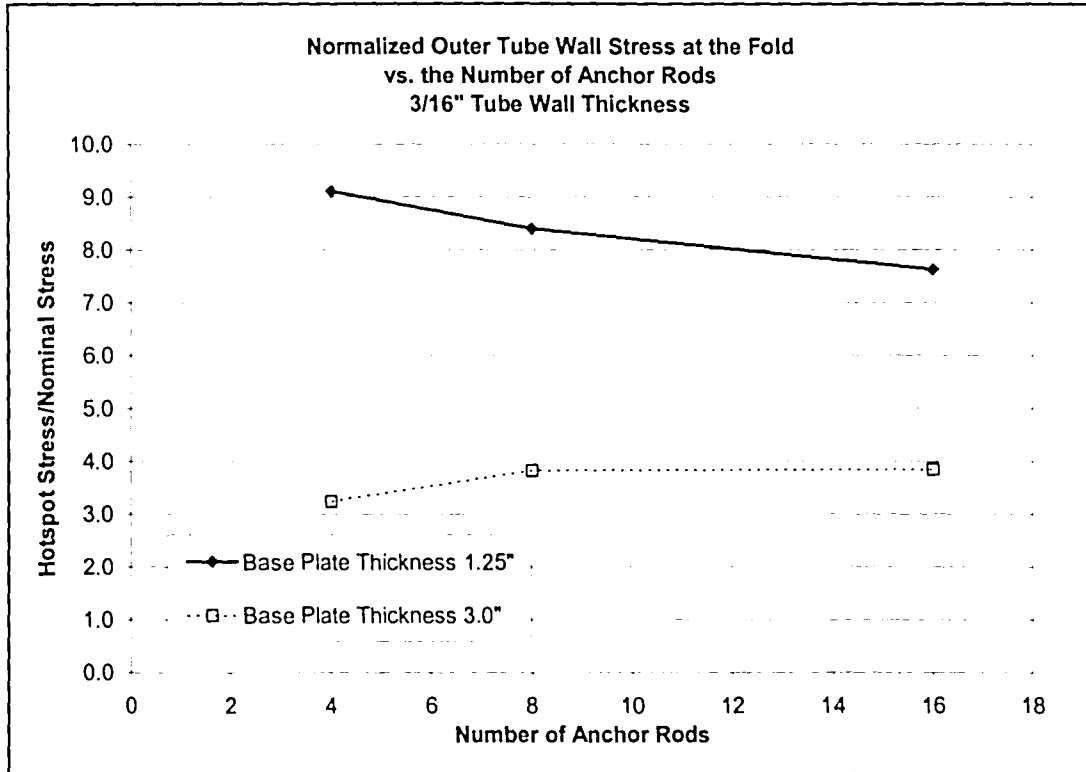


Figure 4.29: Results of Studies D and E – Normalized Vertical Tube Wall Stresses at the Fold vs. Number of Anchor Rods for Base Plate Thicknesses of 1.25" and 3.0"

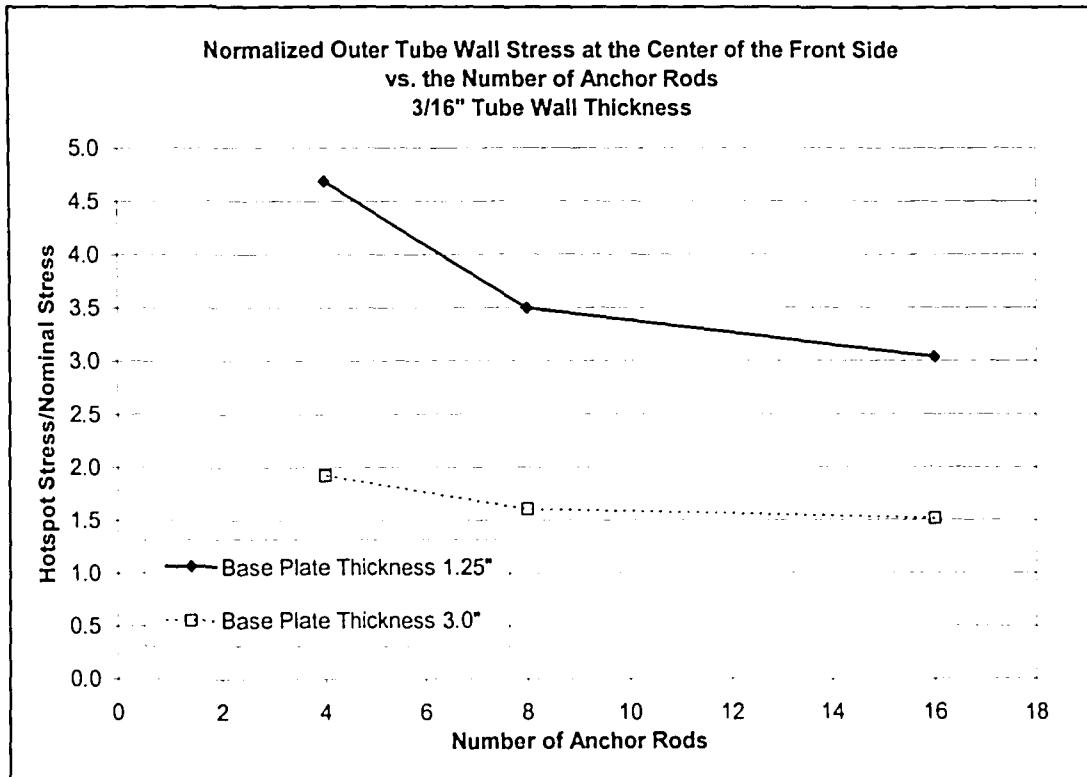


Figure 4.30: Results of Studies D and E – Normalized Vertical Tube Wall Stresses at the Center of the Front Side vs. Number of Anchor Rods for Base Plate Thicknesses of 1.25" and 3.0"

Chapter 5 Conclusions and Recommendations

5.1 Field Investigation Conclusions

Several important conclusions have been made based upon the field investigation of high-mast lighting towers in Iowa. Although these studies were focused on poles in the state of Iowa, the general conclusions are believed to be applicable to all similar structures.

- The frequencies of vibration for the first four modes for all of the high-mast towers fall within the same range (0.25 Hz to 7.3 Hz). The frequencies do not appear to be dependent upon the geometric properties of the base connection.
- There is good agreement between the modal frequencies determined using finite element analyses and the measured modal frequencies at the Clear Lake tower.
- The damping ratio is generally lower in the higher modes of vibration. The high damping ratio in the first mode may be attributed to aerodynamic damping effects. The AASHTO and CAN/CSA Specifications suggested damping ratios that are not always conservative. The values suggested are often significantly higher than the measured damping ratios for the higher modes.
- Improper installation of leveling and locking nuts has a significant effect on the stresses in the tube wall in the vicinity of the loose nut.

5.2 Finite Element Study Conclusions

Based on the results of the finite element model validation studies, the following conclusions can be made:

- The length that the anchor rod is restrained in the concrete foundation does not significantly affect the stress distribution in the tube wall. A longer anchor rod may slightly increase the maximum vertical stress in the tube wall, while the computation time is drastically increased. An extremely long anchor rod is not necessary, especially when the finite element models are not being directly compared to field studies.
- The method of modeling the restraint of the solid anchor rod is to constrain the outer surface of the rod. This method is more conservative than the centerline constraint approach used in a two-dimensional structural analysis. Also, the method of restraining the surface of the anchor rod more closely represents the actual behavior of the anchor rods.

Based on the results of the finite element parametric studies performed, the following conclusions can be made:

- This research has shown that base plate flexibility has a considerable influence on the stress behavior in the tube wall adjacent to the socket welded connection of a high-mast lighting tower. The assumption that the tube is fixed at the connection with the base plate (a common assumption used in design practice) is not consistent with the real behavior of these

structures and future designs need to take the base plate flexibility into consideration.

- The parametric studies show that the major influence of base plate flexibility is the base plate thickness and the best (and most cost effective) method to decrease the flexibility of the base plate is to increase the thickness. Based on the trend determined from the base plate thickness study, a minimum thickness of 3" is recommended.
- This research showed that as the maximum vertical stress in the tube wall decreased with increasing base plate thickness, the amplification factor, or normalized stress, also decreased. Increasing the tube wall thickness was not shown to have an advantageous effect on stiffening the base plate. Instead, a stiffer tube applied more load to the base plate. In order for a thicker tube wall to improve the fatigue performance of a high-mast tower, the base plate must be proportionally increased.
- It is suggested that the tube wall thickness in the lower fifteen feet of the tower be greater than the thickness used in previous designs of high-mast towers. A minimum thickness of 1/2 inch is recommended for poles that are between 100 to 120 feet tall and a minimum of 5/8 inches thick for poles greater than 120 feet tall in the absence of detailed analysis.
- Based on the parametric studies, the current eight-anchor rod configuration is adequate and there is no need to use a greater number of rods. The four-rod configurations may be acceptable for high-mast towers with smaller

diameters, however it is not recommended to use the four-anchor rod configuration on towers similar to the BASE model. The 16-rod configuration is unnecessary. The added benefit from doubling the number of anchor rods can not be justified because improvement in base plate flexibility is not significant enough to validate the increase in cost.

5.3 Future Work

- The parametric studies conducted for this study focused on one basic high-mast lighting tower with specific parameters such as the diameter, height, base plate shape, tube wall cross section, weld connection, and anchor rod pattern. Future parametric studies are recommended to determine the stress behavior of different types of high-mast lighting towers.
- The base plate flexibility of cantilevered structures needs to be incorporated into the design of these structures, most likely in the form of an amplification factor applied to the design structures. Two possible methods, not discussed in this report, are presented in Hall's Master's thesis [Hall, 2004]. Unfortunately, this may not occur until more comprehensive data regarding the stress behavior of many typical cantilevered structures is available.
- One area of interest that could not be investigated in this research study due to time constraints is the bend radius of the fold in the tube wall. Future parametric studies could be conducted to study the effects of the bend

radius on the stress behavior in the tube. This type of study may provide suggestions regarding the cross section of the tube wall. Also incorporated into this study would be the differences between towers with a varying number of sides and circular towers, as the bend radius changes depending upon the geometric parameters of the tube.

- Experimental fatigue testing of these details is needed to determine the influence of base plate thickness, as well as the other parameters studied, on the fatigue resistance of the base plate connection. It would be beneficial to develop a simplified method to estimate fatigue resistance of the detail as a function of these parameters.

Appendix A: Vertical Stress Profiles

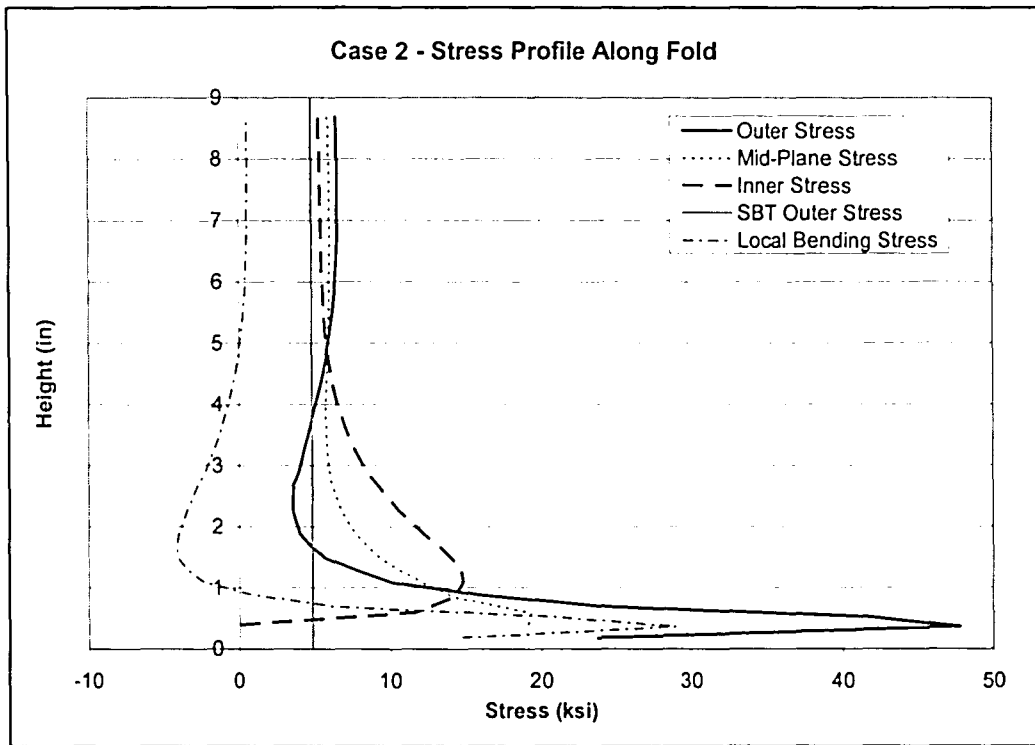


Figure A.1: Case 2 – Stress Profile Along Fold

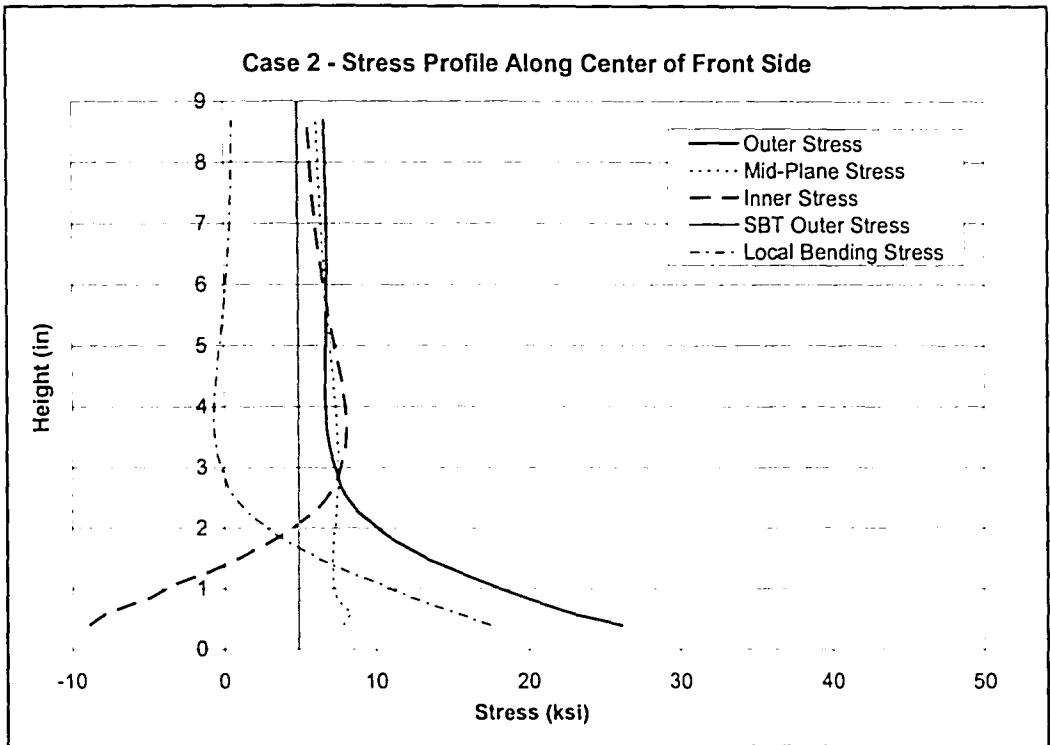


Figure A.2: Case 2 – Stress Profile Along Center of Front Side

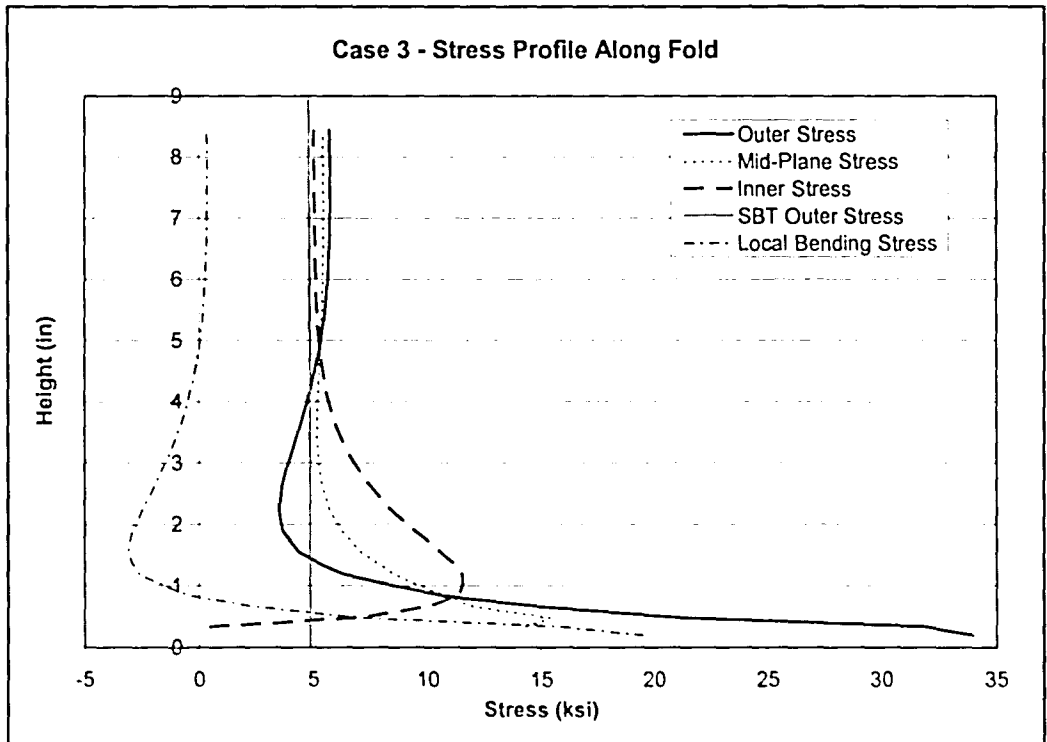


Figure A.3: Case 3 – Stress Profile Along Fold

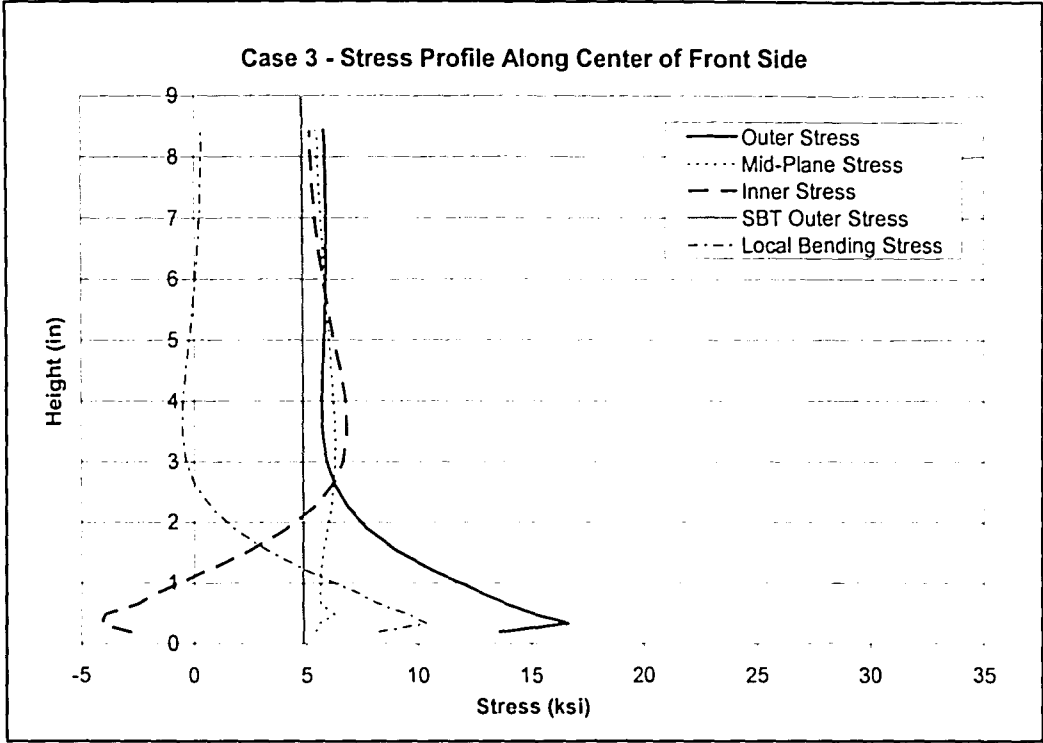


Figure A.4: Case 3 – Stress Profile Along Center of Front Side

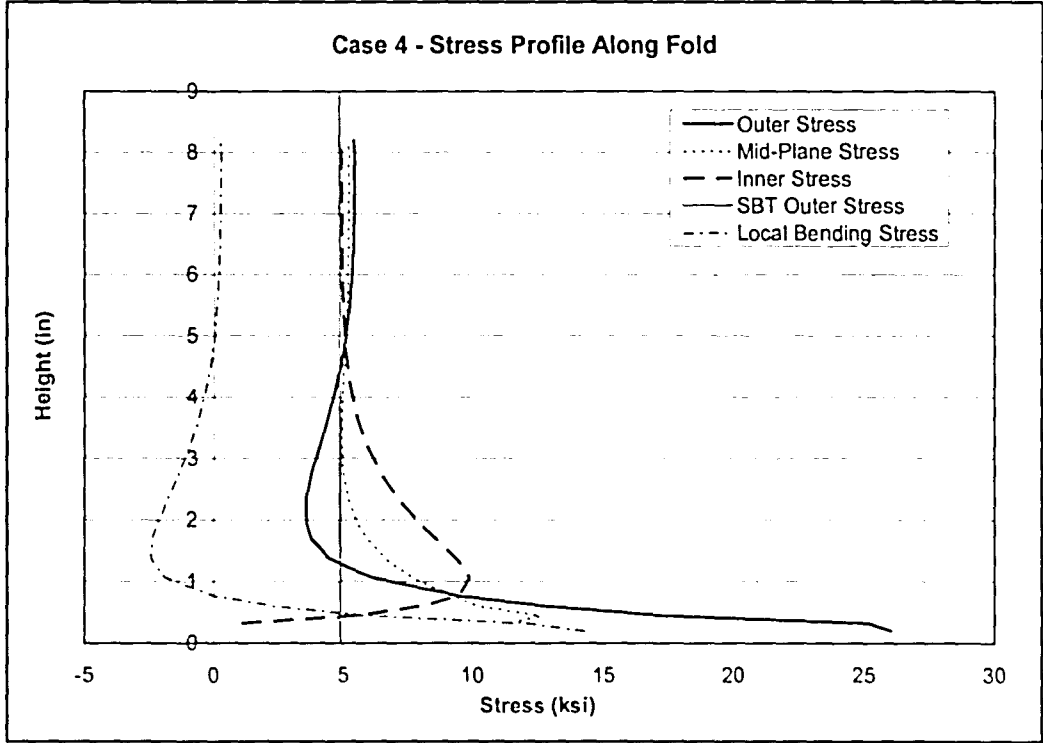


Figure A.5: Case 4 – Stress Profile Along Fold

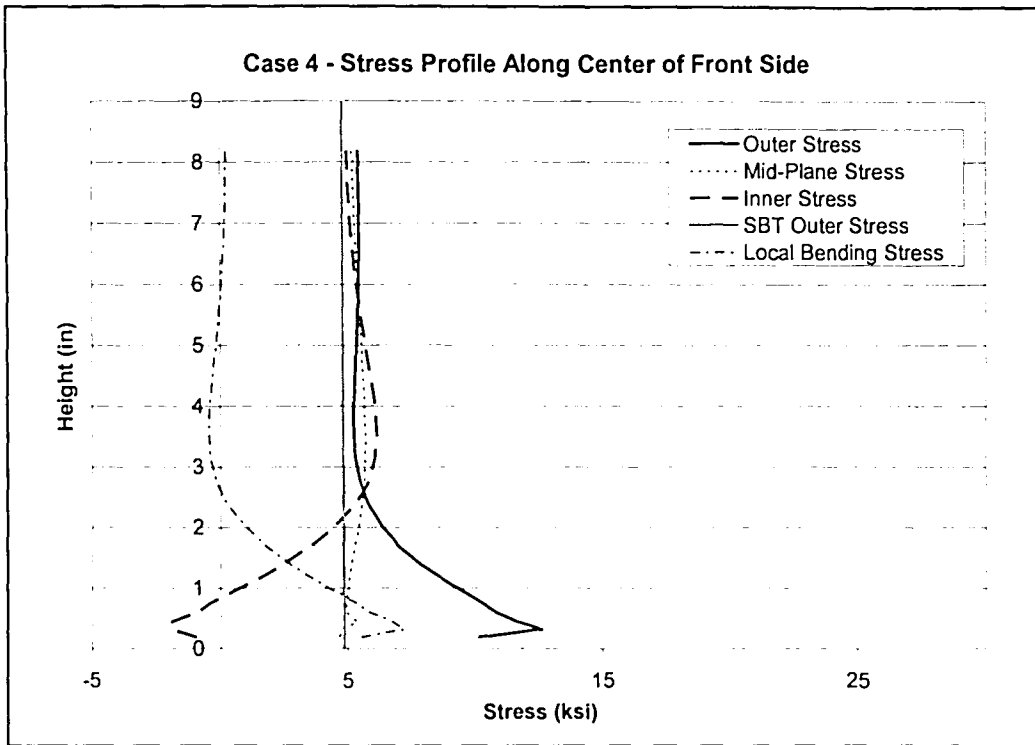


Figure A.6: Case 4 – Stress Profile Along Center of Front Side

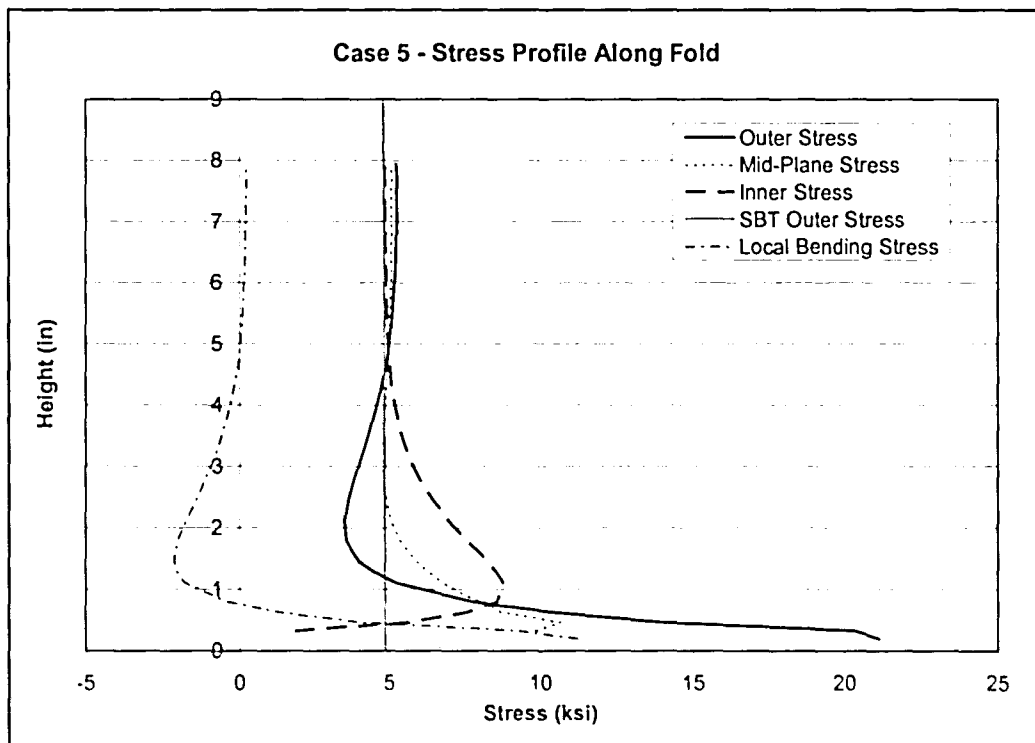


Figure A.7: Case 5 – Stress Profile Along Fold

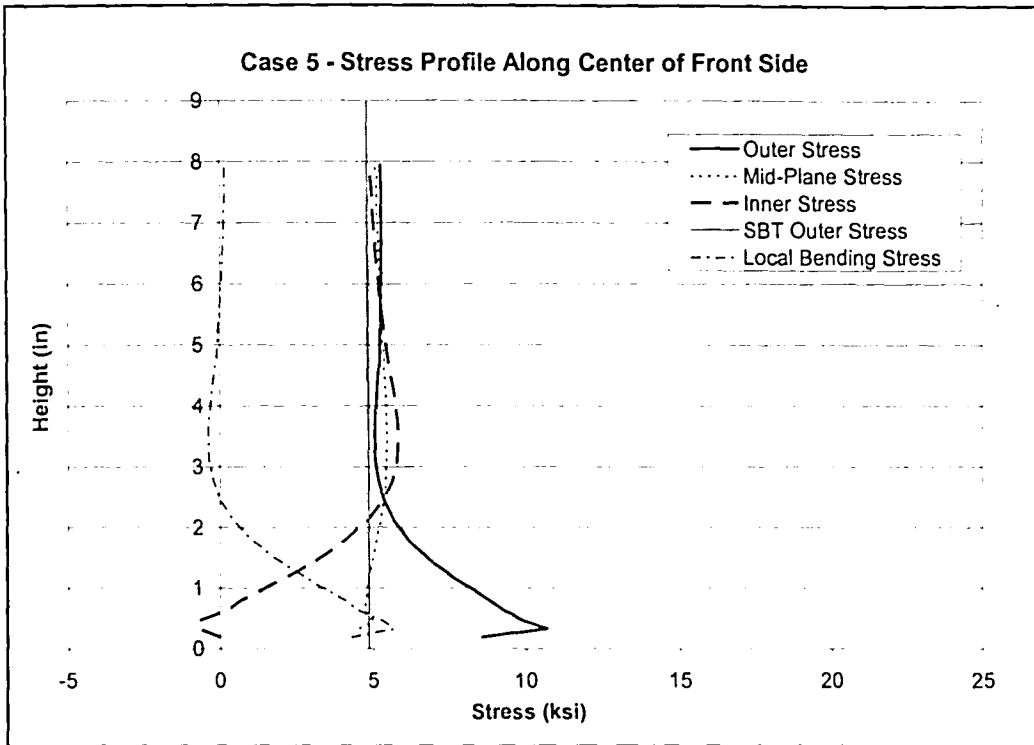


Figure A.8: Case 5 – Stress Profile Along Center of Front Side

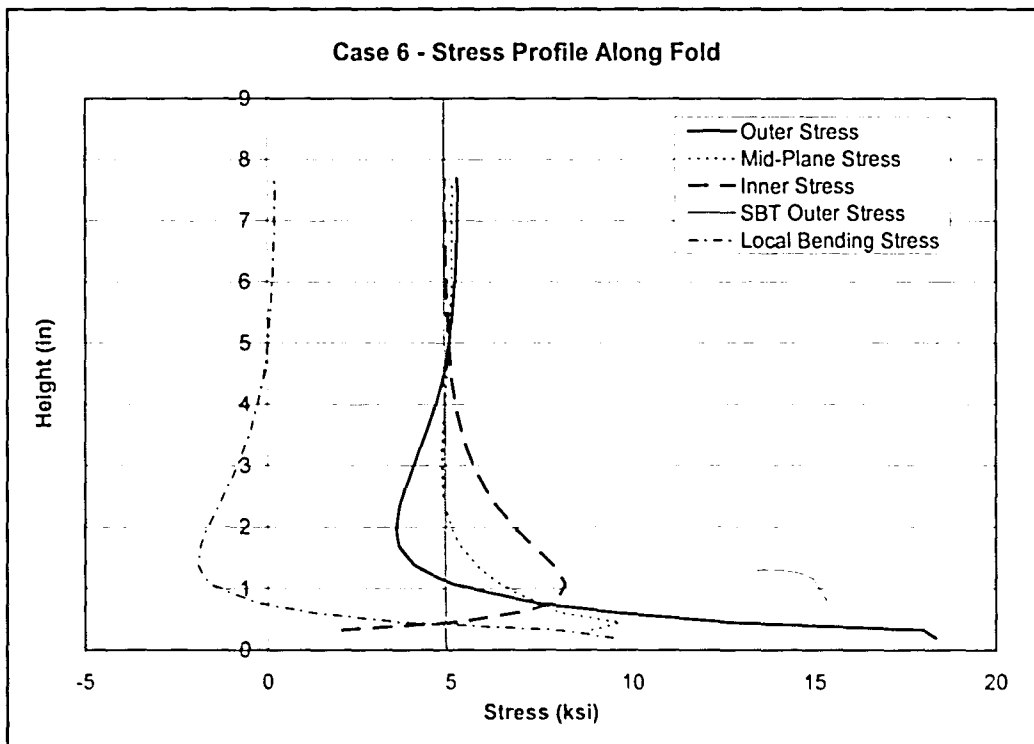


Figure A.9: Case 6 – Stress Profile Along Fold

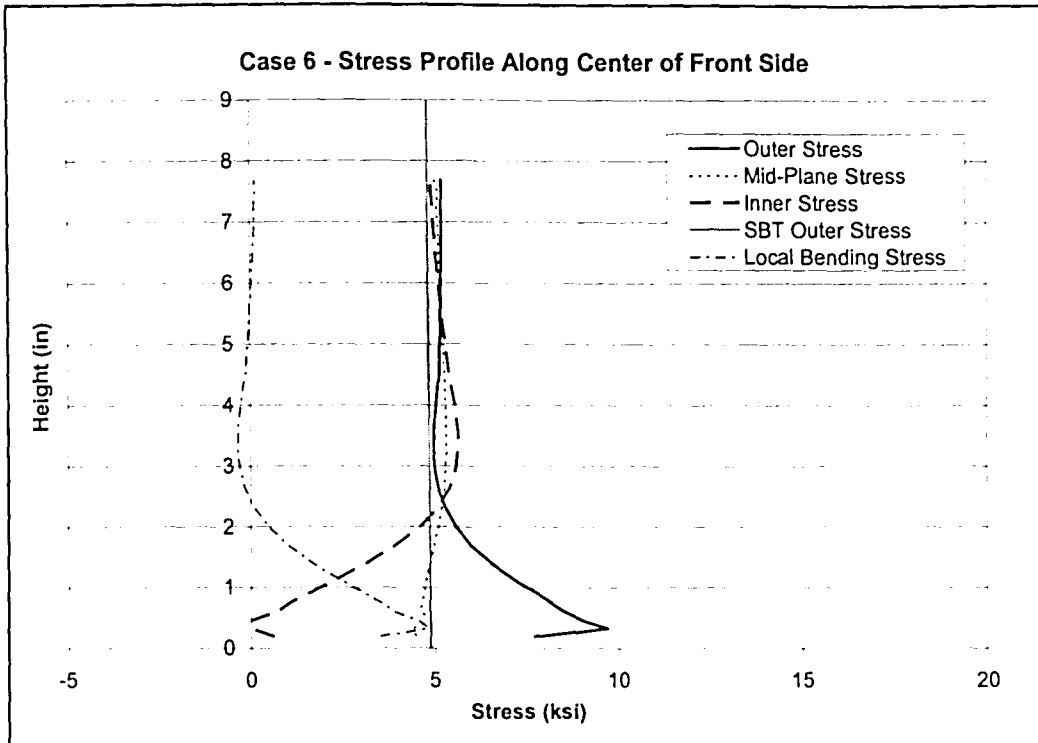


Figure A.10: Case 6 – Stress Profile Along Center of Front Side

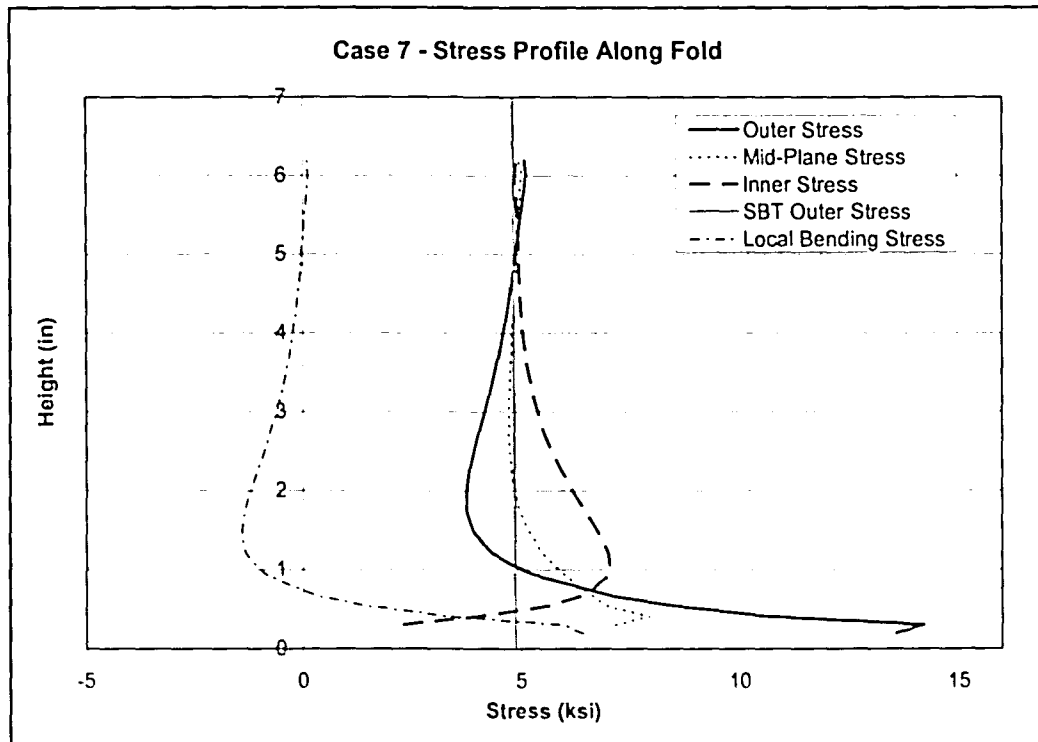


Figure A.11: Case 7 – Stress Profile Along Fold

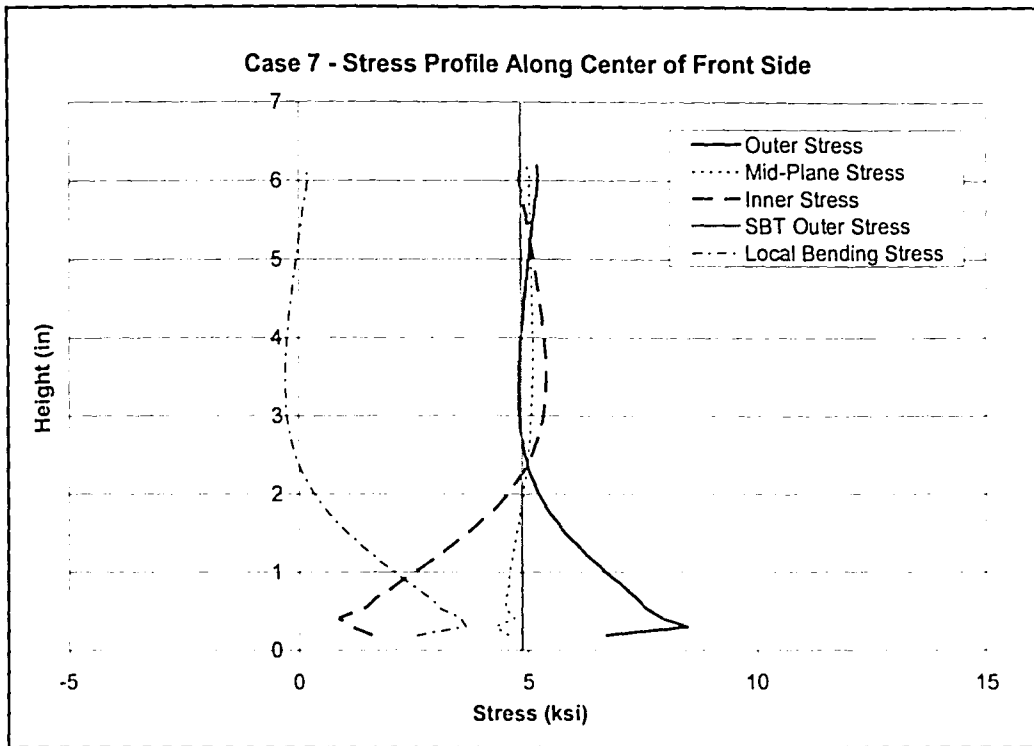


Figure A.12: Case 7 – Stress Profile Along Center of Front Side

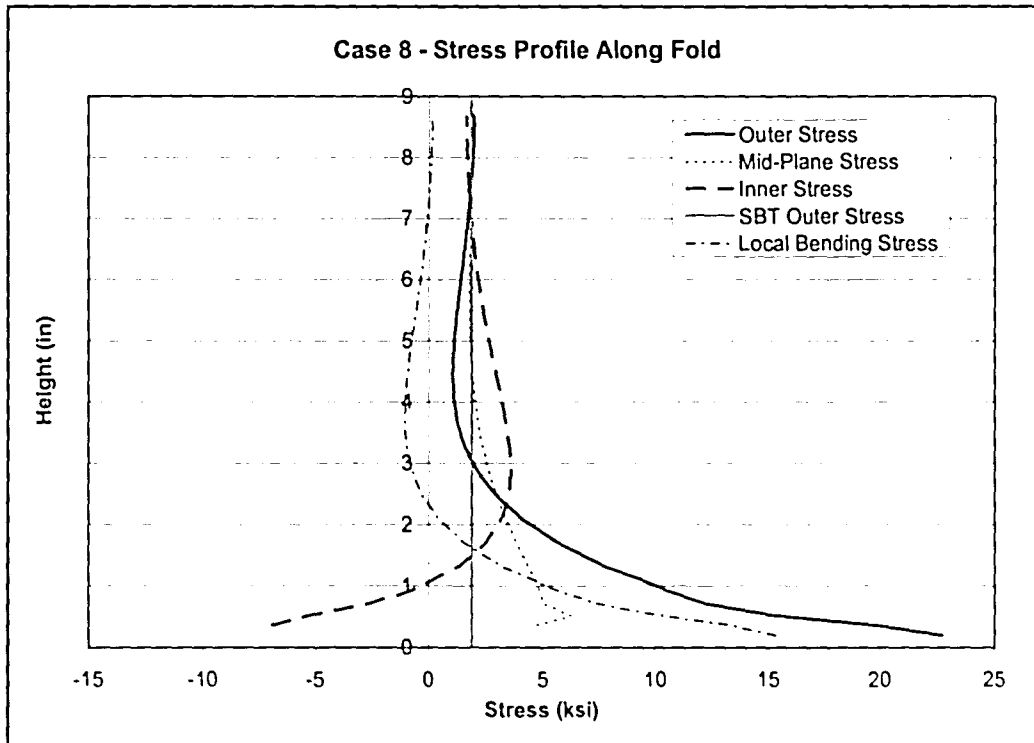


Figure A.13: Case 8 – Stress Profile Along Fold

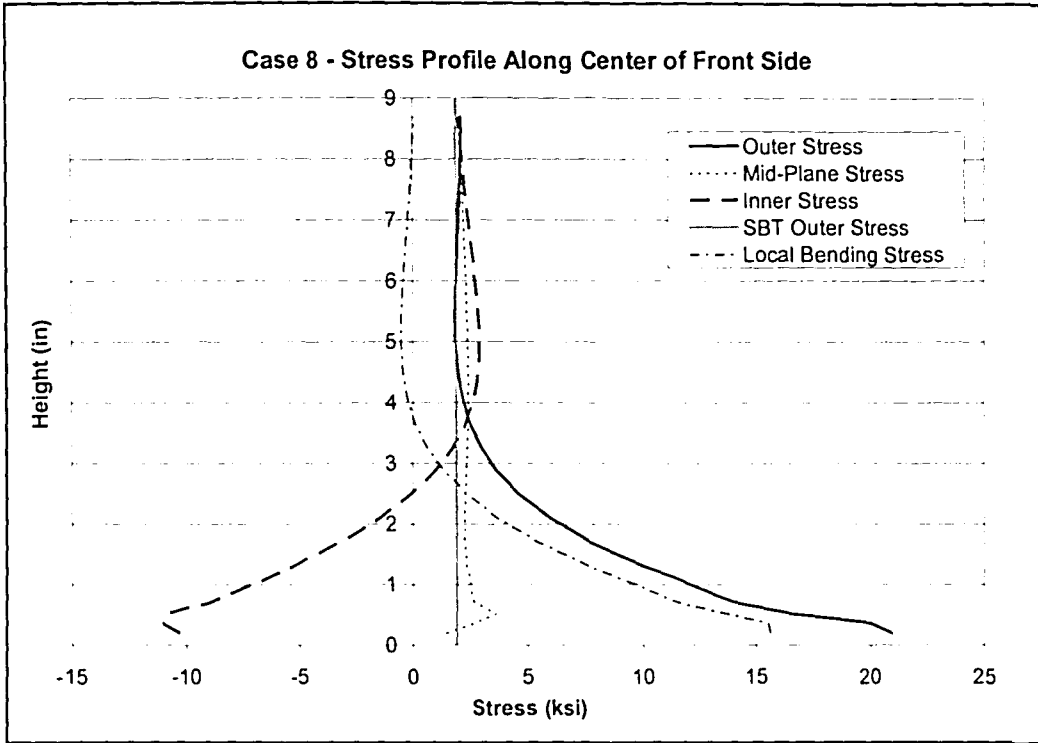


Figure A.14: Case 8 – Stress Profile Along Center of Front Side

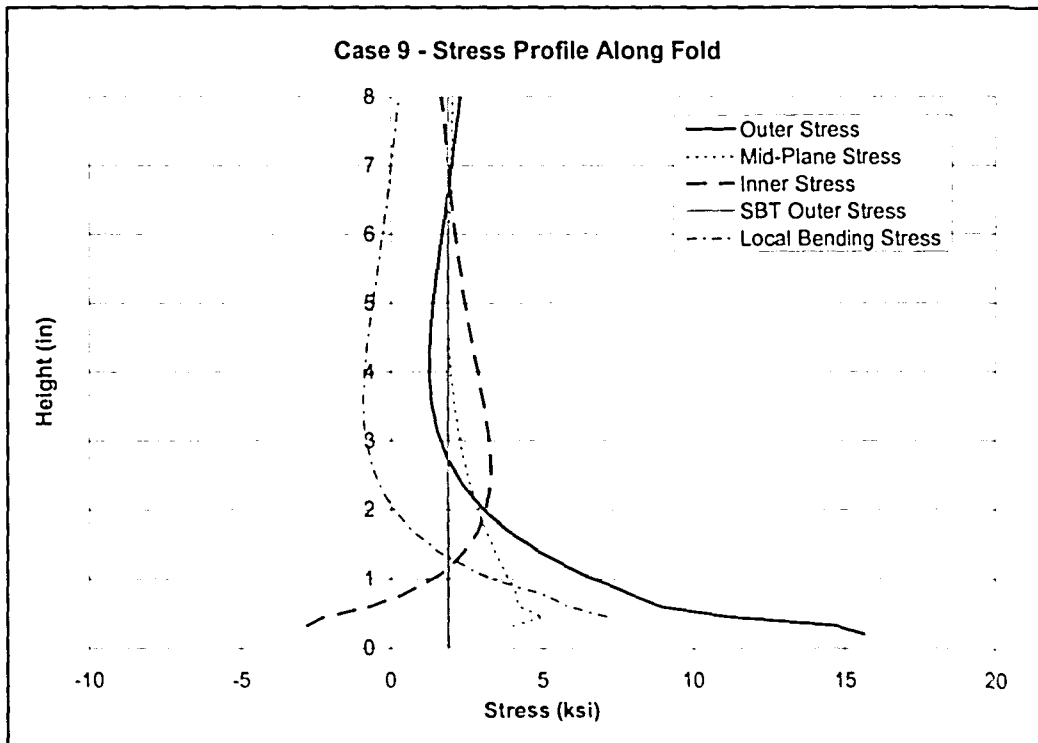


Figure A.15: Case 9 – Stress Profile Along Fold

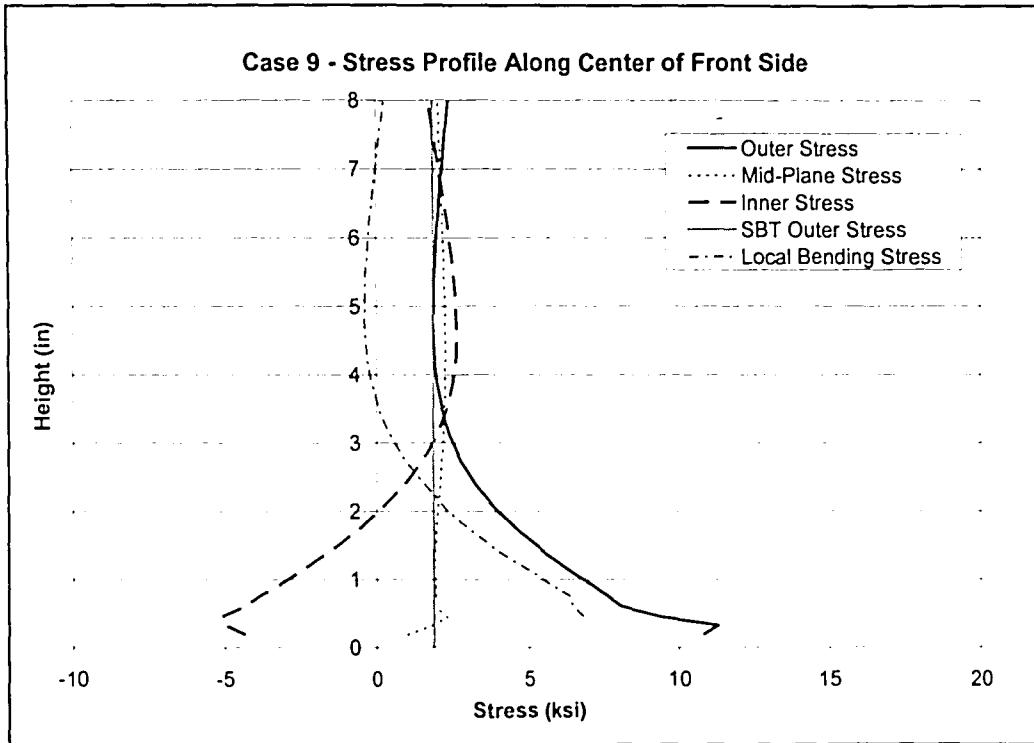


Figure A.16: Case 9 – Stress Profile Along Center of Front Side

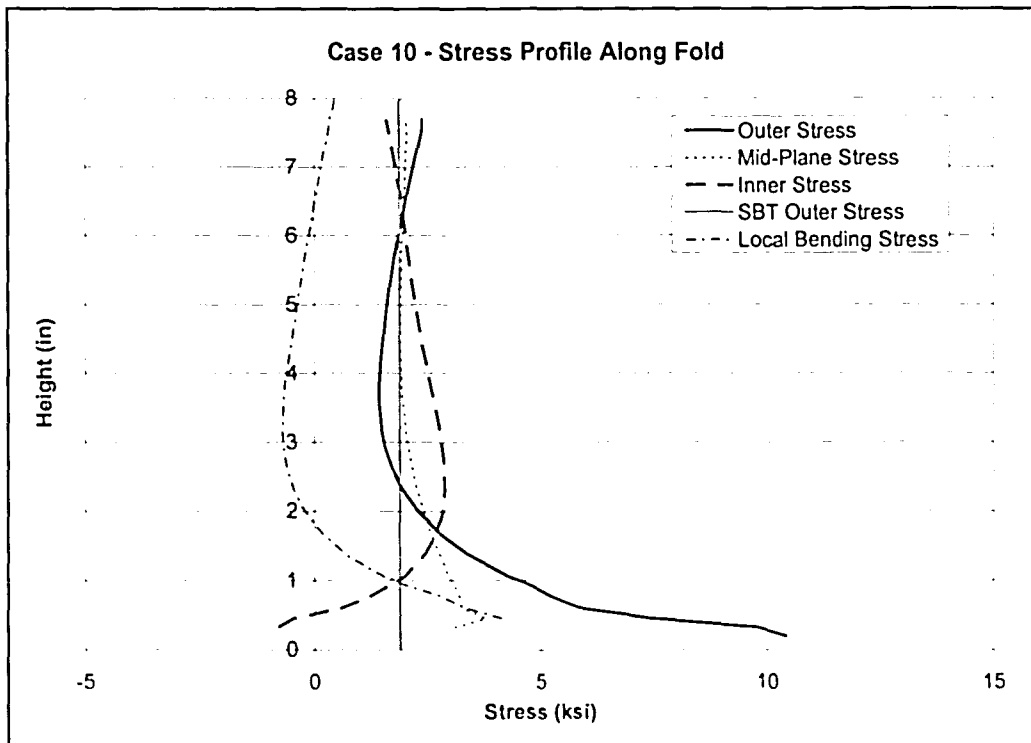


Figure A.17: Case 10 – Stress Profile Along Fold

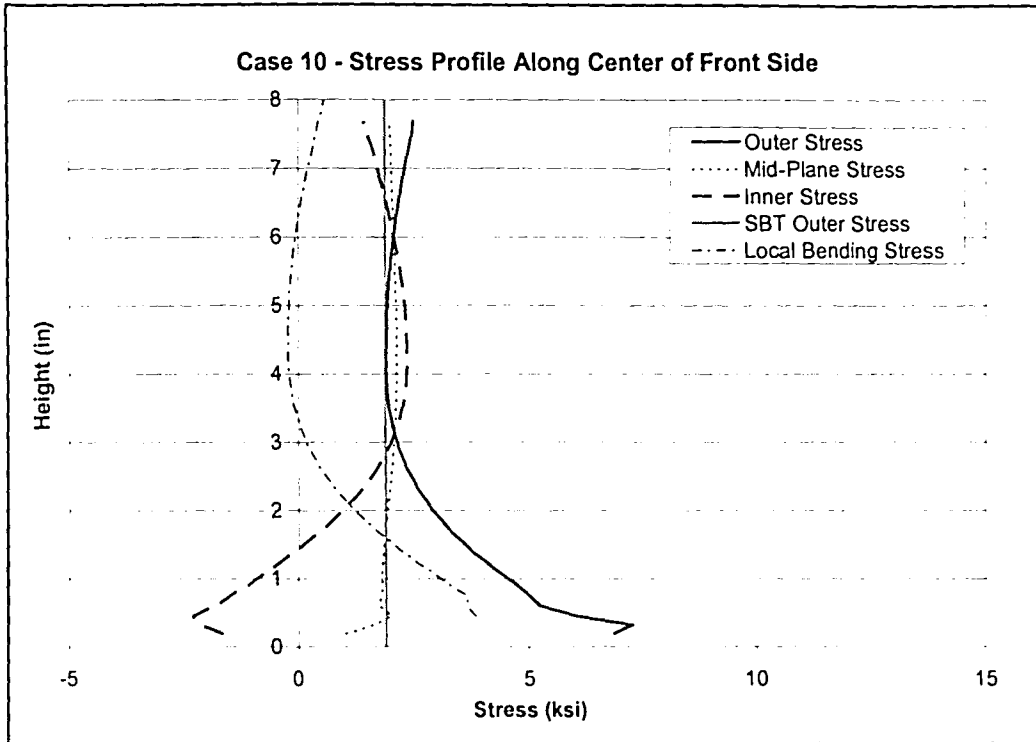


Figure A.18: Case 10 – Stress Profile Along Center of Front Side

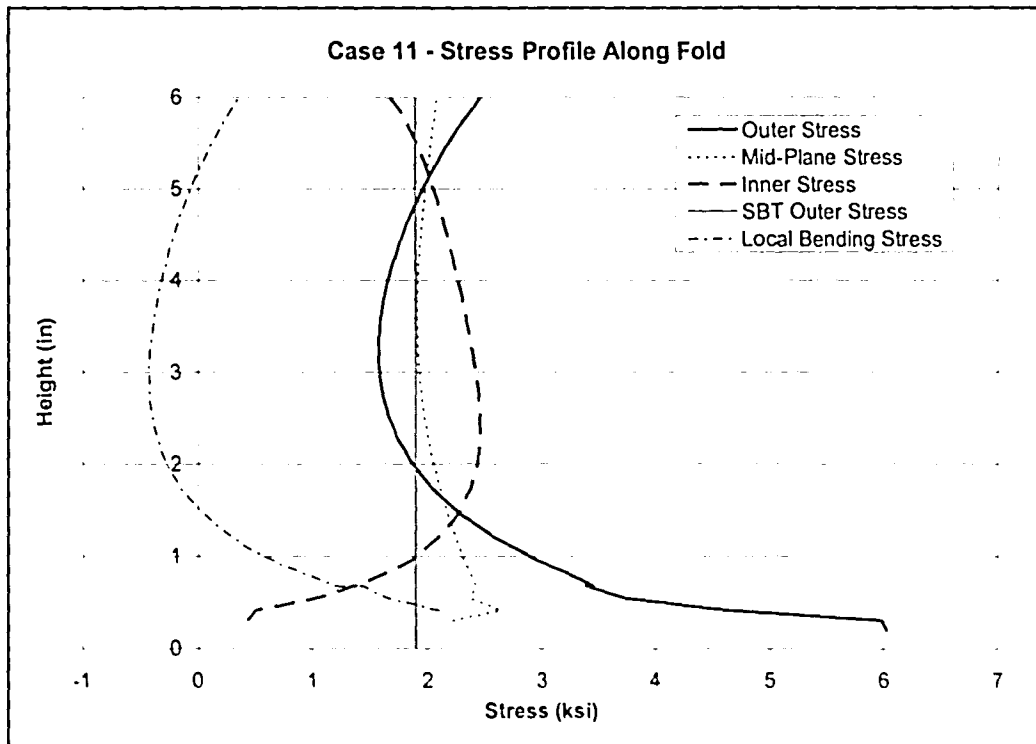


Figure A.19: Case 11 – Stress Profile Along Fold

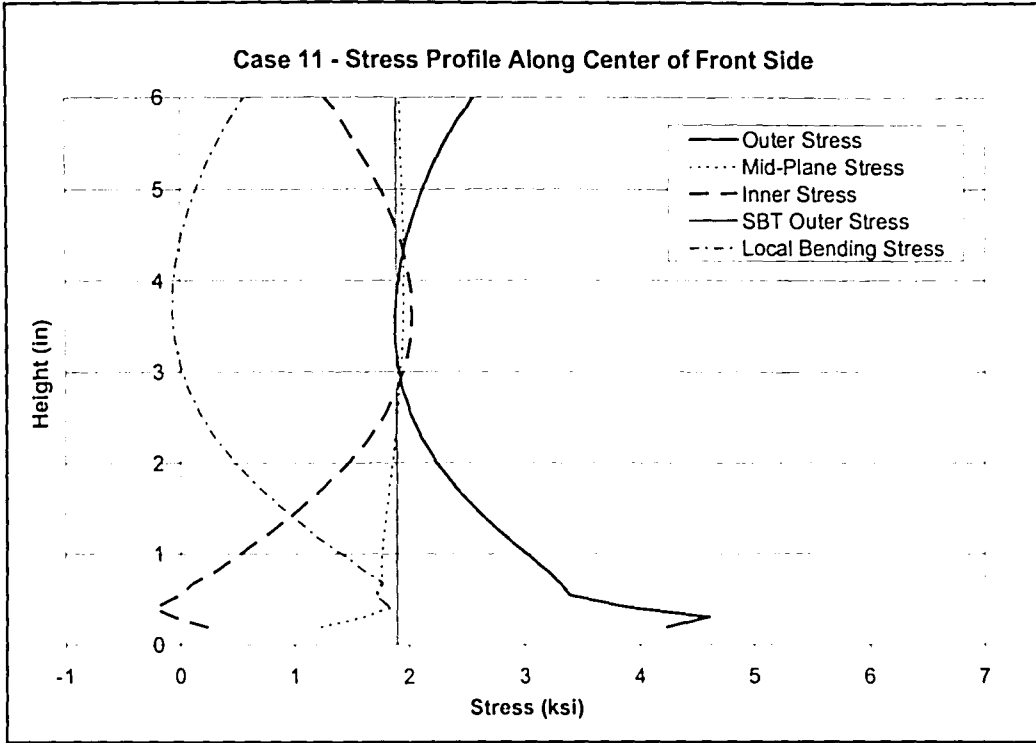


Figure A.20: Case 11 – Stress Profile Along Center of Front Side

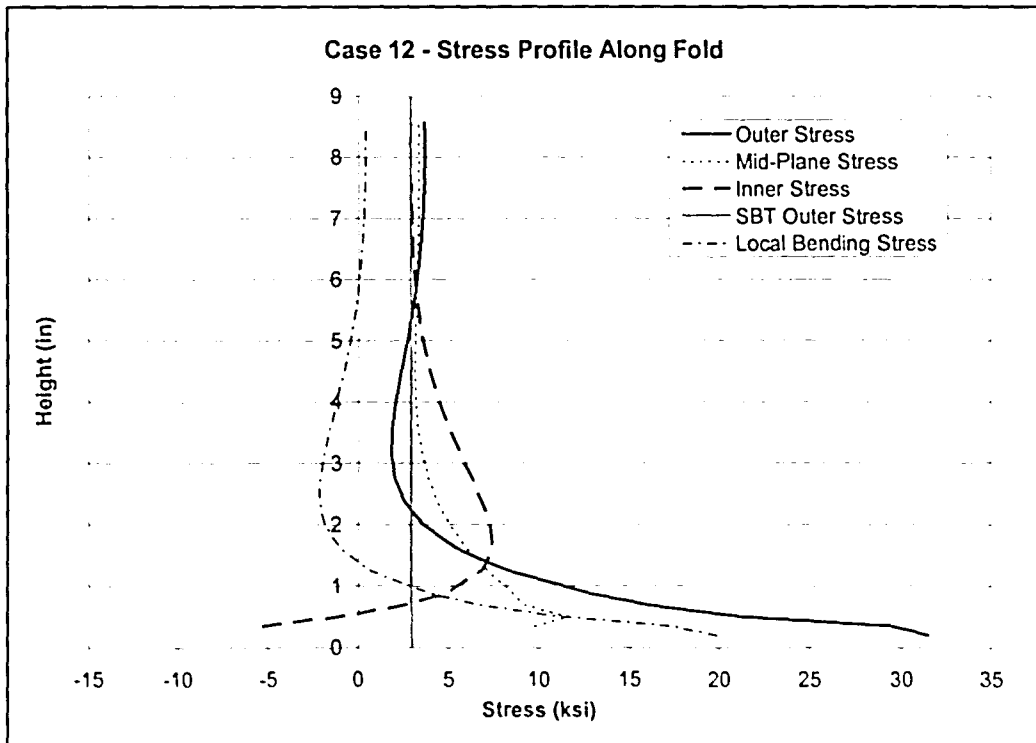


Figure A.21: Case 12 – Stress Profile Along Fold

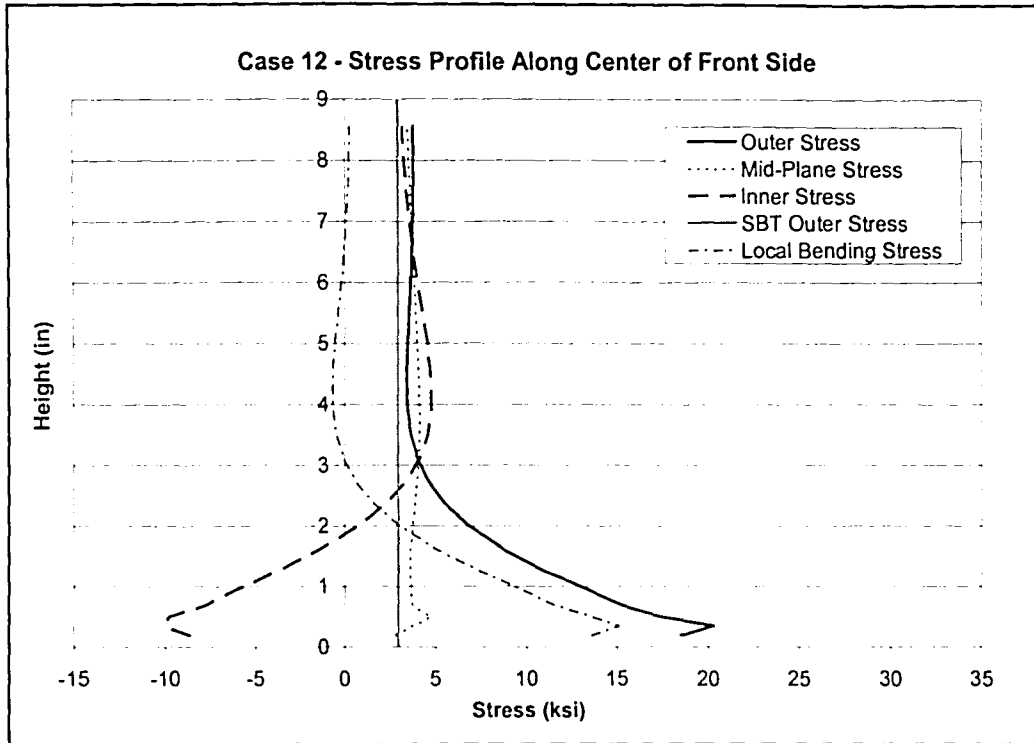


Figure A.22: Case 12 – Stress Profile Along Center of Front Side

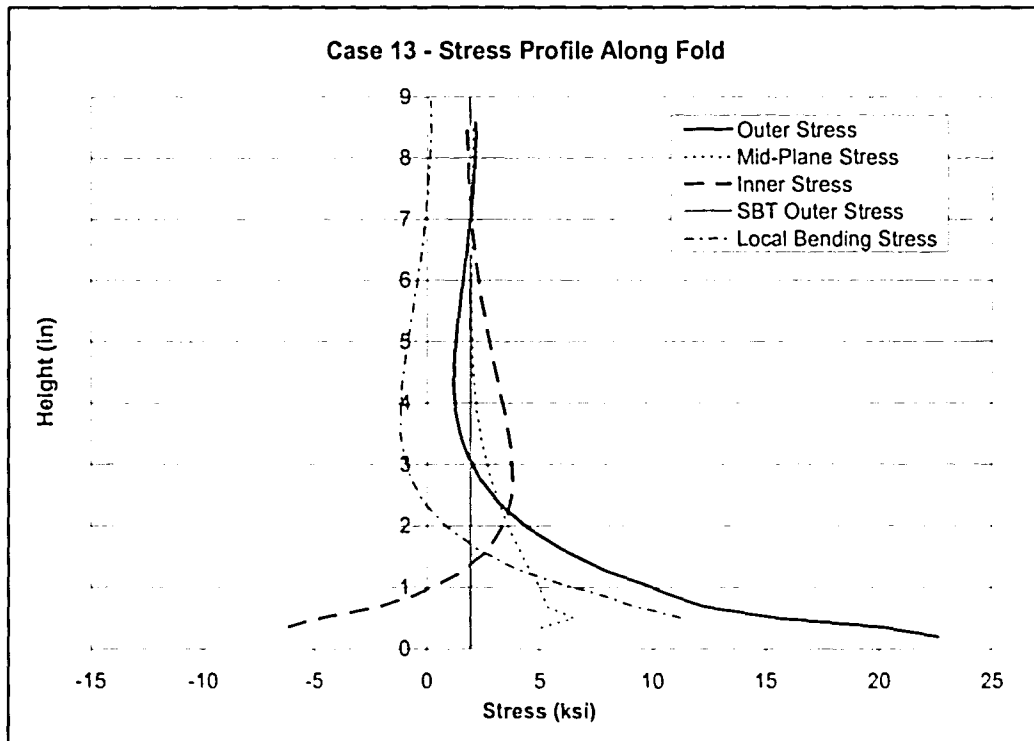


Figure A.23: Case 13 – Stress Profile Along Fold

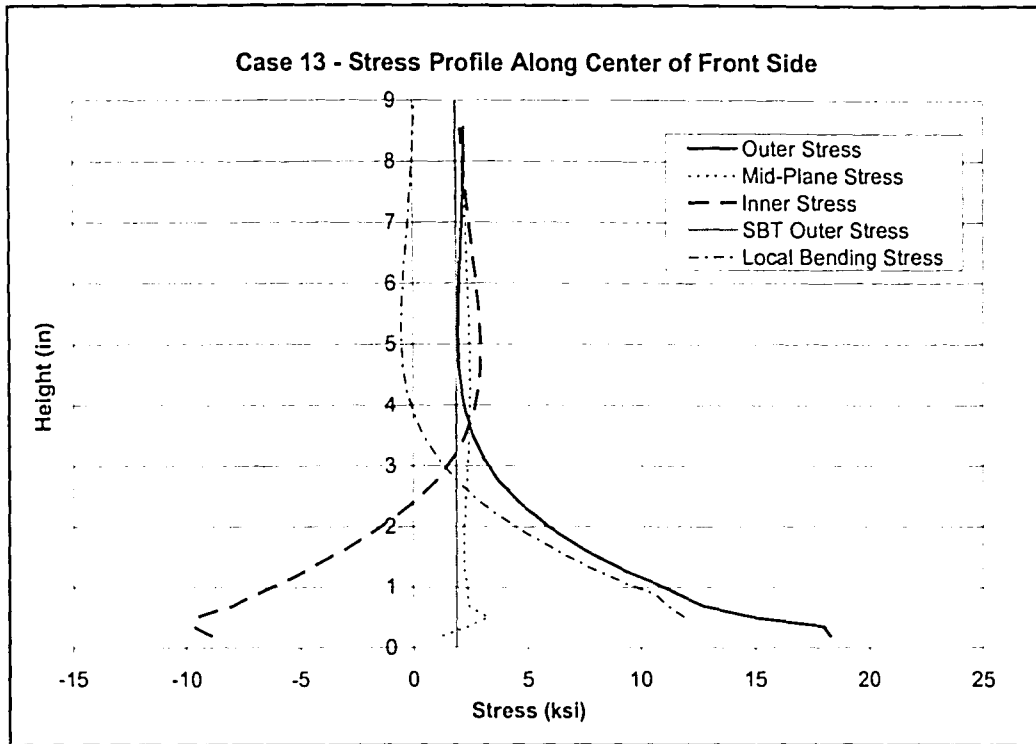


Figure A.24: Case 13 – Stress Profile Along Center of Front Side

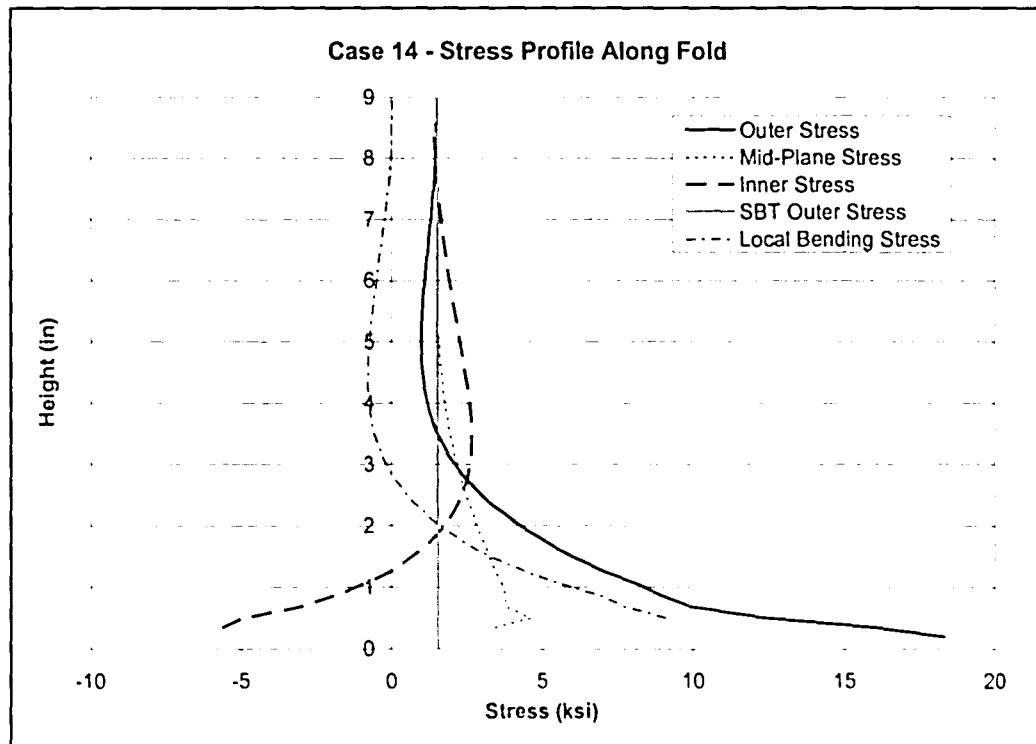


Figure A.25: Case 14 – Stress Profile Along Fold

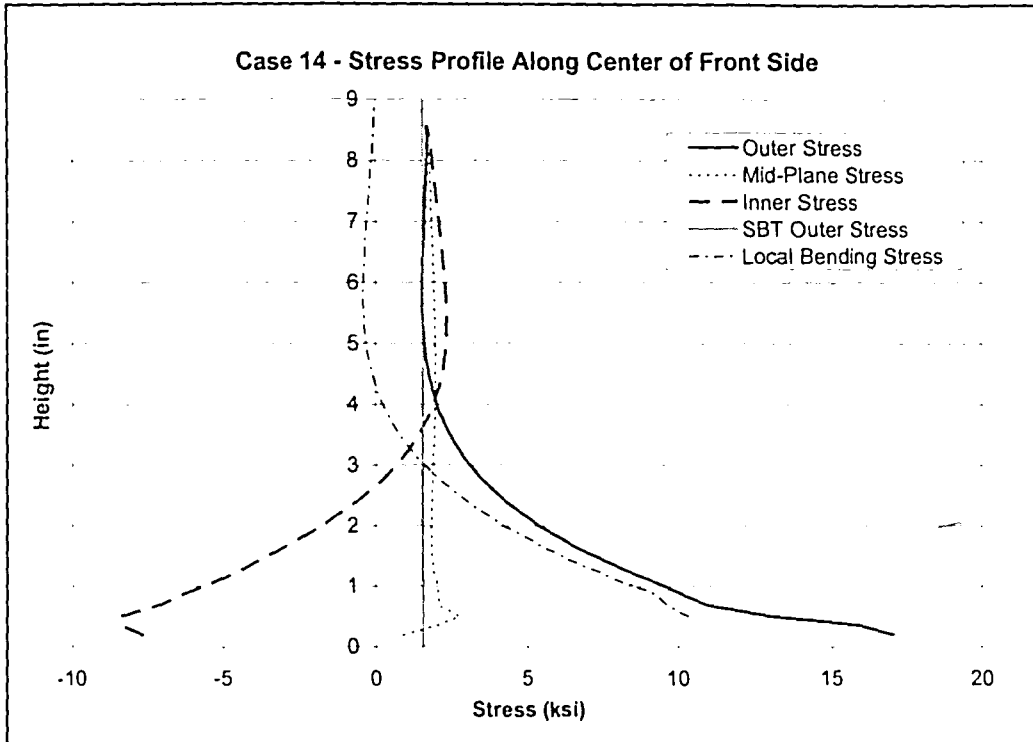


Figure A.26: Case 14 – Stress Profile Along Center of Front Side

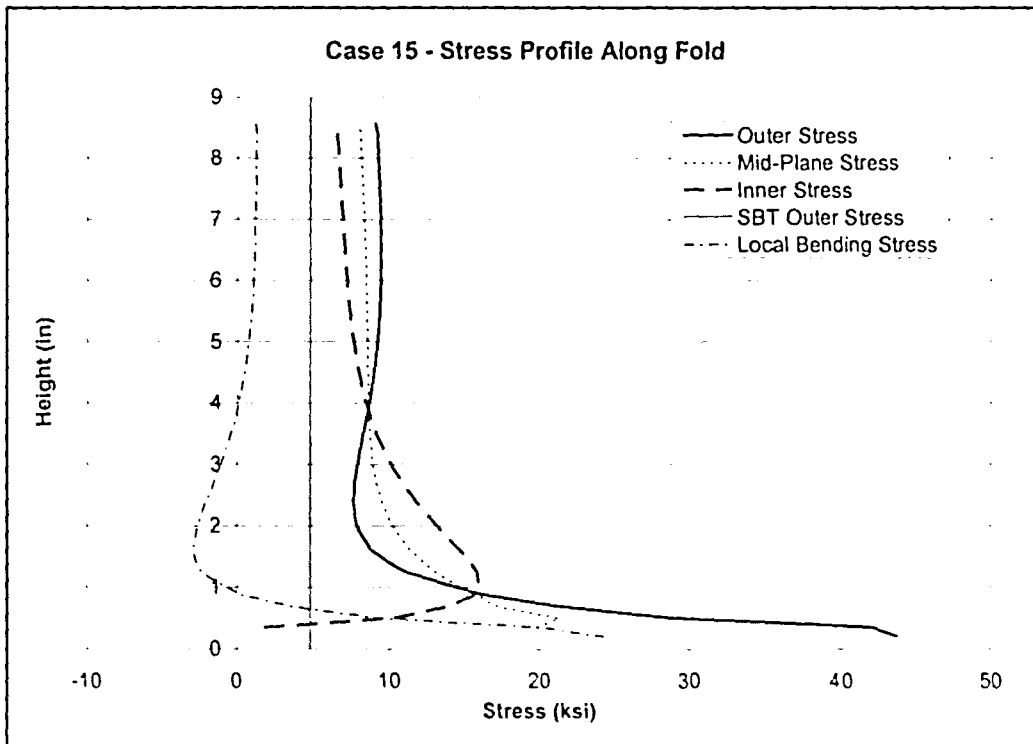


Figure A.27: Case 15 – Stress Profile Along Fold

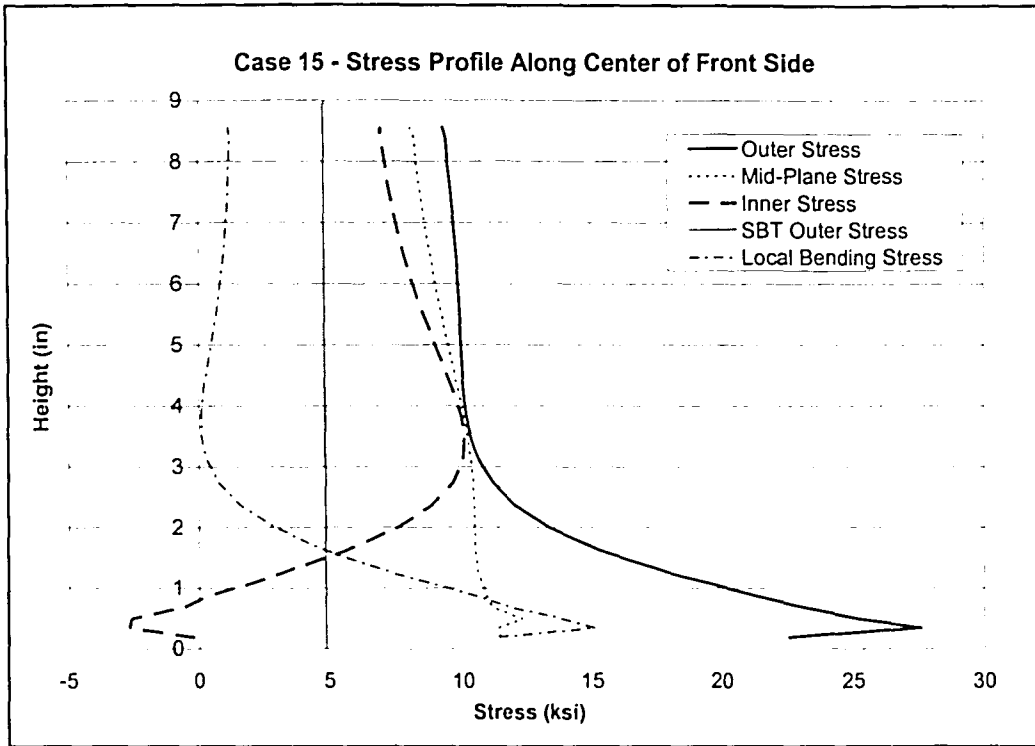


Figure A.28: Case 15 – Stress Profile Along Center of Front Side

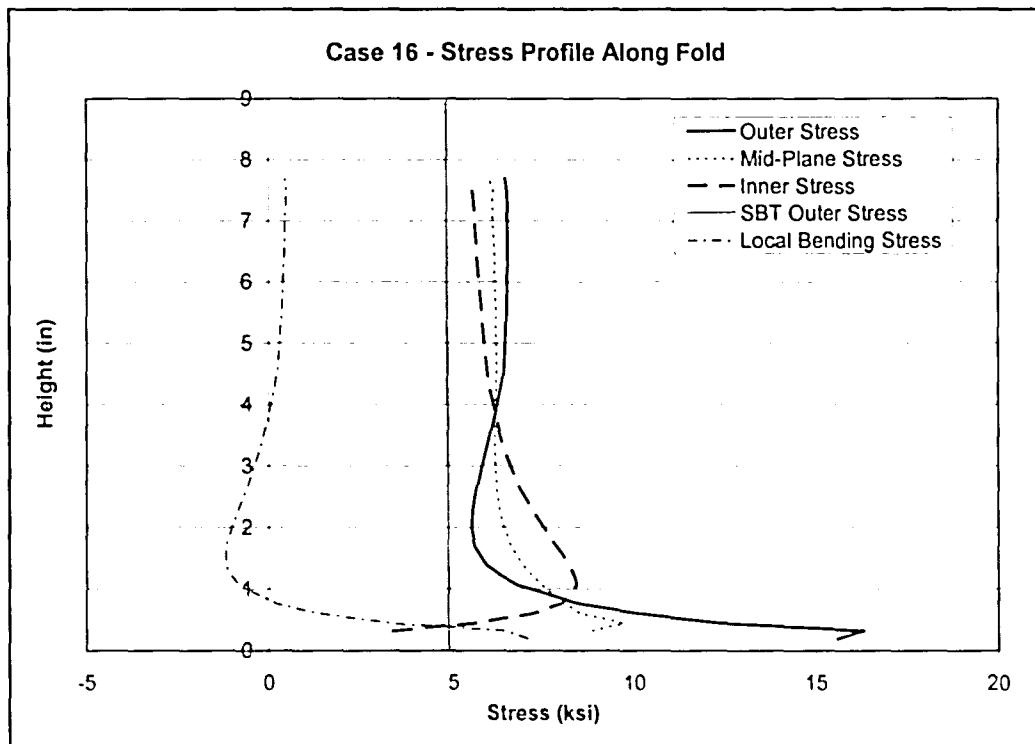


Figure A.29: Case 16 – Stress Profile Along Fold

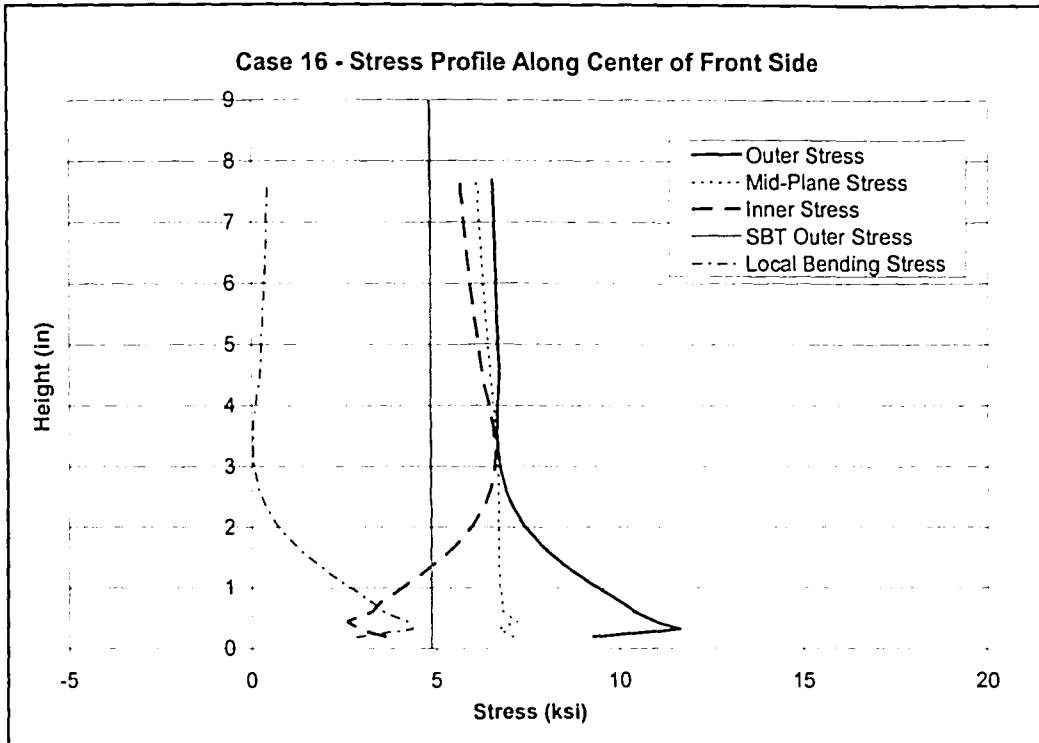


Figure A.30: Case 16 – Stress Profile Along Center of Front Side

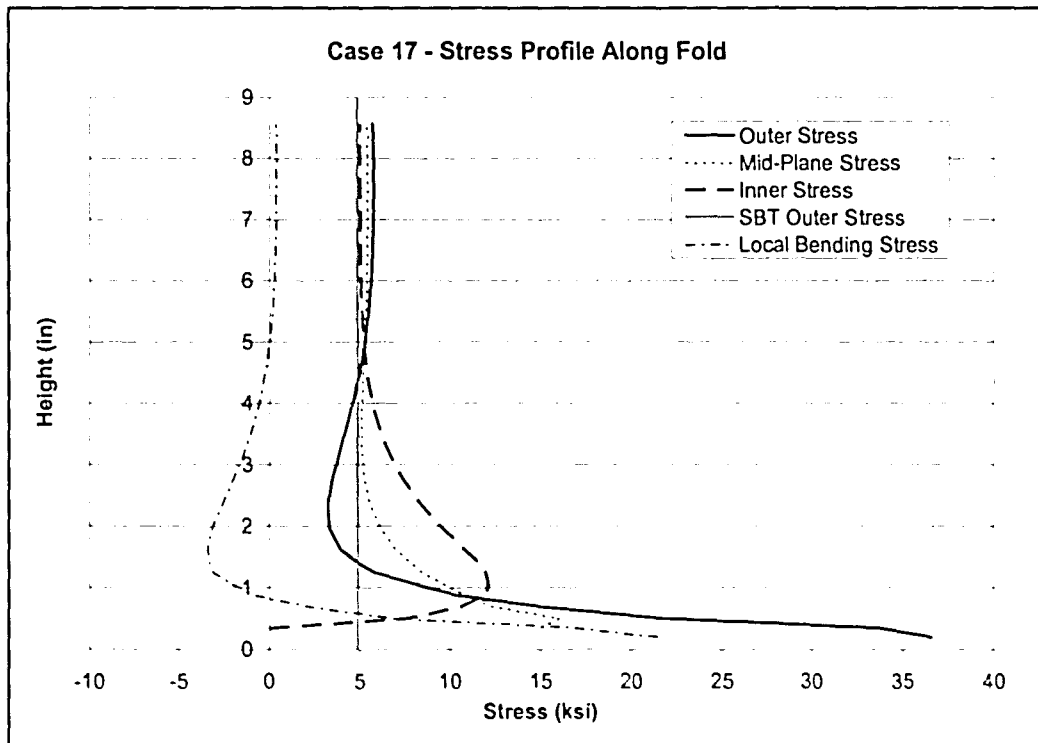


Figure A.31: Case 17 – Stress Profile Along Fold

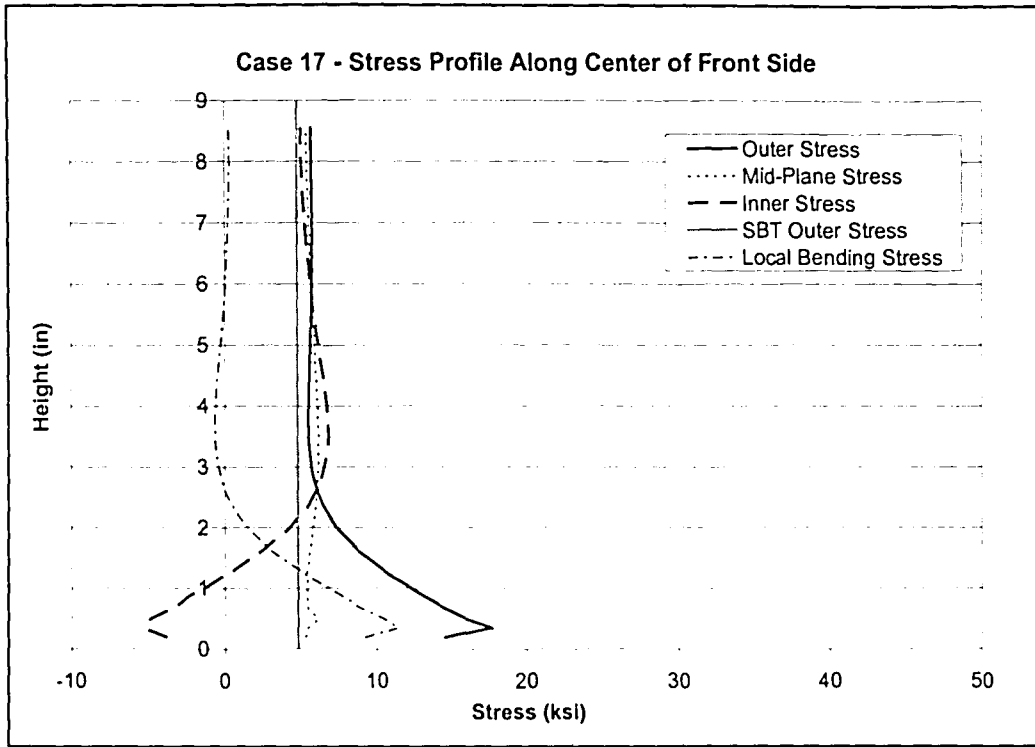


Figure A.32: Case 17 – Stress Profile Along Center of Front Side

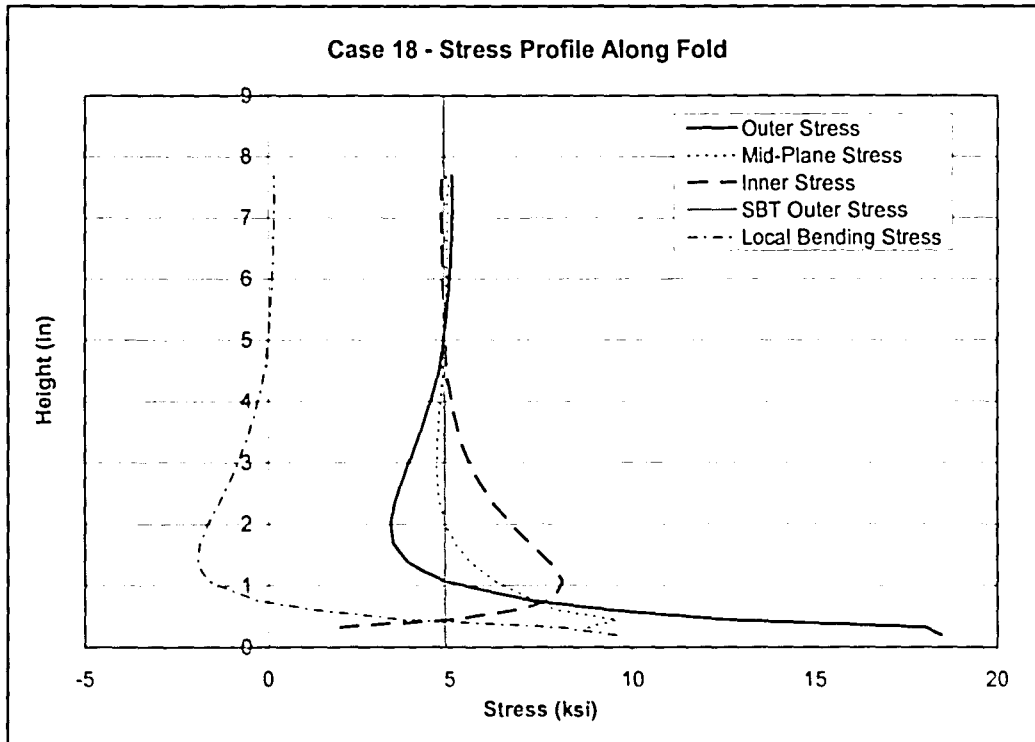


Figure A.33: Case 18 – Stress Profile Along Fold

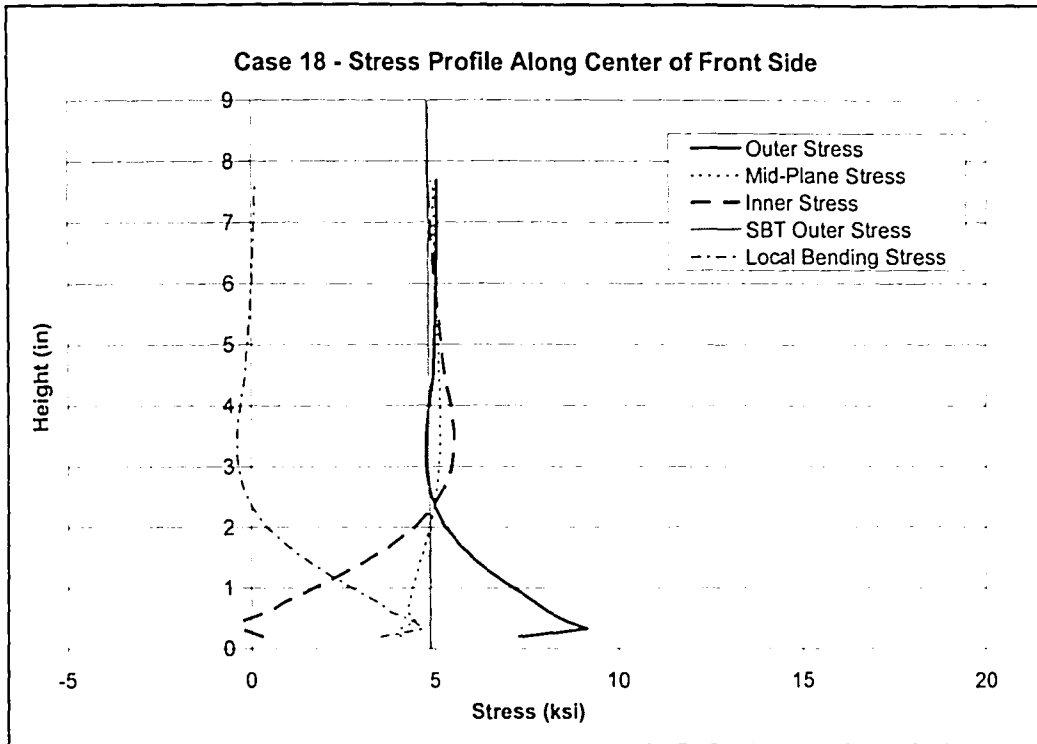


Figure A.34: Case 18 – Stress Profile Along Center of Front Side

References

1. ABAQUS/Standard Users Manual, Version 6.3, Hibbitt, Karlson & Sorensen, Pawtucket, Rhode Island, 2002.
2. American Association of State Highway and Transportation Officials, AASHTO Standard Specifications for Structural Supports for Highway Signs, Luminaries and Traffic Signals, Fourth Edition, AASHTO, Washington, D.C., 2001.
3. Brakke, B., Iowa Department of Transportation, Internal department documentation of high-mast lighting tower inventory, 2005.
4. Chopra, A. K., Dynamics of Structures: Theory and Applications to Earthquake Engineering, Second Edition, Prentice Hall, Upper Saddle River, New Jersey, 2001.
5. Connor, R.J., et al., Field Instrumentation and Testing of High-mast Lighting Towers in the State of Iowa, Iowa Department of Transportation, Ames, IA, 2006.
6. CSA International, CAN/CSA-S6-00, Canadian Highway Bridge Design Code, Toronto, Canada, December 2000.
7. CSA International, Commentary on CAN/CSA-S6-00, Canadian Highway Bridge Design Code, Toronto, Canada, December 2000.
8. Dexter R.J., et al., Fatigue-Resistant Design of Cantilevered Signals, Sign and Light Supports, National Cooperative Highway Research Program, NCHRP Report 469, Transportation Research Board, Washington, D.C., 2002.
9. Dexter, R.J., Investigation of Cracking of High-mast Lighting Towers, Iowa Department of Transportation, Ames, IA, September 2004.
10. Fisher, J. W., et al., Fatigue Behavior of Steel Light Poles, California Department of Transportation, Sacramento, CA, 1981.
11. Hall, J.H., The Effect of Base Plate Flexibility on the Fatigue Performance of Welded Socket Connections in Cantilevered Sing Structures, M.S. Thesis, Department of Civil and Environmental Engineering, Lehigh University, Bethlehem, PA, 2005.

12. Kaczinski, M.R., et al., Fatigue-Resistant Design of Cantilevered Signals, Sign and Light Supports, National Cooperative Highway Research Program, NCHRP Report 412, Transportation Research Board, Washington, D.C., 1998.
13. Koenigs, M. T., Fatigue Resistance of Traffic Signal Mast-Arm Connection Details, M.S. Thesis, Department of Civil Engineering, The University of Texas at Austin, Austin, Texas, 2003.
14. Neudorff, L.G., et al., Freeway Management and Operations Handbook, Federal Highway Administration, Report FHWA-OP-04-003, FHWA, September 2003.
15. Simi, El, et al., Wind Effects on Structures: An Introduction on Wind Engineering, Third Edition, John Wiley & Sons, New York, 1996.
16. Van Dien, J. P., Fatigue Resistant Design of Cantilevered Sign, Signal, and Luminaire Support Structures, Department of Civil Engineering, Lehigh University, Bethlehem, PA, 1995.

Vita

Margaret K. Warpinski, “Meg”, was born in Albuquerque, New Mexico on September 16th, 1981 to Norman Raymond and Kathleen Mary Warpinski. After completing her work at Sandia High School in Albuquerque, New Mexico in 2000, she enrolled at The University of Texas at Austin. She received a Bachelor of Science in Civil Engineering from The University of Texas at Austin in May of 2004. Meg enrolled in the graduate program at Lehigh University in August of 2004.

Permanent Address: 7129 Kiowa Ave N.E.
 Albuquerque, New Mexico 87110
 megwarp@gmail.com

**END OF
TITLE**